Instrumentation of erosion function apparatus and evaluation of a new erosion characterization methodology

by

Tri Van Tran

B.S., Can Tho University, 2005
M.S., Kansas State University, 2015

AN ABSTRACT OF A DISSERTATION

submitted in partial fulfillment of the requirements for the degree

DOCTOR OF PHILOSOPHY

Department of Civil Engineering
College of Engineering

KANSAS STATE UNIVERSITY
Manhattan, Kansas

2018

Abstract

Surface soil erosion is a widespread problem that impacts the natural and built environment. Many disciplines, such as hydrology, soil science, agriculture, and geotechnical engineering, have investigated soil erosion. Although empirical equations to predict soil erosion exist, they are typically inaccurate, so several devices have been developed to quantify the erodibility of soil. The erosion function apparatus (EFA) was developed to predict the erosion potential of soil for evaluating bridge scour; however, it has been used for several other geotechnical applications. The main disadvantages of the EFA are that it is unable to directly measure the shear stress, it remains operator dependent, and it is time consuming as a standard test requires at least eight hours. Moreover, as erosion occurs, it affects the water quality and makes it difficult to observe the soil sample surface during the test, affecting the operator judgement. The research objective of this project is to instrument the EFA to address the limitations of the device. A stereo-photogrammetry system was developed to measure the soil surface roughness following an EFA test and reduce operator dependency. Turbidity sensors were added to provide a secondary measurement of erosion. The newly instrumented EFA was used to develop a new methodology for interpreting erosion results. Lastly, the new methodology and instrumentation were used to explore the influence of natural and engineered soil properties on soil erosion.

Instrumentation of erosion function apparatus and evaluation of a new erosion characterization methodology

by

Tri Van Tran

B.S., Can Tho University, 2005
M.S., Kansas State University, 2015

A DISSERTATION

submitted in partial fulfillment of the requirements for the degree

DOCTOR OF PHILOSOPHY

Department of Civil Engineering
College of Engineering

KANSAS STATE UNIVERSITY
Manhattan, Kansas

2018

Approved by:

Major Professor
Stacey E. Tucker-Kulesza

Copyright

Abstract

Surface soil erosion is a widespread problem that impacts the natural and built environment. Many disciplines, such as hydrology, soil science, agriculture, and geotechnical engineering, have investigated soil erosion. Although empirical equations to predict soil erosion exist, they are typically inaccurate, so several devices have been developed to quantify the erodibility of soil. The erosion function apparatus (EFA) was developed to predict the erosion potential of soil for evaluating bridge scour; however, it has been used for several other geotechnical applications. The main disadvantages of the EFA are that it is unable to directly measure the shear stress, it remains operator dependent, and it is time consuming as a standard test requires at least eight hours. Moreover, as erosion occurs, it affects the water quality and makes it difficult to observe the soil sample surface during the test, affecting the operator judgement. The research objective of this project is to instrument the EFA to address the limitations of the device. A stereo-photogrammetry system was developed to measure the soil surface roughness following an EFA test and reduce operator dependency. Turbidity sensors were added to provide a secondary measurement of erosion. The newly instrumented EFA was used to develop a new methodology for interpreting erosion results. Lastly, the new methodology and instrumentation were used to explore the influence of natural and engineered soil properties on soil erosion.

Table of Contents

List of Figures

List of Tables

Acknowledgements

I would like to first express my deepest appreciation and gratitude to my major professor Dr. Stacey E. Tucker-Kulesza for her giving me an exciting project to work on during my doctoral degree. I thank her for her guidance and patience throughout my time here at Kansas State University. I am also grateful to her for providing me financial support throughout my study. I could not finish my study without her support.

In addition, I would like to thank my committee members, Dr. Michelle L. Bernhardt-Barry, Dr. Eric J. Fitzsimmons, Dr. Gretchen Sassenrath, and outside chairperson Dr. Catherine C. Lavis for their kind supports. Special thanks to Dr. Michelle L. Bernhardt-Barry for her kindness and guidance, providing information during the photogrammetry project.

I would also like to extend a thank you to those students who help me to finish my research; including Michael Snapp, Abady Al-Ali, Weston Koehn, Lisa Shofstall, Andrew Crowder, Luke Augustine, Mark Mathis, and Zahidul Karim. I also acknowledge the kind help of Mr. Cody Delaney for helping me with all kind of technical issues in my research. I would like to thank the Civil Engineering Department at Kansas State University for their financial support during my time at Kansas State.

Finally, I would like to thank my family for their support and encouragement during my time at KSU. Especially, I still do not have enough words to express my love for my wife and my children, who gave me strength when I was weak, who helped me out when I was stressed and who shared with me everything in my life.

Dedication

The dissertation is dedicated to my family, my parents. Without their inspiration and continued support, I would not be able to come this far. Thank you so much for everything.

Chapter 1 - Introduction

Surface soil erosion is a widespread problem that impacts the environment, agriculture, and infrastructure in both rural and urban areas. Soil erosion is the displacement of soil particles due to water flow or wind. Water flow erosion, the focus in this study, occurs when hydraulic forces exerted by the flowing water exceed the resistive forces of the soil. Soil erosion also impacts river/stream banks and when it occurs over agricultural lands erosion causes water contamination by carrying nutrients from fertilizers as well as pesticides into nearby water bodies and groundwater resources (Hansen et al., 2002; Verstraeten et al., 2003). Moreover, soil erosion in agriculture removes farmable surficial soil. In claypan regions of the US, including in Kansas, removing the surficial soil exposes the impermeable claypan layer at the surface (as shown in Figure 1.1) and decreases crop yield (Tucker-Kulesza et al. 2017).

Figure 1.1 Soil erosion in agriculture

In civil engineering, soil erosion affects the stability of infrastructure, specifically structures over and around water bodies. According to the Federal Highway Administration

(FHWA), there are 615,002 highway bridges in the USA and approximately 500,000 of these bridges are built over water (Richardson et al. 2003). Over 26,000 of these bridges are classified as scour critical. Scour, shown in Figure 1.2, is the removal of soil due to erosion from around infrastructure. When erosion occurs around a scour critical bridge, the structure may be undermined or may not be able to support the design loads during flood events, resulting in a collapse. This phenomenon is a wide spread occurrence. For example, there were at least 1,502 bridge failures and 58% of them were due to scour from 1966 to 2005 (Calappi et al. 2010). While scour can be dangerous for the safety of the traveling public, characterizing soil erosion potential is needed to evaluate infrastructure and reduce the scour risk.

Figure 1.2 Scour around bridge pier (U.S. Department of the Interior, U.S. Geological Survey)

Currently, the most accurate way to determine the erosion potential of soil is through experimental testing. Although empirical equations exist, they typically underestimate soil erosion because the equations were built on a series of soil parameters for clean sands. Therefore,

numerous testing devices were developed to directly measure soil erosion rate and critical shear stress to evaluate soil erodibility. Erosion rate and critical shear stress are the two parameters that determine the erodibility of soil. Erosion rate is the rate of removal of soil material per unit time. Critical shear stress is the minimum amount of applied hydraulic shear stress required to initiate erosion (Bernhardt et al. 2011). Each erosion testing device is unique and induces a different erosion mechanism. For example, the jet erosion test (JET), developed by Hanson and Cook (2004), produces erosion using a submerged hydraulic jet to determine the erodibility coefficient and critical shear stress of the soil *in situ*. The JET test is one of the few field erosion methods. Laboratory testing devices include the Hole Erosion Test (HET), the Rotating Erosion Testing Apparatus (RETA), the Sediment Erosion Rate Flume (SERF), the Ex-situ Scour Test Device (ESTD), and the Erosion Function Apparatus (EFA). The EFA, a flume style apparatus, was instrumented in this project and used to measure the erosion of reconstituted soil samples, undisturbed samples collected from the field, and engineered soil samples. More details about erosion testing apparatuses are described in Chapter 2.

The objective of this research is to instrument the K-State EFA, primarily so detailed experiments can be conducted to improve the understanding of fine-grained soil (cohesive soil) erosion mechanisms by future researchers. Erosion in non-cohesive soils, or cohesionless soils, is primarily controlled by the median particle size (Briaud et al. 2001). However, erosion in cohesive soils is a complex function of physical, geochemical, and biological soil properties (see Figure 1.3; Grabowski et al. 2011). These complex interactions have caused empirically derived models to remain inaccurate. Grabowski et al. (2011) recommended that the interactions among the physical, geochemical, and biological properties of soil be further investigated to find the correlations

between multiple properties and erodibility; however, these interactions could not be studied with the original EFA due to the limitations discussed below.

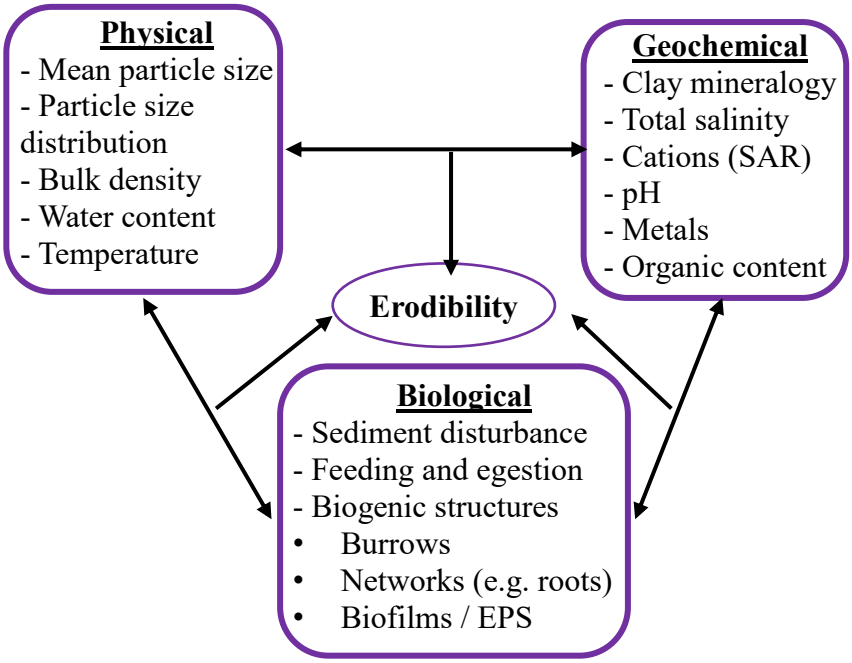

Figure 1.3 Physical, geochemical, and Biological properties affecting erosion of cohesive soil (Grabowski et al. 2011)

Two critical components of the K-State EFA were instrumented to allow for more detailed erosion measurement to investigate soil property interactions: surface soil roughness and the turbidity of the eroding fluid. The soil roughness is used for determining the hydraulic shear stress in an erosion test. The existing methods for measuring surface roughness are currently user dependent and time consuming. A surface roughness measurement using digital photogrammetry gives a repeatable roughness measurement and the results are less variable than the traditional method (Tran et al. 2017). Two turbidity sensors were installed in the K-State EFA to calibrate the relationship between turbidity measurements and the volume of soil eroded during EFA test. The combined photogrammetry and turbidity measurements were used to create a new erosion characterization chart as a function of volume of soil eroded and turbidity. This new methodology

uses the same erosion characterization classifications from traditional EFA testing but allows researchers to see data before erosion occurs. This will help to disaggregate the impact of soil properties on fine-grained soil erosion to improve erosion models as data are not lost with the new methodology. Furthermore, future researchers can use the new erosion characterization methodology to evaluate the erodibility of materials that are difficult to measure such as really soft rock or engineered soils, as was done in this study.

The second phase of this research will be to use the instrumentation to evaluate fine-grained soil erosion. The physical properties of soil, including mean particle size, particle size distribution, bulk density, and water content have been studied intensively in the past (Briaud et al. 1999; Debnath et al. 2007; Bale et al. 2007; Sang et al. 2015). However, the influence of temperature (a physical property in Figure 1.3) on soil erosion has not been fully investigated. This study investigated both water temperature and soil temperature influences on soil erosion as there was no previous literature where both properties were investigated simultaneously. The newly instrumented EFA was also used to characterize the erodibility of claypan soils. This research is significant because the novel instrumentation and new erosion characterization methodology will contribute to and allow future researchers to improve soil erosion models. Additionally, novel methods to reduce soil erosion have been developed, including soil strengthened by microbially induced carbonate precipitates (MICP). The newly instrumented EFA could be used to measure the impact of MICP on soil erodibility.

This research is divided into five chapters. The background and research objective are described in Chapter 1. Chapter 2 is a literature review of the parameters that affect soil erosion and soil erosion testing devices. Details regarding the fundamental of the proposed instrumentation, the photogrammetry technique and turbidity system, are described in Chapter 3.

Chapter 4 presented the results and discussions in this research. Scientific contribution of this research is presented in Chapter 5. Finally, conclusion and recommendations, including some of the future research are provided in Chapter 6.

Chapter 2 - Literature Review

Predicting soil erosion is a challenge for researchers as well as practicing engineers. The parameters that affect soil erosion are presented first in this chapter in order to have a better understanding what will influence the erodibility of soils. Because the main objective of this research is to instrument an erosion testing device and to utilize it for research purposes, an overview of soil erosion devices similar to what will be utilized in this study is then described. A literature review about the photogrammetric techniques and the turbidity sensors system used in this research are also presented.

2.1 Parameters that affect soil erosion

According to Grabowski et al. (2011), there are three main groups of properties that affect the erodibility of cohesive sediment. These included physical, geochemical and biological properties (Figure 1.3). Kimiaghalam et al. (2015) stated that physical, mechanical, and electrochemical properties of cohesive sediments have a significant impact on the soil erodibility. Most importantly, physical properties of the sediment that influence the erodibility of cohesive soil have been studied by many researchers. These properties are the mean particle size, grain size distribution, plasticity index, bulk density and water content, and temperature. The geochemical properties, such as clay mineralogy, geochemistry of water, and organic content that affect soil erosion are also discussed herein. There has been limited research in biological properties to date, however, researchers are beginning to investigate engineered biofilms/EPS as shown in Figure 1.3 to improve soil erosion resistance, specifically for surficial erosion control (Shanahan and Montoya 2016) and to wind erosion (Hamdan et al. 2016). This research investigated the effects of an engineered biofilm on soil erosion resistance (Wang et al. 2018); however, other biological properties are beyond the scope of this project.

2.1.1 Mean particle size and particle size distribution

The median particle size of soil is widely used as a crucial factor for the erodibility of soils. Dade et al. (1992) created Hjulstrom and Postma plots to illustrate that soil particles with a larger diameter than sand are more difficult to erode than sand. The plots also showed that clay particles are much more difficult to erode than silts and sand. Thomsen and Gust (2000) found a negative correlation between critical shear stress and mean particle size for natural marine clay from a field survey. However, a positive relationship between critical shear stress and mean particle size was observed in laboratory studies when particle size and floc density were proportional (Lau and Droppo 2000; Droppo et al. 2001). In general, effective particle size can be either positively or negatively correlated with erodibility depending on the conditions under which the aggregates are formed.

Erodibility is also a function of particle size distribution. Houwing (1999) conducted a field study and found that erosion rates decreased two times with increasing clay content (4-35%) for intertidal sediment. Other researchers have confirmed that critical shear stress increases with increasing clay contents (Panagiotopoulos et al. 1997; Van Ledden et al. 2004; Winterwerp and Van Kesteren 2004).

2.1.2 Plasticity index

Plasticity index (*PI*) is a measure of the plasticity of a soil. Shan et al. (2015) developed an empirical relationship between critical shear stress (τ_c) and *PI* with several other soil parameters. The empirical model was derived from experimental testing on fine grained soil samples using an in-house flume-style erosion device as

$$\tau_c = 0.1\left(\frac{w}{F}\right)^{-2} PI^{1.3} q_u{}^{0.4} \qquad \textbf{Equation 2.1}$$

where w is the water content, F is the fraction of fines by mass, and q_u is the unconfined compressive strength. The equation shows that critical shear stress increases with increasing plasticity index. Similarly, Kimiaghalam et al. (2015) found that the coefficient erodibility (k_d) decreases with increasing plasticity index. Figure 2.1 shows the correlation between critical shear stress, k_d and *PI*. Note that although a relationship was established, the root mean squared (R^2) error showed a weak correlation with both τ_c and k_d.

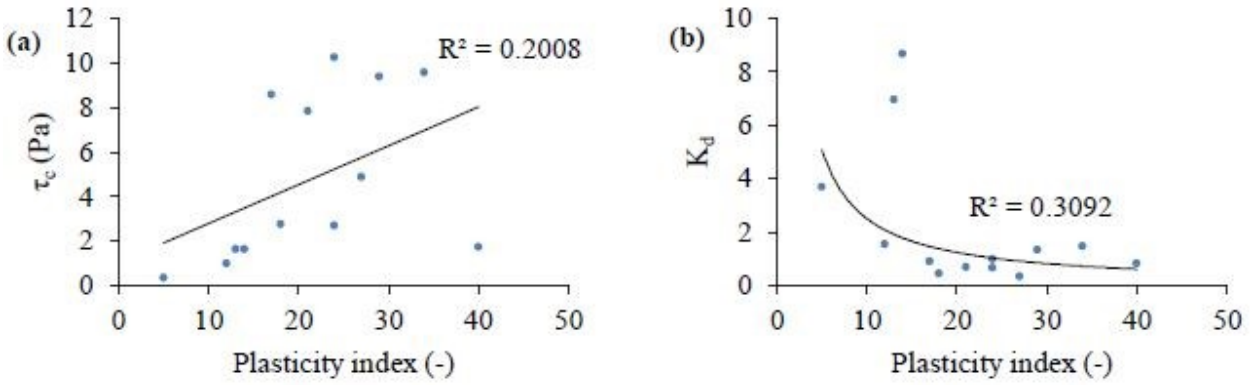

Figure 2.1 Critical shear stress and k_d versus plasticity index

2.1.3 Bulk density and water content

The relationship between bulk density and soil erodibility have been well studied in the literature (Jepsen et al., 1997; Lick and McNeil, 2001; Amos et al., 2004; Bale et al., 2007; Kimiaghalam et al. 2015). Jepsen et al. (1997) revealed an inverse relationship between bulk density and erosion rates. A high bulk density typically results in lower erosion rates (Jepsen et al., 1997; Lick and McNeil, 2001); or alternatively less dense soils have higher erosion rates (Bale et al., 2007). Amos et al. (2004) provided an empirical relationship between bulk density and critical shear stress (τ_c) for marine soils as

$$\tau_c = 5.44x10^4(\rho_b) - 0.28 \qquad \textbf{Equation 2.2}$$

where ρ_b is the wet bulk density from 800 to 2000 kg/m^3.

Water content also plays an important role on the erodibility of soil. Larionov et al. (2014) conducted vertical water jet tests of the loamy clay samples and found that the erosion parameters of the samples strongly depend on the soil moisture. The erosion rate was the smallest for samples with a water content of 22 – 24%. Larionov et al. (2014) showed that the erosion rate increased, and the variability of the results decreased with both decreasing and increasing the water content as presented Figure 2.2.

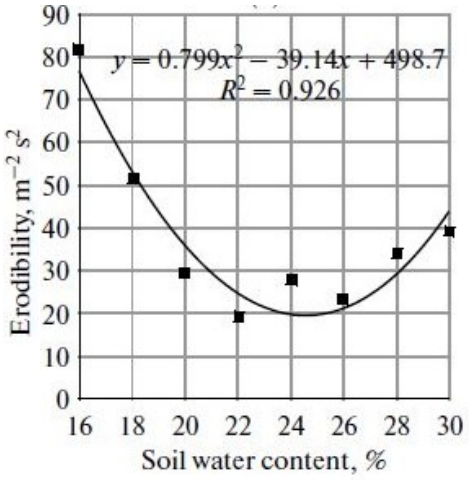

Figure 2.2 Erodibility of model soil samples as a function of water content

2.1.4 Temperature

Researchers have found a relationship between water temperature and the erosion of soil; however, there are at least two different hypotheses that explain the effects of temperature on erodibility. According to Zreik et al. (1998) and Mehta and Parchure (2000), an increase in temperature causes an increase in erodibility of soil due to the weakening of inter-particle connections of the soil. Winterwerp and Van Kesteren (2004) stated that the viscosity of the pore water decreases with an increase in temperature. This causes the velocities of the flow at the bed surface to be higher and thus the erodibility of the soil is increased. According to Larionov et al.

(2014), the erosion rate of soil strongly depends on the water temperature used in the test. The soil erosion rate increases with the water temperature, which can be explained with the Van't Hoff rule. Larionov et al. (2014) believed that the rupture of bonds between soil particles was caused by electrostatic forces appearing between the monomolecular water layers around the adjacent soil particles similarly oriented with respect to the soil solid phase. This explanation would be true for fine-grained soil. However, the Larionov et al. (2014) samples were coarse-grained.

No evidence of effects of increased water temperature on soil temperature was noted in any previous studies. Therefore, there is a need for determining what factor predominantly causes the change in soil erosion so that a unifying theory on temperature effects can be established. Moreover, identifying the critical temperature parameter is needed to support the hypothesis that temperature must be controlled to match field conditions during erosion testing to more accurately measure soil erosion.

2.1.5 Clay mineralogy

Clay mineralogy has been investigated as a factor that affects soil erodibility. These studies have been limited to three common clay minerals: kaolinite, illite, and montmorillonite. Kaolinites have the largest particles and the lowest cation exchange capacity (CEC), whereas montmorillonites have the smallest particles and the highest CEC (Partheniades, 2007). CEC is the total capacity of a soil to hold exchangeable cations. For soils with minerals with high CEC, water infiltration between the particles, pushes the soil particles apart. The more they are pushed apart, the more erodible the clays become. Therefore, montmorillonites are considered to have the highest erodibility; conversely, kaolinites have the lowest erodibility. Illites represent an intermediary in erodibility categories (Morgan, 2005).

2.1.6 Geochemistry of water

Geochemistry of water plays a vital role in determining erodibility of soil. Sodium adsorption ratio (SAR) and total salinity are the parameters that have been studied the most in the literature (Rowell, 1994; Brady and Weil, 2002; Winterwerp and van Kesteren, 2004; Debnath et al., 2007). SAR is a ratio of the sodium to the combination of calcium and magnesium in relation to known effects on soil dispersibility. Soils with high SAR (> 13-15) absorb more water and result in a soil with high porosity, low permeability, and high erodibility (Rowell, 1994; Brady and Weil, 2002). Figure 2.3 shows the relationship between critical shear stress with SAR and total salinity in a study of Winterwerp and Van Kesteren (2004). As shown in the figure, critical shear stress decreased with increasing SAR and increased with high total salinity. Soil is most resistant to erosion with total salinity of 5%.

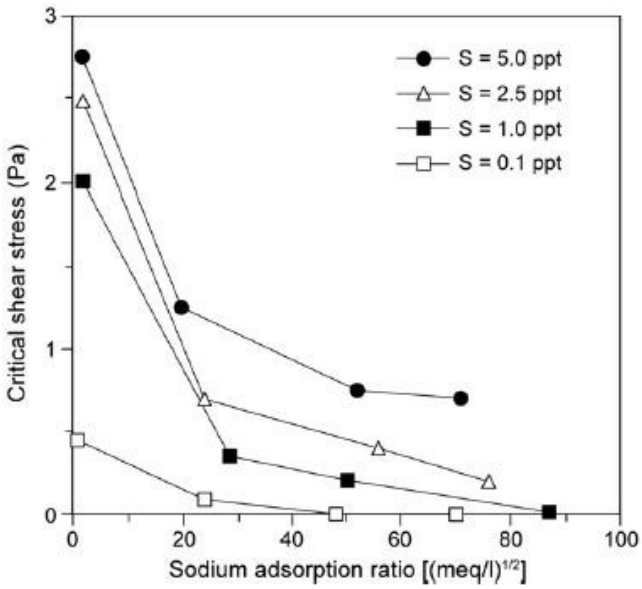

Figure 2.3 Critical shear stress versus SAR and total salinity (Winterwerp and Van Kesteren, 2004)

There has been little research in the past that investigate the effect of pH on soil erosion. Kandiah (1974) conducted an experimental study on a homogeneous kaolinite and

montmorillonite. The author found that erosion rate increased with high pH at a uniform shear stress. However, there is currently no field studies that investigate a pH effect on erodibility of soil.

2.1.7 Organic content

Organic content is defined as the quantity of organic matter per unit mass of sediment. It has been recognized as an important factor affecting the soil erosion (Brady and Weil, 2002; Morgan, 2005). For soils with organic content from 0 to 10%, the erosion rates are negatively correlated with organic content. It is noted that for natural sediment, organic content has a positive correlation with water content and an inverse relationship with bulk density according to Avnimelech et al. (2001).

2.2 Erosion testing devices

Several erosion testing devices have been developed and each laboratory device induces a different soil erosion mechanism (surface erosion, gully, rill, and inter-rill). Erosion testing devices can be divided into four categories: rotating apparatus tests; jet erosion tests; flume-style erosion tests; and internal erosion tests. These devices are discussed briefly herein. However, this research will focus on surface erosion, also known as bank erosion, which is typically measured using flume-style erosion devices. Therefore, this literature review covers the main flume-style erosion devices currently in use (sediment erosion rate flume, ex-situ scour test device, and erosion function apparatus).

2.2.1 Jet Erosion Test (JET)

Jet Erosion Testing (JET) apparatus was developed by Hanson and Cook (2004), which is a portable device that measures soil erodibility in the field. The main components consist of an

adjustable head tank, jet tube, nozzle, point gage, and a jet submergence tank. The test set up in the field is shown in Figure 2.4.

Figure 2.4 JET set up in the field (Hanson and Cook, 2004)

The jet submergence tank is pushed into the soil until the plate ring is level with the soil surface and then the tank is filled with water. Water is pumped from the source to the head tank where the water level is kept constant during the test. Water is expelled from the nozzle and impinge the soil surface. The depth of the eroded hole is measured using the point gage every 5 to 10 minutes. The critical shear stress in a JET is a function of the maximum stress due to the jet velocity at the nozzle, the potential core length, and the equilibrium depth. The equilibrium depth is the scour depth at which the stress is no longer enough to cause the erosion.

The advantage of the JET is that it is a quick test, simple to conduct, and relatively inexpensive to perform. It can be conducted at different locations at a specific site and the combined results are used to predict erosion. This gives a more holistic assessment of the testing area. However, the excess stress parameters obtained from the JET results cannot be measured

directly. They are based on the measured scour depth and determining the equilibrium scour depth is still operator dependent. Additionally, if no water source is available at the site, the JET requires large amounts of water to be transported to the site, making the JET applications limited. Most importantly, the jet test generates the flow through an impinging jet, which does not represent the actual flow conditions in the field.

2.2.2 FLUME apparatus

Another in-situ testing device is the FLUME apparatus. Ravens (2007) described the FLUME as a 3 m long straight flume with the cross section of 10.1 x 12.7 cm, deploying in-situ via a boat. Figure 2.5 shows the diagram of the FLUME.

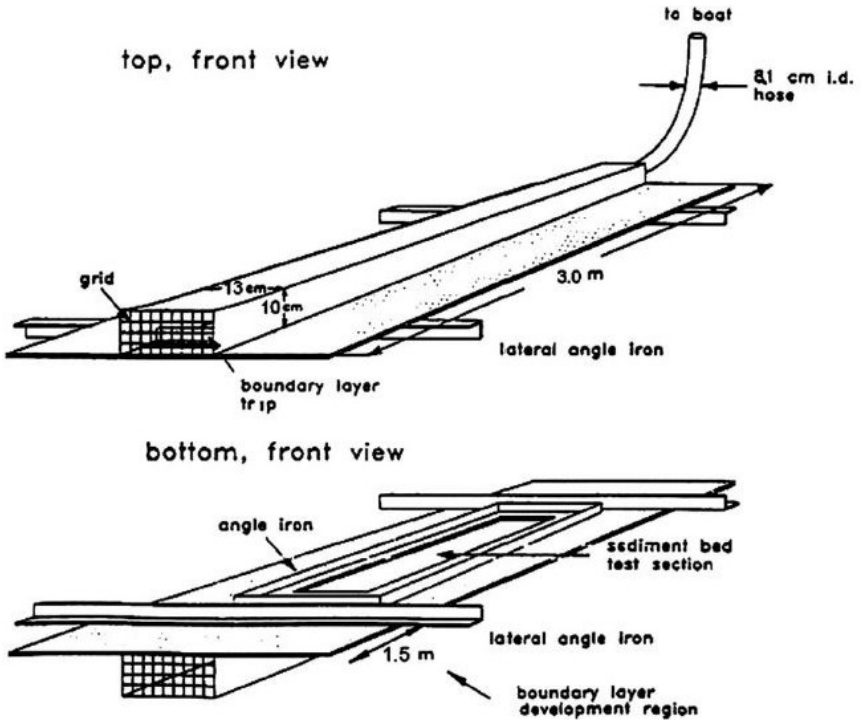

Figure 2.5 Diagram of FLUME (Ravens 2007)

The flume contains three sections: a 1.5 m long inlet section, a 1.1 m long erosion test section, and an outlet section. The water flows through the flume via an onboard pump and the flow rate is monitored with a Paddlewheel Flow Sensor. Fine sand is glued on the bottom of the

inlet section to reduce the change in roughness as flow passed to the test section. The particle concentration is monitor based on turbidity measurements and a calibration curve in order to calculate the erosion rate of sediment bed. The advantages of this system are that the flume is directly placed on the sediment using an onboard winch system and more erosion is induced as flow rate increased. However, the limitation of this device is that the roughness of the sediment bed is assumed to be zero. When the erosion depth exceeds 4 cm, scour develops at the entrance and exit of the test section making the results unreliable.

2.2.3 Pocket Erodometer Test

The two devices above need to transport large and heavy equipment to a site and results are not immediate. The pocket erodometer test (PET) was developed by Briaud et al. (2011) to address these limitations. The PET is a simple, inexpensive, light weight instrument, that provides a quick field estimate of the erodibility of the soil sample. The PET is a water gun that produces an 8 ± 0.5 m/s velocity jet, with a nozzle diameter of approximately 0.5 mm. The device is pointed at the face of the sample with a distance of 50 mm. The trigger is then squeezed 20 times at a rate of 1 squeeze per second. The depth of the hole in the surface soil sample is recorded and the erosion rate is calculated. The results are compared to an erosion chart to determine the erodibility category of the soil. Figure 2.6 shows the PET test progression.

Figure 2.6 Photo of the PET test progression (Briaud et al. 2011)

Despite the advantages of PET as mention earlier, this device is not suitable for rock erosion testing and it remains to be an operator dependent device. Furthermore, calibration of the PET device is difficult and therefore results are highly variable between devices.

2.2.4 Hole Erosion Test (HET)

The HET was developed to evaluate the internal potential for embankment dams. In an HET, the soil specimen is compacted in a standard proctor mold. A 6 mm diameter hole is drilled at the center along the soil sample to represent a crack or a concentrated leak. Water flows from an upstream tank through the control valve to the first chamber, then through the preformed hole, and exits into the downstream chamber. The flow rate is recorded every 10 seconds during the test through an overflow. The test is finished when the hole is too big and reaches the mold or the flow rate is too high that cannot be measured accurately anymore by the device. After the test, the soil specimen is removed, and diameter of the hole is measured. The erosion rate is calculated as the change in diameter of the hole divided by the time of flow. Figure 2.7 illustrates the schematic of HET. The HET is easy to set up; however, the preformed hole can be difficult in soils without sufficient cohesion.

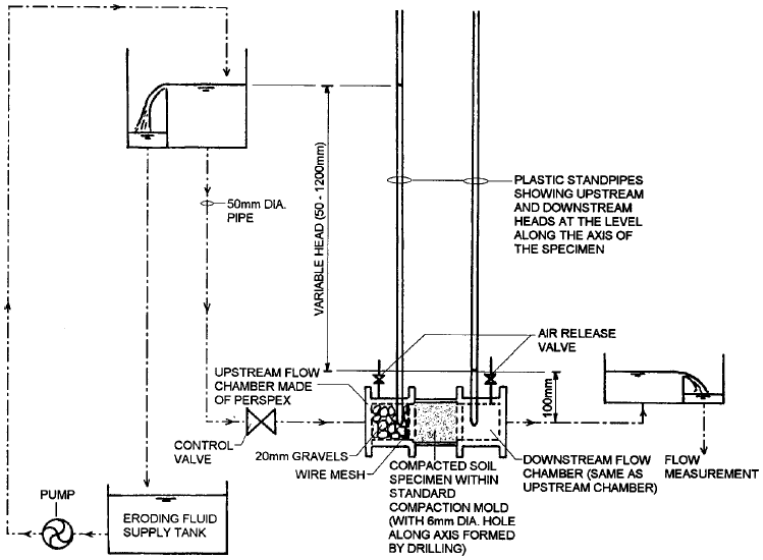

Figure 2.7 Schematic of the hole erosion test (Wan and Fell, 2004)

2.2.5 Rotating Erosion Testing Apparatus (RETA)

Bloomquist et al. (2012) developed the RETA for measuring the erosion rate versus shear stresses of rock and stiff clay. The RETA is an updated version of the original erosion testing device, the rotating cylinder apparatus, developed by Moore and Masch (1962). The RETA consists of a housing that contains an electric motor, a rotating outer cylinder, a support frame with slide rails for inserting or removing the sample into the outer cylinder, torque cell and clutch, and a digital touch screen control/monitoring unit. A 7.9 mm diameter hole is drilled through the center of the sample for the insertion of a support rod. The lower end of the support rod is connected to the motor, while the upper end of the support rod connects to the clutch-torque-cell. Then the sample is placed inside the rotating outer cylinder, and the annulus is filled with water that allows the sample to saturate. When the cylinder is rotated at the desired torque or rotational speed (controlled by the control/monitoring system), flow in the annulus is generated which induces shear stress on the outer surface of the sample. After testing, the sample was raised of the outer cylinder. The container with the water and eroded sediment is placed in the oven for the water to vaporize and then is weighed. The mass of eroded sediment is determined by subtracting the total mass from the known mass of the container. A minimum of three tests are performed in the RETA to get the relationship between erosion rate and shear stress. The advantages of the RETA are that it provides a direct measurement of shear stress and the erosion rate. Moreover, the test can be performed for a long period of time in low erodibility samples (such as rock) and at higher shear stress levels. However, the erosion rate in RETA tests are conducted on the vertical surface of the sample while erosion actually occurs on the horizontal surface *in situ*. Lastly, the average shear stress in this test is nearly constant during testing and this device can only be tested for self-supporting samples such as rock and stiff clay.

2.2.6 Sediment Erosion Rate Flume (SERF)

Crowley et al. (2012) performed a study of the SERF, which measures soil erosion rate and its applied shear stress directly. The SERF was developed at the same time as the EFA used in this study and is quite similar to the EFA. The apparatus consists of two pumps, a 3 m long rectangular aluminum flume divided into five sections, a shear stress sensor, three fiber optic lasers and three corresponding fiber optic photoelectric sensors, a temperature probe, an ultrasonic ranging system, a pressure transducer, a temperature control system, and the 4164 liters stainless steel reservoir. To perform an erosion rate test, the sample is inserted into the test section and the flume is filled with water at a low speed to remove the air bubbles. During the test, the fluid velocity is controlled, and the temperature is maintained at a constant value via the cooling system and the sample surface is kept at the same level with flume bottom by an ultrasonic array and laser system. The flow velocity and shear stress are recorded. Finally, the test is repeated with some different flow velocities. The advantage of this device is that it was built with different sections so that different sized samples (diameters) can be tested. Moreover, the shear stress of a sample with a given roughness can be measured directly, so it removes operator dependency from an erosion test and provides real time erosion data.

2.2.7 Ex-situ Scour Test Device (ESTD)

The ESTD uses a moving belt and a pump to drive the flow in a channel with dimensions of 120 mm x 20 mm and a length of 580 mm. The system consists of the inlet and outlet tanks which are connected with the channel located in the ESTD tank. The flow meter and a direct force gauge are attached into the device to measure flow velocity and the force imparted by flowing water on the soil sample. Two cascaded filter cylinders are used to filter the water to ensure that the water near the soil sample is always clear for observation during testing. Figure 2.8 shows the

schematic of the ESTD. The flow velocity profile driven only by the moving belt is S-shaped and a parabola in the rectangular channel when the belt is not moving. A log-law velocity profile in the channel is generated when both the belt and the pump are operating.

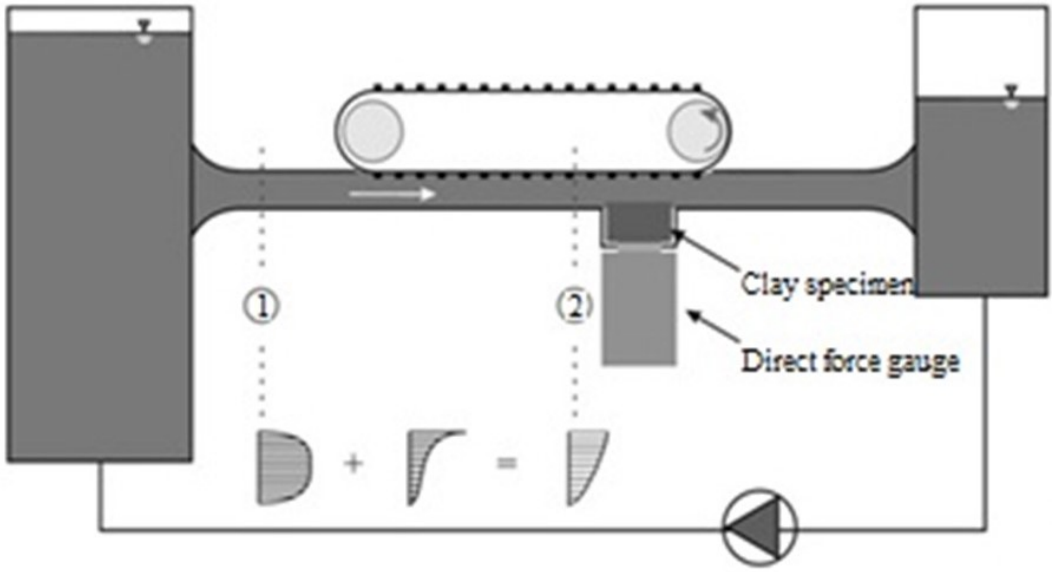

Figure 2.8 Schematic of the ESTD (Shan et al. 2015)

The soil sample with diameter of 63.5 mm is mounted on a sensor disk. The sensor disk is placed on the platform, which is on top of the direct force gauge. At the beginning of the test, the soil sample is placed flush with the channel bottom. As erosion occurs after a certain period, the test is stopped, and the sample is pushed up to keep the flush condition. The weight loss of the sample is used to calculate the erosion rate of the sample, and the shear stress is calculated from the measured forces by the direct force gauge. The erosion then starts again, and the above procedure is repeated until the test finished. One advantage of this device is that the bed shear stress is directly measured. In addition, the soil samples are automatically pushed up as erosion occurs to keep the top of the soil sample at the same level of the flume in the ESTD test. However, the length of the soil sample is limited to 20 mm which can make sample preparation difficult.

2.2.8 Erosion Function Apparatus (EFA)

The EFA (used in this study) was developed to measure the erosion function of a soil by measuring the erosion rate and hydraulic shear stress of a soil sample for a given flow velocity of water (Briaud et al. 1999). The EFA has been used extensively in research. For example, Samuel et al. (2003) conducted EFA tests for soil samples collected from 20 bridge sites in Alabama to determine soil erodibility. Similarly, an EFA was used to characterize the erodibility of cohesive soils at bridge sites in Maryland, South Dakota, and Illinois (Brubaker et al. 2004; Larsen et al. 2010; Straub and Over 2010). Bernhardt et al. (2011) investigated the erodibility of field-retrieved soil samples from levees in an EFA. More recently, Karim and Tucker-Kulesza (2018) developed a relationship between *in situ* electrical resistivity and soil erodibility measured in an EFA.

In an EFA test, water flows at different velocities in a rectangular pipe with the cross-sectional dimensions of 101.6 mm x 50.8 mm and a length of 1.22 m. The apparatus is equipped with a pump to drive flow through the test section and back to the water reservoir located at the rear end. An ASTM standard Shelby tube containing the soil sample is mounted over a motor-controlled piston. The top of the Shelby tube is inserted into a circular opening in the test section and kept flush with the flume's bottom. A piston is pushed upward to extrude the sample from the Shelby tube and keep the top of the sample at the same level with the bottom of the flume as erosion occurs during testing. The distance traveled by the piston (amount of soil eroded) is recorded during testing. In addition to a flow meter, a thermometer is fixed downstream from the test section to measure the flow rate and temperature of the water in the flume, respectively. Circular PVC pipes are used to guide the flow from the reservoir to the test section and back to the reservoir. A standard erosion test is run on a sample at six different velocities. Each velocity

circulates for one hour. Typically, a velocity of 1 m/s is conducted first, and the procedure is repeated for velocities 2, 3, 4, 5, and 6 m/s. A photograph of KSU-EFA is given in Figure 2.9.

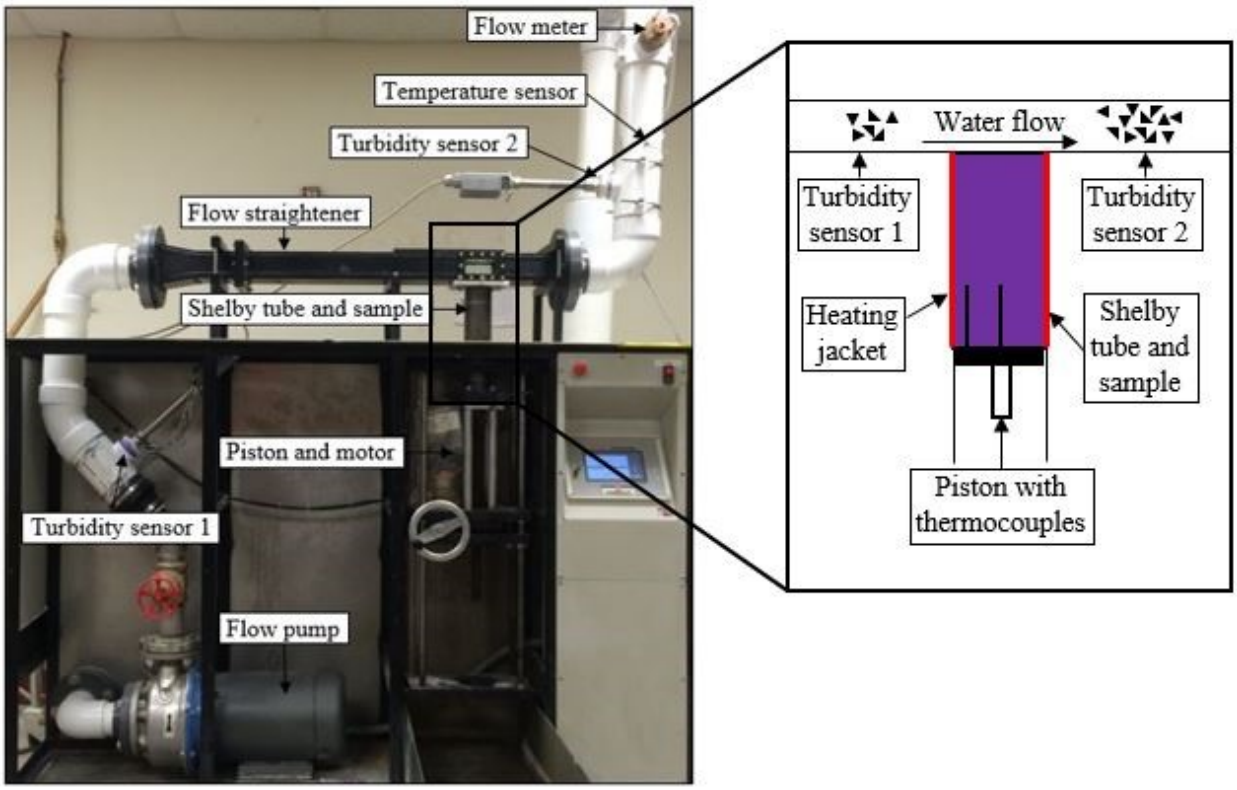

Figure 2.9 Erosion function apparatus – Kansas State University

The objective of an EFA test is to obtain the plot of erosion rate, $\dot{z}$ (mm/hr), versus hydraulic shear stress, τ (Pa). The erosion rate at each velocity in erosion test is calculated as

$$\dot{z} = \frac{h}{t} \qquad \textbf{Equation 2.3}$$

where h is the length of soil sample eroded and t is the duration of the test. The hydraulic shear stress is computed as

$$\tau = \frac{1}{8} f \rho v^2 \qquad \textbf{Equation 2.4}$$

where ρ is the mass density of the water, v is the flow velocity in the test, and f is the friction factor obtained from the Moody chart (Moody 1944). The friction factor is a function of the Reynolds number, R and the pipe roughness ε / D. The Reynolds can be obtained by

$$R = \frac{vD}{\nu} \qquad \textbf{Equation 2.5}$$

where D is the pipe diameter and ν is the kinematic viscosity of water. Briaud et al. (2001) stated that the roughness, ε can be assumed as $D_{50} / 2$, where D_{50} is the mean particle diameter for the soil. This relationship is likely valid for coarse grained soil. For cohesive soil, the surface roughness is measured using calipers (a hand measurement). The results using the HEC-18 methodology, presented as erosion rate versus velocity and erosion rate versus shear stress, are shown in Chapter 3. A disadvantage of a traditional EFA test is that it remains operator dependent. Therefore, there was a need to develop a new non-contact roughness measurement method that was not user dependent and could accurately measure surface roughness while being cost effective. The photogrammetry technique was investigated as a solution to this problem in this research.

2.3 Photogrammetric techniques

In soil erosion testing, as well as in numerical or physical soil erosion models, soil surface roughness is an important parameter used to obtain the hydraulic shear stress. According to Thomsen et al. (2015), soil surface roughness was defined as the anomalies of the soil surface, and it was recognized that it was difficult to quantify. Currently, hand calipers or point gages are the common way to measure the surface roughness depending on the need of application. Calipers was used for small-scale roughness measurements (such as in an EFA test), while point gages were used to measure roughness in large scale tests or *in situ* in agriculture. For example, Karim and Tucker-Kulesza (2018) obtained the soil surface roughness in EFA tests by using hand calipers. They measured ten points where the soil surface elevation changed from a predefined horizontal

plane (the Shelby tube plane). Lanca et al. (2013), Simon et al. (2007), and Ballio and Radice (2013) used point gages to measure the depth of scour hole to an accuracy of ± 1 mm in a flume test. The method above is very simple, inexpensive, and easy to use; however, it is user dependent. The selected points that are measured and the number of points measured for each sample can be highly subjective.

Other methods to quantify surface roughness are using echo sounder or laser sensors. They were employed in the laboratory and in the field by previous researchers (Coleman et al. 2003; Sheppard and Miller 2006; Stahlmann and Schlurmann 2010; Porter et al. 2014; Isakson and Chotiros 2015). The advantages of these methods are fast results and removing operator dependency. On the other hand, these devices require a large capital investment and special operator skills. Similarly, Poon and Bhushan (1995) utilized a stylus profiler (SP), atomic force microscope (AFM), and non-contact optical profiler (NOP) to measure surface roughness of a glass-ceramic disk substrate in comparison between the three techniques. The authors concluded that the AFM was the most suitable for surface measurement on glass-ceramic substrate. The SP required a small stylus tip radius to get the precise measurement, while the NOP was not suitable for measurement if the lens had magnification lower than 40. These techniques were simple and suitable for small scale tests; however, they are not an appropriate method for soft material like soils because the surface can be easily damaged during measurement. Moreover, the equipment for these methods are costly and highly specialized.

Each of the methods mentioned above is either user dependent or expensive. Recently, researchers have used the photogrammetric techniques across many fields for measuring physical quantities, including the deformation, position, and shape of an object (Derenyi 1982; Luhmann et al. 2007). The advantages of the photogrammetric technique are that it is a non-contact method,

data processing is automated, and it provides quick results. In the photogrammetric technique, common points of two or more images of an object taken from different positions are identified. The 3D coordinates of these common points are then computed using the triangulation method based on the derived camera location. Ultimately, the shape of a 3D object can be reconstructed. This method has been applied in material and structural testing (Whiteman et al. 2002; Maas and Hampel 2006), architecture (Liu and Kang 2014; Alexandru 2016), geology (Fischer at el. 2006; Bemis et al. 2014), aerospace (Liu et al. 2012), transportation (Cooner and Balke 2000), and in agriculture (Alarcon and Sassenrath 2011).

For example, Alarcon and Sassenrath (2011) conducted a study using the photogrammetric technique to develop a geometrically accurate model of cotton crop canopy. This model was adequately capturing the three-dimensional structure of the leaves and the changes in leaf shape and size over the growing season. In the model, each leaf position was determined by using two points: leaf origin (the point of intersection of the surface of the leaf with its leafstalk) and central lobe tip (the outermost point of the leaf). Five benchmark points were set up within the cotton crop rows and a vertical photograph of the crop canopy were then taken. The location of the camera was known by using at least three benchmark points. Once the position of the camera is known, the location of the other points in the picture is possible to obtain. The model in this study is a useful tool for developing a realistic crop canopy. It could also be used to investigate the insect distribution, and the spreading of insecticides and pesticides within the canopy.

Similarly, photogrammetry was used in a study by Cooner and Balke (2000) for investigation of traffic incident scenes. In order to process an incident scene, several photos of an incident scene or an object were taken. These photos were then input into the software (PhotoModeler). The points of interest were marked in each photo. The software then combined

the photos and located the marked features in three dimensions. The marks became accurately measured points and a 3-D model of an accident were reconstructed. The use of photogrammetry for incident management application is cost effective and it is a time saving tool to process an incident scene.

Based on an extensive literature review, no previous studies have used photogrammetric techniques, or precisely stereo-photogrammetry, for soil surface roughness measurements. Therefore, the first goal in this research was to develop a stereo-photogrammetry method that can accurately measure surface roughness, while being cost effective and not operator dependent. The method was then validated by taking the roughness measurement of a manufactured object and compared the results with a structured light scanner. Details about the method are described in Chapter 3.

2.4 Turbidity sensors

The K-State EFA was also modified with two turbidity sensors, installed before and after the soil sample in the EFA to measure the soil particles concentration during erosion testing (Figure 2.9). The purpose of installing the turbidity sensors is to provide a secondary measurement of erosion, particularly for low erodibility samples where determining measurable erosion is difficult. Turbidity is an optical measurement commonly used in water quality studies that measure the scattering of light in a liquid due to suspended materials, measured in nephelometric turbidity units (NTU). Several researchers have used turbidity sensors to obtain particle concentration in their erosion devices (Schaaff et al. 2006; Ravens 2007; Debnath et al. 2007; Benahmed and Bonelli 2012; Haghighi et al. 2013). For example, Schaaff et al. (2006) installed a turbidity sensor at the bottom downstream of the test section of the recirculating flume to measure resuspended particulate matter (SPM). Two water samples were collected every 3 minutes and were then filtered to quantify

the SPM and to calibrate the turbidity sensor. Based on the SPM, the critical shear stress and erosion rate were estimated.

Ravens (2007) used a turbidimeter during FLUME *in situ* testing to obtain particle concentration. The particle concentration was obtained based on turbidity measurements and a calibration curve. The calibration curve was based on the total suspended solids measurements of water samples taken during the test; therefore, it is dependent on soil types. The turbidity was recorded every 15 seconds. The plot of turbidity (NTU) versus time (min) allowed the researchers to identify when erosion occurred.

Debnath et al. (2007) used two turbidity sensors on a flume *in situ* testing device to monitor the water turbidity in the test. One sensor was mounted at the entrance of the test section to observe background conditions, while the other was located at the downstream of the channel. Turbidity readings were calibrated against suspended sediment concentration for each experiment independently by taking at least six in-situ water samples near the sampling locations. The resuspension rate was then estimated from the turbidity reading and it was used for calculating the bed-load component of erosion in the flume in-situ testing.

Benahmed and Bonelli (2012) used a turbidity sensor to study the effects of dry density, water content, degree of saturation, and clay content on cohesive soils susceptible to internal erosion via a HET. A similar study was conducted by Haghighi et al. (2013). The author utilized the turbidimeter, which was placed after the exit chamber in the HET to measure the turbidity of the fluid flowing from sample. The measured turbidity was proportional to the concentration of soil. Based on the mass of soil eroded in the erosion test, the coefficient of the measured turbidity was estimated, and it was further used to calculate the shear stress and erosion rate for the sample.

Chapter 3 - Methodology

3.1 Overview

The primary objective of this study was to instrument the K-State Erosion Function Apparatus (EFA), so detailed experiments can be conducted to improve the understanding of fine-grained soil (cohesive soil) erosion mechanisms. The EFA can be used to study many erosion issues including: scour at bridges, sheet flow over levees, and agricultural surface erosion problems. More accurately determining the erodibility of soil will allow future researchers to study the parameters that affect soil erosion. Systematically controlling individual soil properties will provide a deeper understanding of mechanisms of the cohesive soil erosion; this is needed for improving existing soil erosion models that are typically over conservative. This chapter includes the research methodology for this study, focusing on laboratory work. The first phase of this study was the instrumentation of the EFA. The next phase was the evaluation of the instrumentation. The findings from these two phases were used to develop a new erosion characterization methodology for fine-grained soils. The overall methodology is shown in the flow chart below:

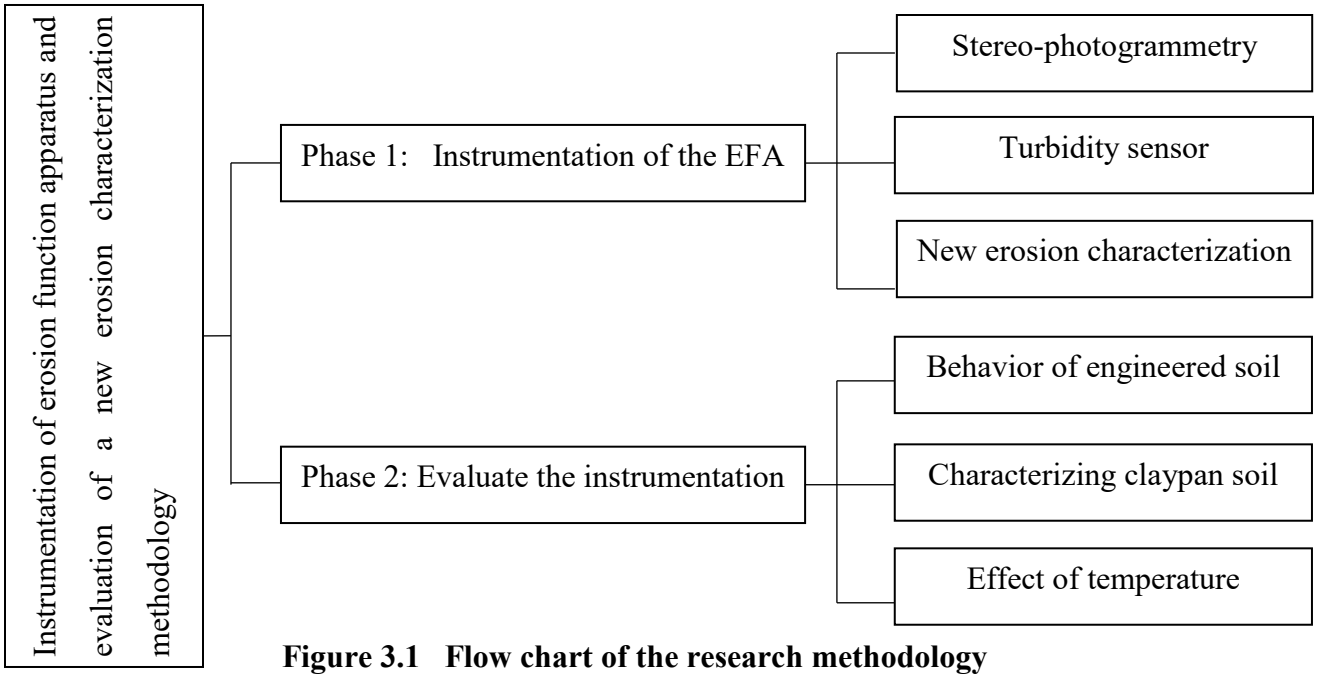

Figure 3.1 Flow chart of the research methodology

3.2 Stereo-photogrammetry technique

There are currently no prescribed methods for determining the surface roughness in soil erosion tests, even though it is an important parameter in numerical and physical geotechnical soil models. Different researchers have their own ways to measure this parameter; however, these methods are operator dependent, not applicable to small-scale experiments, or cannot be used for very soft soil. Some of the methods also required highly specialized equipment, making them cost prohibitive. Photogrammetric techniques are used across many fields but have not been used for soil surface roughness measurements based on an extensive literature review. This section describes the developed photogrammetric technique for soil, specifically stereo-photogrammetry (Tran et al. 2017).

The stereo-photogrammetry system in this project consisted of a 24.2-megapixel Nikon D5300 digital SLR camera with an 18–55-mm lens (a 30-mm lens was used in this study), a checkerboard pattern, and MATLAB R2015a (The MathWorks Inc., Natick, MA, 2000). The photogrammetric technique comprised of two basic steps: camera calibration and reconstruction of the 3D image of the soil surface following the erosion test. Camera calibration was used to estimate the camera parameters using multiple images of a special calibration pattern, the checkerboard (MathWorks, 2015). The checkerboard must not be square. One side of the checkerboard contained an even number of squares and the other side contained an odd number of squares. This allowed the MATLAB camera calibrator app to determine the orientation of the checkerboard. The longer side of the pattern was the x-direction. At first, the pattern was placed on a flat surface to ensure the accuracy of the calibration. At least ten images of the checkerboard pattern were taken. In this study, total of 93 images were used to estimate camera parameters. These images were captured at different orientations. The distance from the camera to the

checkerboard was roughly equal to the distance from the camera to the surface of the soil sample in the actual EFA test. Note that, these photos were taken in the camera's manual mode without changing any settings between images and always keeping the checkerboard pattern in focus. Focal length is the distance from the sensor to the rear of the lens. The f-stop (the ratio of the focal length to the diameter of the aperture) was set to f/29 and the shutter speed (the length of time that the camera's shutter is open) was 3/10 second. This setting allowed to get the picture in focus when photos were taken throughout this study. The optimal distance and angle between the camera and soil samples were determined by taking a photo and then systematically increasing the distance from the sample by 5 mm and/ or increasing the height of the camera to change the angle by one degree until the highest number of points detected by the camera were obtained. This process continued until the photo quality degraded resulting in fewer points. The optimal distance from the center of the camera lens to the center of the soil sample was found to be 140 mm and the angle between the camera and the sample was 28°. Figure 3.2 shows the schematic of the experimental setup when photo of surface soil sample was taken.

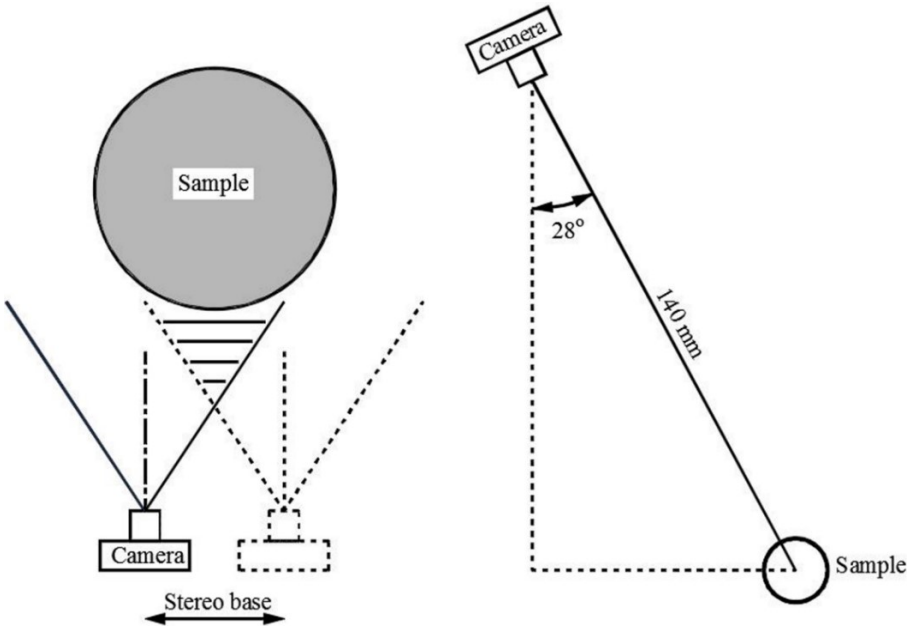

Figure 3.2 Schematic of the experimental setup (Tran et al. 2017)

Photos of the checkerboard were processed in the camera calibrator app in MATLAB to estimate camera intrinsic, extrinsic, and lens distortion parameters. The intrinsic parameters include the focal length, the principal point, and the skew coefficient. The extrinsic parameters consist of a rotation and translation which are used to define the location and orientation of the camera. These parameters were used for the next step (reconstructing the 3D image of the sample surface). Figure 3.3 a shows the image of the checkerboard pattern where the green circles were the measured points, the red square was the checkerboard origin and the plus sign inside the squares were the projected points. The bar graph of the mean reprojection error per image along with the overall mean error after calibration is shown in Figure 3.3 b. The reprojection errors are the distances, in pixels, between the points detected from the image and the reprojected points as shown in Figure 3.3 c. These errors were calculated automatically by the program. In this study, the overall mean error was found to be 1.97 pixels. The resolution of each image was 4,000 by 6,000 pixels. Therefore, the reprojection error was less than 0.05 % or an error of 0.04 mm for the surface roughness measurement (calipers typically used in EFA testing have accuracy of 0.2 mm). After the camera was calibrated, the camera parameters including the focal length and principal point were obtained from the calibration program. These parameters were needed for reconstructing the 3D image of the sample surface.

A custom computational program was developed in MATLAB 2015 that can reconstruct the 3D image of the soil sample's surface following an EFA test with two images of the sample's surface. The code followed the same procedure as described in Hartley and Zisserman (2004). First, a set of feature points in both images were detected and extracted with the aid of the Computer Vision System Toolbox in MATLAB. Next, the two sets of feature points were compared to identify common points in the two images. Random sample consensus (RANSAC)

was used to determine the fundamental matrix by locating the matching points in the two images from the previous step. It is an algorithm that identifies the outliers in a data set and also be used for determining the depth of objects in stereo vision.

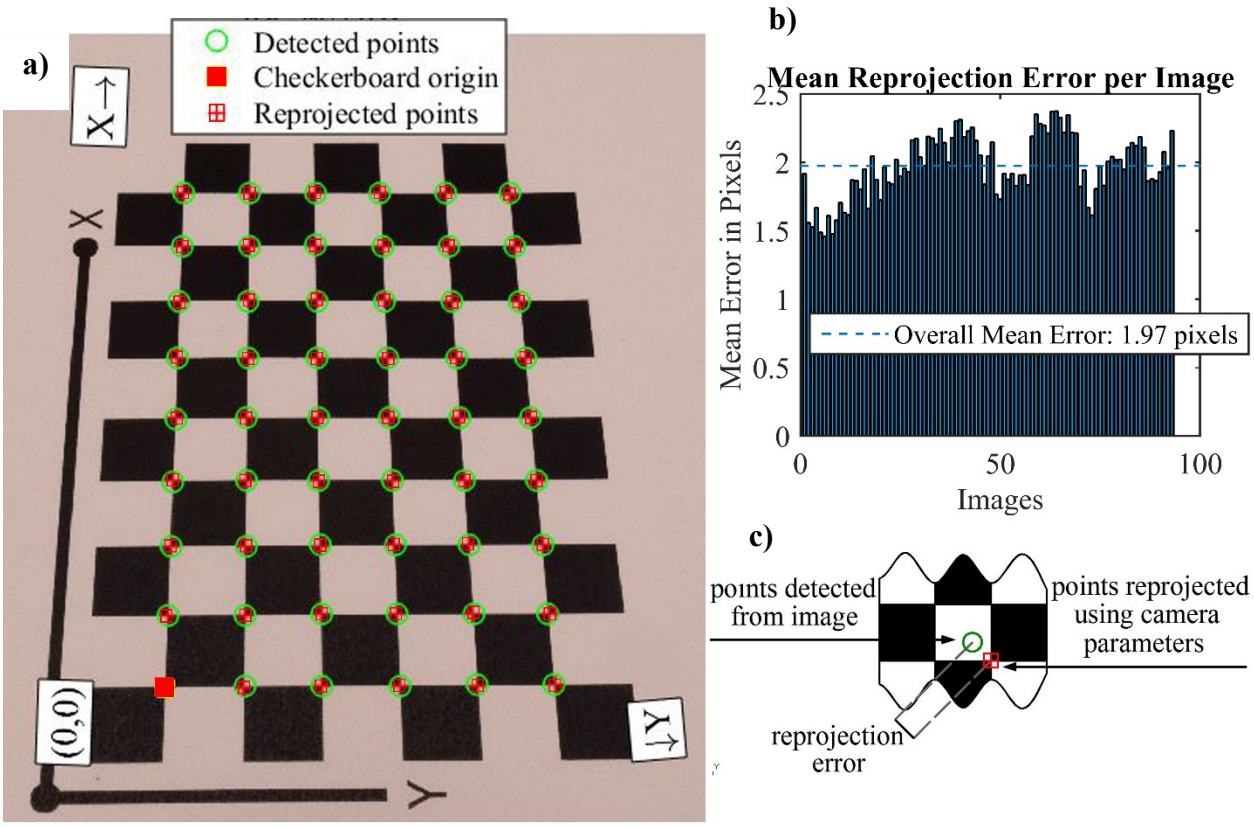

Figure 3.3 a) Checkerboard pattern; b) mean reprojection error per image; c) reprojection error (Tran et al. 2017)

The camera calibration matrix was obtained based on the camera parameters (determined from the calibration step previously described). Then, the essential matrix (the 3 by 3 matrix that relates corresponding points in stereo images) was computed, which was the product of the inverse camera calibration matrix, the fundamental matrix, and the camera calibration matrix. The camera matrix (used to project 3D world points in homogeneous coordinates into an image) was found corresponding to a given essential matrix. After obtaining the corrected camera matrix, the 3D coordinates of the corresponding points (i.e., point clouds) were calculated using triangulation.

Triangulation is the process of determining the location of a point by forming triangles to it from known points. At the end, the 3D plot of these point clouds was created, and the image of sample surface was constructed. These point clouds were then used to calculate the surface roughness for each of the samples.

To validate the new method, a 3D printed red disk (Figure 3.4) was created to measure the surface roughness because it would provide a standardized object to compare measurement techniques. The red color was chosen because it was similar to natural soil colors and would simulate the difficulty of a dark, uniform color on identifying common points. The results were compared with measurements made using calipers, the stereo-photogrammetric technique, and a structured light scanner. Structured light scanners typically consist of a projector and two cameras. The cameras are used to capture images of patterns cast across a 3D object; then the object can be reconstructed into a 3D model based on the distortion of the patterns. The scanner used in this project was a Geomagic Capture system by 3D Systems, Inc. A calibrated turntable was used to aid in orienting multiple scans of the disk. The 3D object was reconstructed using the scanner software. Point clouds was generated and exported to AutoCAD software to obtain the 3D point coordinates. Figure 3.4 shows the photograph of the 3D printed red disk (a), 3D model of the disk surface (b), and the point clouds obtained using the structured light scanner (c). The resolution of the structured light scanner is much higher than the photogrammetry method. A high-density point cloud comprised of 720,389 total points was originally obtained. Two additional point clouds were created by reducing the number of points randomly to 2,166 and 1,027 using the structured light scanner, which were similar to the number of points obtained through the photogrammetry technique. This helped to understand the influence of the number of points on the roughness measurement and also to verify that the number of points obtained by

photogrammetry would yield accurate results. These point coordinates were then imported into MATLAB and a measurement of roughness was made. The results of the validation of the stereo-photogrammetry method for measuring soil roughness in EFA testing are presented in Chapter 4- Results and Analysis and in Tran et al. (2017).

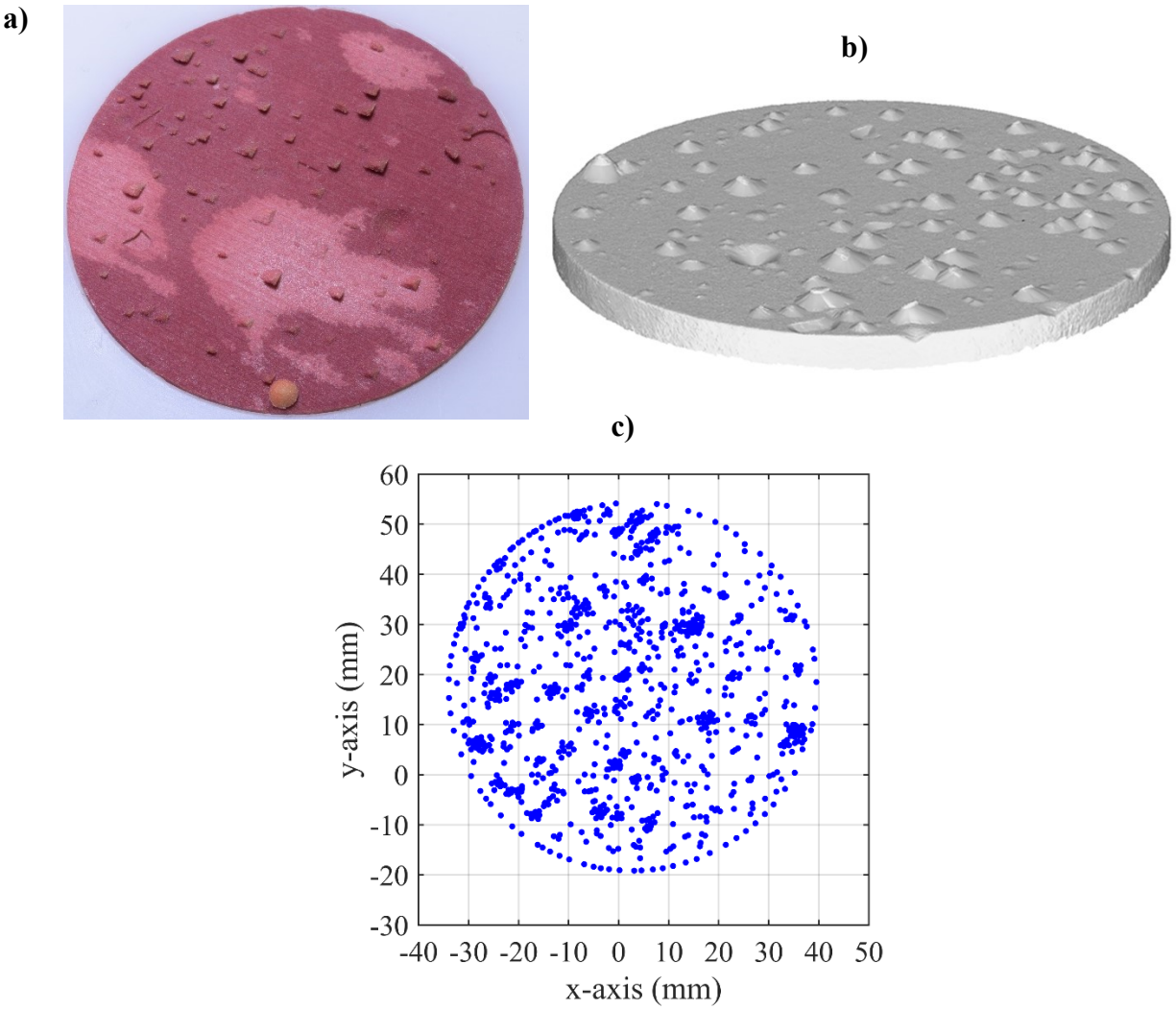

Figure 3.4 a) 3D printed red disk; b) 3D model using structured light scanner; c) 2D image of the surface sample

3.3 Turbidity sensor

The main goal of implementing the turbidity sensor in the EFA was to create a secondary measurement of erosion by measuring the turbidity of water as erosion took place. Moreover,

developing the relationship between turbidity and the amount of soil eroded in erosion testing was used to investigate the erodibility of highly resistant samples. A Confab Instrumentation Turbidimeter (Model 850I) was used in this project. The turbidimeter consisted of a sensor and a panel/wall mount enclosure that display the readings. It has four ranges from 0–2 NTU to 0–2000 NTU. The unit of turbidity is called the Nephelometric Turbidity Units (NTU) which is the amount of light that reflects for a given amount of particles and is dependent upon the shape, color, and reflectivity of these particles. Two turbidity sensors were installed in the plastic pipe, one upstream and one downstream of the sample, in the EFA to obtain the particle concentration coming before and after erosion of the sample. In order to block the wavelength of light that the sensor uses from getting into the white plastic pipe and to eliminate outside light from getting through, metallic tape was used to wrap the pipe up to 0.3 m upstream and downstream of each sensor. A National Instrument data acquisition system, NI 9203, was used and LabView 2015 was used to record the turbidity measurements with time. The distance between the two sensors was approximately 2.15 m. The minimum sampling rates were chosen depending on the flow velocity and the phase shift between the two sensors in the erosion tests as shown in Table 3.1. Note that at high water flow velocities such as 5 and 6 m/s, the turbidity measurements were affected by bubbles in the flume; therefore, the turbidity data were not collected at these velocities.

Table 3.1 Sampling rate of turbidity measurements at different water velocity

Velocity (m/s)	Phase shift (s)	Minimum sampling rate (samples/s)
1	2.15	20
2	1.075	40
3	0.717	60
4	0.538	80
5	0.430	100
6	0.358	120

The turbidity measurement is sensitive to small changes in particle concentration and air bubbles in the water flow, thus the output of the sensor needed to be filtered (Lambrou et al. 2009). Gaussian filter was implemented so trends in the output signal could be more clearly observed by removing data outliers. Gaussian filtering was more effective at smoothing the data. Thus, it was used in this study to get the final result for turbidity measurements.

3.4 Soil erosion test

In this research, the goal of the erosion test was to find the critical shear stress, so the instrumentation could be quantitatively validated. Critical shear stress is the applied hydraulic stress required to initiate erosion (Bernhardt et al. 2011) and a higher critical shear stress indicates that a soil is more resistant to erosion. Critical shear stress is obtained from the erosion plot which includes the erosion rate (mm/hr) versus shear stress (Pa). All erosion tests were run using cold tap water because the temperature of water effects soil erosion (Larionov et al. 2014; Zreik et al. 1998; Tran et al. in review). Water temperature was maintained at constant value (15±2°C) for all tests by continuously filling and sum-pumping the reservoir with cold or hot water from a connected water line. The soil sample was run at room temperature (18±1°C) except where the effects of soil temperature were explored.

3.4.1 Soil sample preparation

Soil samples for erosion testing in this research included both laboratory reconstituted and field-retrieved soil. Samples from the field were directly brought to the humidity-controlled room after drilling to ensure soil samples did not lose the moisture. All remolded samples in this research were prepared using manufactured kaolin clay and sand (d_{50} = 0.24 mm) at a target water content depending on the requirements of each project. The mixture was selected so samples would be cohesive but also erode at low water velocities (e.g., 1 m/s flow). All physical soil properties (i.e.,

density, particle size, water content) were kept constant throughout the study. Samples were initially mixed for ten minutes with a mixer fit with a paddle blade and allowed to rest in a humidity room for a minimum of 24 hours in sealed containers. The mixture was then further mixed in a clay pugger mixer for five minutes while the vacuum was running under the pressure of 25 psi; and then extruded directly into a 76.2 mm outside diameter Shelby tube. The clay pugger mixer was used following the recommendation of Shan et al. (2015) to reduce the amount of slaking (loss of soil when immersed in water) in erosion testing of benchmark samples. Samples were then kept in a moisture room until EFA testing.

3.4.2 Test description

Each sample was tested under four or six different velocities in the EFA depending on the sample type and project objectives. The range of velocities was typically from 1.0 to 6.0 m/s, in 1 m/s increments. Each sample was brought from the moisture room right before the test to ensure that the test was run at the target or in-situ moisture content. The moisture content was measured before the test according to ASTM standard D2216 (ASTM 2010a). The 0.38 m long Shelby tube containing the soil sample was placed on the platform of the EFA. The bottom of the Shelby tube was tightened with a bracket attached to the platform. This ensured that when the piston was pushed upward in order to extrude the soil sample for trimming before the test or when the soil eroded during testing, only the soil was moved (as opposed to the whole tube). After trimming the top of the soil sample, the top of the Shelby tube was inserted into the opening of the flume by lifting the platform with the help of a crank wheel. The top of the soil sample was kept at the same level with the bottom of the flume. The 0.5 m/s flow velocity was chosen to initiate the water flow first by pressing the flow button on the interactive LCD screen and then increased to 1 m/s for the first velocity. During testing, the water temperature and flow velocity were measured (by the

temperature sensor and flow meter attached in the EFA), monitored and recorded continuously on the LCD screen. When soil eroded, the piston was pushed upward (by pressing the push button on the LCD) to extrude the soil sample and maintain its position flush with the bottom of the flume. The amount of pushing was recorded and displayed on the LCD screen. It was used to calculate the erosion rate of the soil sample. Normally, each velocity was conducted for 60 minutes. However, the EFA was set to run within 50 minutes for each velocity in this research due to the EFA factory setting. Figure 3.5 shows the surface soil sample before and after EFA testing.

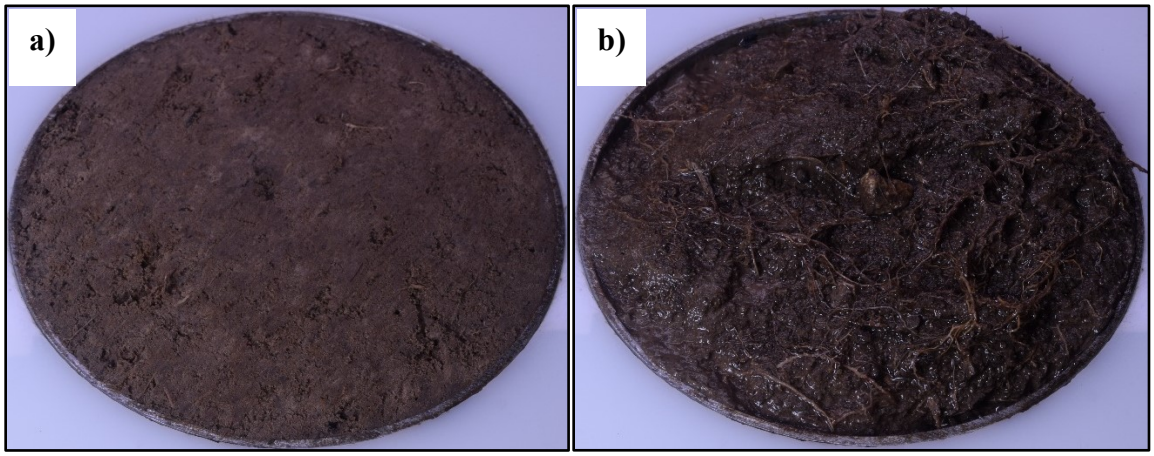

Figure 3.5 a) Surface soil sample before the test; b) Surface soil sample after the test

After the EFA test was done, two photos of the soil surface were taken and then processed with the custom photogrammetry computational program as described earlier to quantify the surface roughness for determining the applied hydraulic shear stress. Before starting the test for the next velocity, the top of the soil sample was trimmed again so that the soil sample was flush with the bottom of the flume. The above process was repeated for other water flow velocities.

3.4.3 Calculating shear stress

The hydraulic shear stress, τ was computed with the $\tau = \frac{1}{8} f \rho v^2$ Equation 2.4 shown in Chapter 2. The friction factor, f was obtained from the Moody chart (Figure 3.6) and it is a

function of the Reynolds number, R and the pipe roughness ε / D. The Reynolds number can be obtained by using $R = \frac{vD}{\nu}$ Equation 2.5. The relative roughness, ε / D is the ratio of the average height of the roughness elements on the pipe surface over the pipe diameter. In the EFA, the pipe has a rectangular cross section; therefore, D is taken as

$$D = 2\frac{ab}{a+b} \qquad \textbf{Equation 3.1}$$

where a and b are the sides dimension of the rectangle pipe.

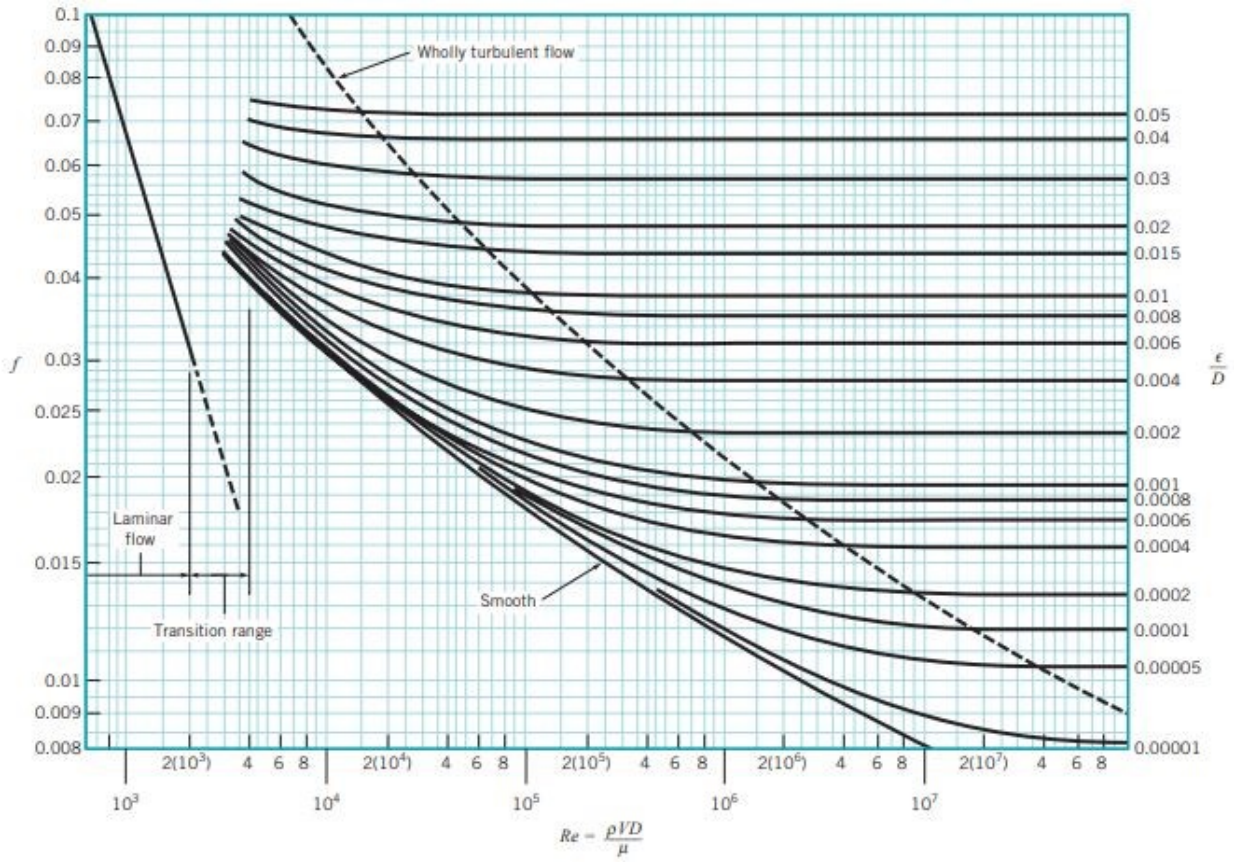

Figure 3.6 Moody chart (Munson et al. 1990)

The surface roughness, ε, was measured using calipers (hand measurement) and using photogrammetry technique in this research. For the hand measurement method, the soil surface roughness following each flow velocity was calculated as

$$\varepsilon = \frac{\sum_{i=1}^{n} A_i h_i}{A} \qquad \textbf{Equation 3.2}$$

where A is the cross-sectional area of the sample; h_i and A_i are the height and corresponding area of the i th roughness element measured by the caliper; n is the total number of roughness elements. In the stereo-photogrammetry technique, the soil surface roughness was taken as the root mean squared (RMS) average roughness, R_q

$$R_q = \sqrt{\frac{1}{N}\sum_{i=1}^{n}(z_i - \bar{z})^2} \qquad \textbf{Equation 3.3}$$

where N is the number of measured points; z_i is the absolute distance of all vertical lines from the mean line (top of Shelby tube); $\bar{z}$ is the arithmetic average height such that

$$\bar{z} = \frac{1}{N}\sum_{i=1}^{n} z_i \qquad \textbf{Equation 3.4}$$

The hydraulic shear stress results from the two methods were compared together, results are presented in Chapter 4 – Results and Analysis.

3.5 Effects of temperature on erodibility of soils

Samples used in the temperature effects project were remolded samples, using 50% manufactured kaolin clay and 50% sand (d_{50} = 0.24 mm) at a water content of 23%. The samples classified as lean clay (CL) according to the Unified Soil Classification System. All samples were prepared using clay pugger mixer as previously described. The effects of temperature on erodibility of soils were conducted in two separate experiments in order to investigate whether water or soil temperatures alone, or whether a compounding effect of both parameters, resulted in increased erosion rates as described in the literature (Larionov et al. 2014; Zreik et al. 1998). Six samples were used to investigate the effects of water temperature on soil erodibility. Target water temperatures were 17ºC, 28ºC, and 36ºC and each temperature was tested twice. The control

temperature of 17ºC corresponded to the default external water line temperature. The 36ºC was the maximum temperature from the water line and also a measured maximum water temperature noted from USGS databases (e.g., Arkansas River near Coolidge, KS – http://waterdata.usgs.gov). The third target of 28ºC was selected as the midpoint in the temperature range. The water contents of each prepared sample were measured prior to and following each EFA test to ensure sample consistency. The EFA tests for this experiment followed the procedure mentioned above.

Eight more remolded soil samples were tested at various soil temperatures at the same water temperature of 17ºC to examine whether soil temperatures alone effects soil erodibility. During increased water temperature tests, the temperature of the soil also increased; therefore, the target soil temperatures were 19ºC, 25ºC, 30ºC, and 35ºC to match the measured increase during the first tests. In order to increase and control the soil temperatures in this experiment, a custom heating system (i.e., heating jacket, a plastic piston head equipped with two thermocouple probes, a temperature controller, and a data acquisition system) was integrated into the EFA, as shown in Figure 3.7. A 250-W heating jacket (BriskHeat, #GBH0250) was wrapped around the 76.2 mm outside diameter Shelby tube to heat the soil sample. Two thermocouple probes (Omega, TMQSS-062U-2) were attached to a custom plastic piston head to monitor the internal soil temperature at 11 and 27 mm from the piston centerline. The thermocouples were calibrated in a constant temperature bath against a reference thermometer (Omega, HH41) with an accuracy of ±0.05°C. A BriskHeat temperature controller model X2-120JT regulated the heating jacket temperature to a set value, and soil temperatures up to 35°C were measured. A data acquisition system (National Instruments, cDAQ-9174) and LabVIEW 2015 were used to record and monitor soil temperatures. Samples were heated from room temperature to the desired temperature. Steady state soil temperatures were reached in 25 to 45 minutes. Subsequent erosion testing commenced once the

soil temperature was at steady state. The soil temperature was maintained during erosion testing with the heating system. The water temperature was maintained at the ambient laboratory water temperature (17ºC) by adding cold or hot water to the reservoir.

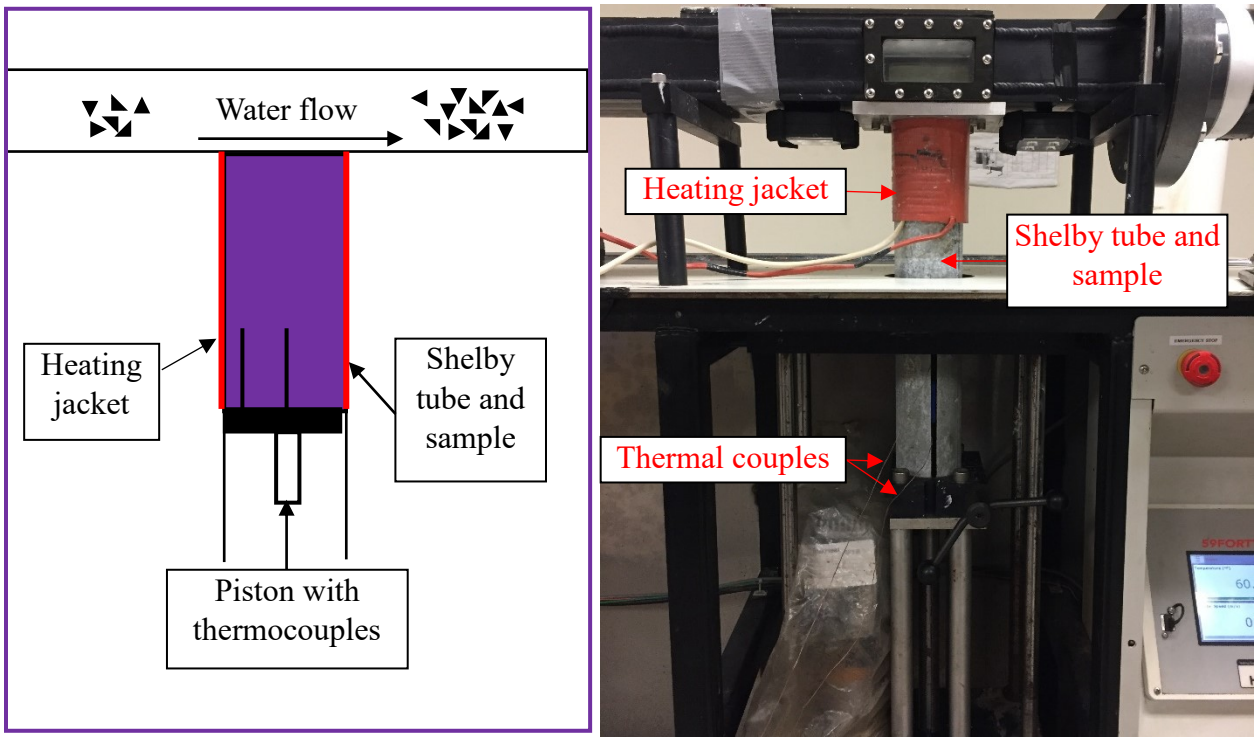

Figure 3.7 a) Schematic of the heating system; b) Photograph of the heating system

3.6 Evaluating the enhanced erosion resistance of engineered soil

In the engineered soils project, both treated and untreated engineered soil samples were used to evaluate the enhanced erosion resistance. Ottawa graded silica sand was used for untreated samples and samples were air pluviated directly into the Shelby tubes before the EFA testing. The treated samples were strengthened with microbially-induced carbonate precipitation (MICP). The MICP samples were a mixture of Ottawa graded silica sand and a solution. The cementation solution for MICP was a water solution of polyvinyl alcohol (Wang et al. 2018). All samples were made at the Department of Civil Engineering, University of Akron and mailed to Kansas State

University for the EFA testing. The treated specimens were originally a rectangular shape and then were reshaped into cylindrical samples with a diameter of 76.2 mm outside diameter and a height of about 50 mm. Each sample was then attached to a plastic piston head using three small prongs. The piston and sample were inserted into a 76.2 mm outside diameter Shelby tube for EFA testing. Figure 3.8 shows the original MICP sample (at University of Akron) and the one after reshaping for the EFA testing at KSU.

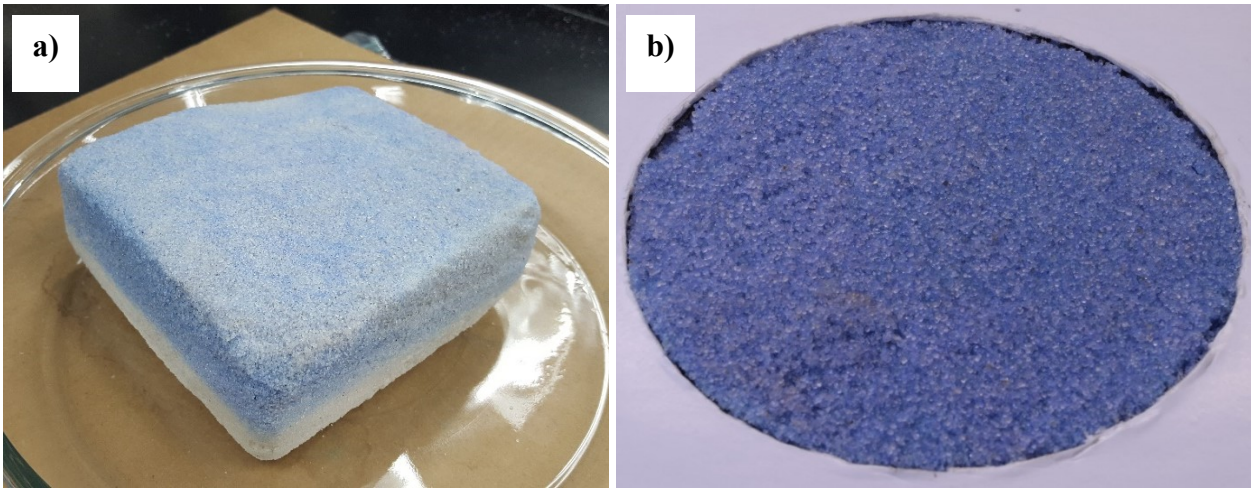

Figure 3.8 a) Soil crust formed by polymer-modified MICP approach; b) Treated sample flush with the top of the Shelby tube before testing in the EFA

Small gaps between the sample and the Shelby tube (less than 1 mm, as shown in Figure 3.8 b) were assumed to be negligible when comparing the applied shear stress between the treated and untreated samples. Furthermore, these gaps increase the turbulence across the sample and thus increase the applied shear stress. Assuming a negligible impact was, therefore, conservative and appropriate for the experiments.

3.7 Summary

This research includes two phases: instrumentation of the EFA and evaluating the instrumentation. Phase 1 included creating a custom stereo-photogrammetry computational

program that measures the surface roughness of the soil samples more accurately in erosion tests; developing the relationship between turbidity and the amount of soil eroded in erosion testing; and creating a new erosion characterization methodology using instrumentation of the EFA. Phase 2 included the investigation of the effects of water and soil temperatures on the erodibility of reconstituted and field-retrieved soil and the evaluation of the enhanced erosion resistance of engineered soil. The major difficulties experienced to carry out the research are described below.

In the stereo-photogrammetry method, two photos of surface sample have to be taken after the erosion test. Finding the two best quality pictures sometime takes time and they need to be loaded into the custom computational program to check whether they will work before doing the next EFA velocity test. Therefore, although this improves the accuracy of the shear stress calculations it increases the time it takes to conduct an EFA test.

The two thermocouple probes were installed into the plastic piston head for the investigation of temperature effect on soil erodibility. The piston head (with the thermocouple probes) was attached to the bottom of the Shelby tube in order to extrude the sample. The piston head must be twisted to attach it to the threaded rod of the step up motor, therefore special care was taken so that the thermocouple probes did not break or disturb the sample.

Chapter 4 - Results and Analysis

This chapter includes the results of the stereo-photogrammetry technique and erosion tests performed in the EFA. Turbidity measurements using turbidity sensors are also presented. Erosion tests are shown as erosion rate with respect to hydraulic shear stress applied by the flowing water and plotted according to the Hydraulic Engineering Circular (HEC) – 18 (Arneson et al. 2012). The HEC–18 is used by engineers to evaluate the erosion potential of soils for transportation infrastructure, such as accounting for scour in bridge design. The effective hydraulic shear stress was obtained using the custom computational program and hand measurements (caliper) so their results could be compared for validation of the new methodology. Moreover, a new erosion characterization was developed using the instrumentation. In the analysis section, the effect of temperature on soil erosion are discussed to improve the understanding of how temperature affects the erodibility of soil. Additionally, the using of engineered soils as a way to reduce projected increases in soil erosion are also described in this section.

4.1 Typical results from the stereo-photogrammetry technique

4.4.1 Validation for the new method

In EFA testing, calculated hydraulic shear stress is an important measurement in order to determine the applied critical shear stress; thus, an accurate determination of the surface roughness measurement (used to calculate shear stress) is vital. As mentioned in Chapter 3, a 3D-printed red disk was used as a standard object for measuring the surface roughness. The results obtained using the photogrammetric method were compared with results obtained using a structured light scanner and using calipers by hand. Surface roughness is typically determined in an EFA test by measuring the relative changes to the soil surface, above and below the Shelby tube plane. Calipers are commonly used to measure the heights of approximately 8-10 locations across the soil surface

after the erosion test. Various equations have been used across many different fields to quantify the surface roughness. Table 4.1 defines each of the roughness parameters as well as their equations.

Table 4.1 Roughness parameters used in various fields (after Raposo, Ferreira, and Ribeiro 2007)

Parameter	Definition
Arithmetic average roughness ($R_{\|a\|}$)	The absolute distances of all vertical lines from the mean line measured, z_i, normalized with the number of points, N $$R_{\|a\|} = \frac{1}{N}\sum_{i=1}^{N}\|z_i\|$$
Arithmetic average height ($\bar{z}$)	General description of height variations $$\bar{z} = \frac{1}{N}\sum_{i=1}^{N} z_i$$
Average roughness (R_a)	Gives the deviation in height. Different profiles can give the same R_a $$R_a = \frac{1}{N}\sum_{i=1}^{N}(z_i - \bar{z})$$
RMS roughness (R_q)	Represents the standard deviation of surface heights $$R_q = \sqrt{\frac{1}{N}\sum_{i=1}^{N}(z_i - \bar{z})^2}$$
Total roughness (R_t)	$$R_t = R_p + R_v$$
Maximum profile peak height (R_p)	Height of the highest peak above the mean line in the profile $$R_p = max(z_i - \bar{z}); 1 < i < N$$
Maximum profile valley depth (R_v)	Deep of the deepest valley below the mean line in the profile $$R_v = \left\|min(z_i - \bar{z})\right\|; 1 < i < N$$
Ten Point Height ($R_{z(iso)}$)	The difference in height between the average of the five highest peaks and the five lowest valleys along the assessment length of the profile $$R_z(iso) = \frac{1}{5}\sum_{i=1}^{5} R_{pi} + \frac{1}{5}\sum_{i=1}^{5} R_{vi}$$

All methods were compared for use in this study. Many were discarded due to the high variability or dependence on the number of points obtained from the measurement. The arithmetic average roughness was initially selected as it was similar to the calculations typically used in an

EFA test. The arithmetic average roughness was calculated as seen in Table 4.1 by summing the absolute value of the heights of each measured point and dividing by the total number of points measured (Gadelmawla et al. 2002; Yatsui et al. 2008). In this study, $R_{|a|}$ was calculated by summing the absolute value of the relative heights of all the points (represented by the vertical lines or residuals shown in Figure 4.1 c and then dividing the total by the number of points.

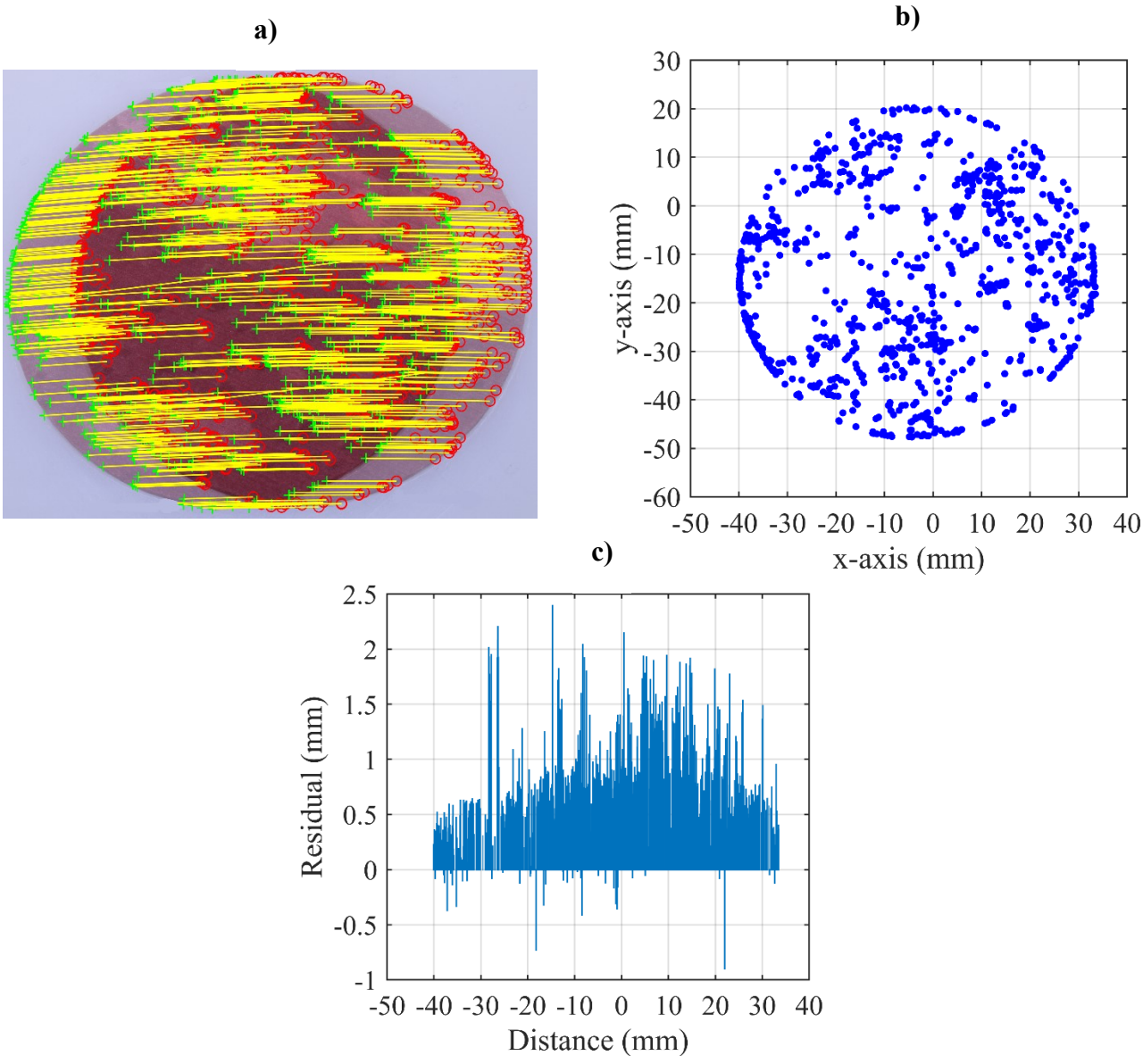

Figure 4.1 Photogrammetry verification for the 3D printed disk (Tran et al. 2017) a) matched feature points; b) 2D image of the sample; c) residuals

Table 4.2 presents the different values of absolute arithmetic roughness obtained for the red disk when different numbers of points and measurement methods were used. The roughness measurements using the structured light scanner or the photogrammetric technique would likely depend on the number of point clouds obtained; therefore, three different sets of point clouds were used for the scanner data to examine the influence of the number of points on the roughness value obtained. Two different sets of photos of the red disk were used for the photogrammetric technique to assess the repeatability of the method. The caliper method was also included to provide a comparison of the digital values with the traditional values obtained by hand. As shown in Table 4.2, the number of points used in the roughness calculations affects the roughness value obtained.

Table 4.2 Absolute arithmetic roughness, $R_{|a|}$, values obtained for the 3D printed red disk

Parameter (indicates residuals removed)	Full scan (720,389 points)	Reduced scan 1 (2,166 points)	Reduced scan 2 (1,027 points)	Photo 1 (1,624 points)	Photo 2 (971 points)	Caliper (87 points)
$R_{\|a\|}$	0.426	0.367	0.369	0.585	0.682	0.817
$R_{\|a\|}$ (0.05 mm)	0.453	0.450	0.463	0.609	0.695	0.817
$R_{\|a\|}$ (0.10 mm)	0.480	0.561	0.564	0.628	0.713	0.817
$R_{\|a\|}$ (0.20 mm)	0.542	0.632	0.649	0.677	0.744	0.817

Note that, in the traditional method (hand caliper), roughness measurements were typically taken only at locations where a peak or valley exists. However, in the photogrammetric technique as well as structured light scanner, some of the point clouds were located on the flat surface. If a large number of points on the flat surface were included in the $R_{|a|}$ calculation, the results were affected. Therefore, Table 4.2 also presented the results from an additional analysis to determine if excluding residuals below a given value would give an accurate and repeatable measure of roughness. Results in Table 4.2 clearly show that removing points below the thresholds did correct some of this skewness; however, the cutoffs values were rather arbitrary. Additionally, no

reasonable selection method or guidelines for the threshold could be determined from the literature. Therefore, it was important to examine some of the additional measures of roughness (shown in Table 4.1) and to find a measurement that would be consistent, yet also provide a reasonable estimate compared to the typical EFA measurement.

Table 4.3 presents the calculated roughness parameters listed in Table 4.1. The average roughness, R_a, was zero in Table 4.3 because it was calculated by summing the different value between the relative heights of each point and the arithmetic average height ($\bar{z}$) and then dividing by the total number of points. From the results, it is clear that some of the parameters are measures of height or amplitude rather than true roughness; thus, they were not valid for the shear stress calculation.

Table 4.3 Various measures of roughness for the 3D printed red disk

Parameter	Full scan	Reduced scan 1	Reduced scan 2	Photo 1	Photo 2	Caliper
Absolute arithmetic average roughness ($R_{\|a\|}$)	0.426	0.367	0.369	0.585	0.682	0.817
Arithmetic average height ($\bar{z}$)	0.369	0.257	0.245	0.490	0.670	0.622
Average roughness (R_a)	0	0	0	0	0	0
RMS roughness (R_q)	0.408	0.465	0.486	0.497	0.431	0.664
Total roughness (R_t)	4.389	3.725	3.666	3.507	3.291	3.500
Maximum profile peak height (R_p)	2.239	1.889	1.901	1.576	1.722	1.378
Maximum profile valley depth (R_v)	2.150	1.837	1.765	1.934	1.569	2.122
Ten Point Height ($R_{z(iso)}$)	0.816	0.484	0.645	0.648	1.621	0.520

As shown in Table 4.3, the root mean squared (RMS) roughness, R_q showed the most consistent and repeatable measure of roughness and did not depend on the number of point clouds obtained used in the analysis. Note that, in the structured light scanner method, the result from the

full scan give the most accurate measurement because of the density of the point clouds retrieved. The measures of roughness for the reduced scan 1 and 2 were approximately 0.06 and 0.08 mm, respectively, larger than the roughness obtained for the full scan. The values obtained from the photogrammetric method were similar to these numbers, where they were 0.09 mm (photo 1) and 0.02 mm (photo 2) over the value of the full scan. Conversely, the surface roughness obtained from hand measurement (caliper method) was almost 63% larger compared with the value from the full scan.

It was also important to examine how the roughness parameters listed in Table 4.1 would influence the resulting hydraulic shear stress. Table 4.4 gives the calculated shear stress values based on the different roughness measures in Table 4.3 for an assumed water flow velocity of 2 m/s. The shear stress was computed by using the Equation 2.4 in Chapter 2. Note that the shear stress for average roughness, R_a, was not applicable (NA) in Table 4.4 because it was zero roughness in Table 4.3. As shown in Table 4.4, several roughness parameters resulted in unrealistically high calculated shear stress values; thus, they were not valid for the roughness calculation. Again, the calculated shear stress using the RMS roughness, R_q, gave consistent results; therefore, the R_q, was recommended as the roughness parameter and used for all future soil surface roughness measures in this research.

The results from the validation study above showed that the photogrammetric technique is an effective and accurate method to compute the surface roughness of the sample. It is a fast, inexpensive method and can be fully automated. The structured light scanner gives the best results with a high-density point cloud; however, the scanner is expensive and the process to obtain the final result needs to be completed in several steps (point clouds must be exported into AutoCAD software, and then extracted to get the coordinates of the point clouds so that calculations of the

residuals can be made in MATLAB program). In comparison, the photogrammetric technique is automated and the entire process is completed in one simple step. Moreover, the photogrammetric technique is also faster than and much more accurate than the caliper method (as discussed above). Most importantly, this method is not as user dependent as the traditional method. With the method validated, the roughness of two different soil samples were determined to show the application of the technique.

Table 4.4 Various measures of shear stress for the red disk

Parameter	Full scan	Reduced scan 1	Reduced scan 2	Photo 1	Photo 2	Caliper
Absolute arithmetic average roughness ($R_{\|a\|}$)	16.5	15.5	15.5	18.0	19.0	20.0
Arithmetic average height ($\bar{z}$)	15.5	14.0	14.0	17.0	18.5	18.5
Average roughness (R_a)	NA	NA	NA	NA	NA	NA
RMS roughness (R_q)	16.0	16.5	17.0	17.0	16.5	18.5
Total roughness (R_t)	39.0	36.0	36.0	35.0	34.0	35.0
Maximum profile peak height (R_p)	29.0	27.0	27.0	25.0	26.0	24.0
Maximum profile valley depth (R_v)	28.5	26.5	26.5	27.5	25.0	28.5
Ten Point Height ($R_{z(iso)}$)	20.0	17.0	18.5	18.5	25.5	17.5

4.4.2 Application to soil samples

Initially dry soil samples were studied to determine the optimal distance and angle between the camera and sample. Next, the surface of the samples was wetted (after the erosion testing) to ensure that the thin layer of water present on top of soil samples would not distort the measured roughness. In order to investigate whether the illumination affects the point clouds obtain using the photogrammetric technique, two photos of each of the soil samples were first taken

immediately following one velocity in the erosion test using ambient light conditions in the laboratory. Next, the effects of illumination were examined by using a lamp to light the surface of the field-retrieved sample and the kaolin sample. There was a slight increase in the number of point clouds when a lamp was used for the field-retrieved sample. However, the number of points was reduced when used on the kaolin clay. This phenomenon was likely due to the uniform color and reflective color of the kaolin clay. Because the additional light reduced the number of the point clouds obtained in the kaolin sample and the lighting resulted in negligible changes in the measured roughness, ambient light condition in the laboratory was used for simplifying the procedure.

Laboratory Sample

Figure 4.2 shows the results of the measured roughness using photogrammetric technique for the kaolin clay sample. Figure 4.2 a is the actual photo of the soil sample taken after the erosion test. Figure 4.2 b shows the detected feature points indicated by red circles in the first image and green crosses in the second image. The yellow lines indicate the corresponding matched feature points between the two images. A total of 6,830 point clouds were detected in this sample. Figure 4.2 c shows the 2D image of the surface sample where each point cloud was represented as a dot with corresponding coordinated. Figure 4.2 d illustrates the residuals. Each vertical line represents the distance of soil sample above or below the reference surface (Shelby tube plane). As seen in Figure 4.2 d, the deepest valley below the Shelby tube plane calculated by the method was 5.54 mm, whereas the caliper method determined it to be 5.5 mm.

Table 4.5 presents the results for the different roughness parameters and the corresponding hydraulic shear stress values for a velocity of 2 m/s for the kaolin clay sample. As shown in Table 4.5, the RMS roughness, R_q, was calculated as 1.52 by using the stereo-photogrammetry system

and was 2.14 using the caliper method. Note that roughness is a unit less measurement (i.e., mm/mm). The relative roughness used in Moody's chart was 0.046 and 0.053 for the photogrammetric and caliper methods, respectively. Therefore, the hydraulic shear stress obtained by using Equation 2.4 was 23.0 Pa for the photogrammetric technique and 26.5 Pa for the caliper method. Note that in this sample, 16 locations across the soil surface were measured after the EFA test to get the roughness measurement for the hand caliper.

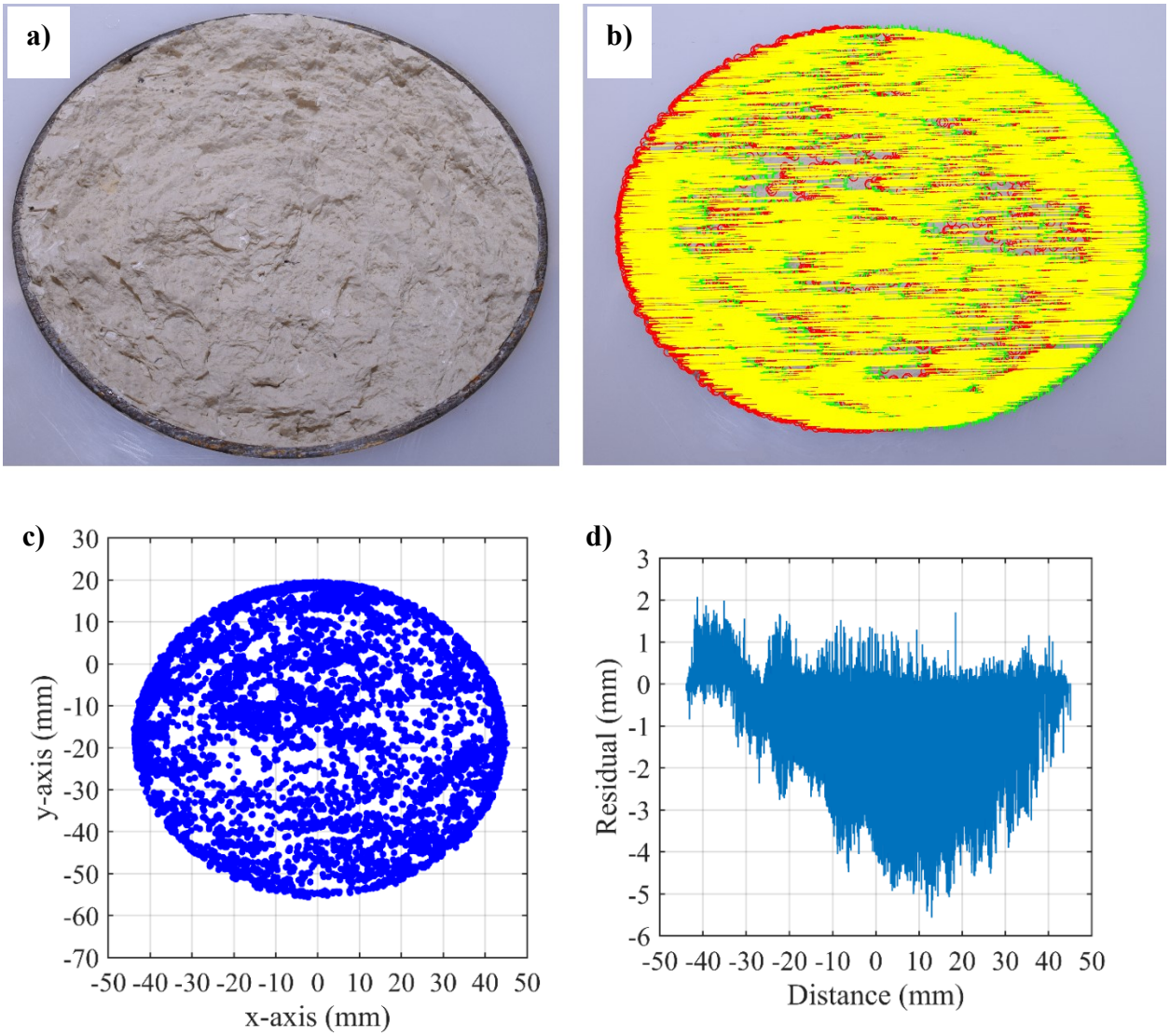

Figure 4.2 Photogrammetry application for the laboratory soil sample (Tran et al. 2017) a) actual photo of the laboratory soil sample; b) matched feature points; c) 2D image of the surface sample; d) residuals

Table 4.5 Various measures of roughness and hydraulic shear stress for the laboratory soil sample using the photogrammetric and caliper methods

Parameters	Roughness measurement (mm)		Shear stress (Pa)	
	Photogrammetric	Caliper	Photogrammetric	Caliper
Absolute arithmetic average roughness ($R_{\|a\|}$)	1.436	2.606	22.5	28.5
Arithmetic average height ($\bar{z}$)	-1.199	-1.856	21.5	25.0
Average roughness (R_a)	0	0	NA	NA
RMS roughness (R_q)	1.524	2.139	23.0	26.5
Total roughness (R_t)	7.601	6.500	47.0	43.0
Maximum profile peak height (R_p)	3.258	3.356	31.5	31.5
Maximum profile valley depth (R_v)	4.343	3.144	35.5	31.0
Ten Point Height ($R_{z(iso)}$)	-3.443	-2.500	32.0	28.0

Field-Retrieved Sample

Figure 4.3 shows the results of the photogrammetry method for the field-retrieved soil. Figure 4.3 a is the actual photo of the field-retrieved sample after the erosion test. The number of point clouds obtained for the field-retrieved soil sample in Figure 4.3 c was approximately two times (13,637 points) as much as the laboratory soil sample. The difference in the number of detected common points for the two samples was due to the surface condition of the samples. The rougher, multicolored and darker surface of the natural sample allowed for more distinct points to be captured by the photogrammetric system compared to the bright, monochromatic surface of the kaolin clay laboratory sample. Using the photogrammetric technique, the RMS roughness was found to be 0.97 whereas the caliper method determined it to be 1.17 as shown in Table 4.6. The relative roughness was 0.039 and 0.042 for photogrammetry and caliper methods, respectively.

The hydraulic shear stress of 19.5 Pa for the laboratory and 21 Pa for the field-retrieved samples was obtained, as shown in Table 4.6.

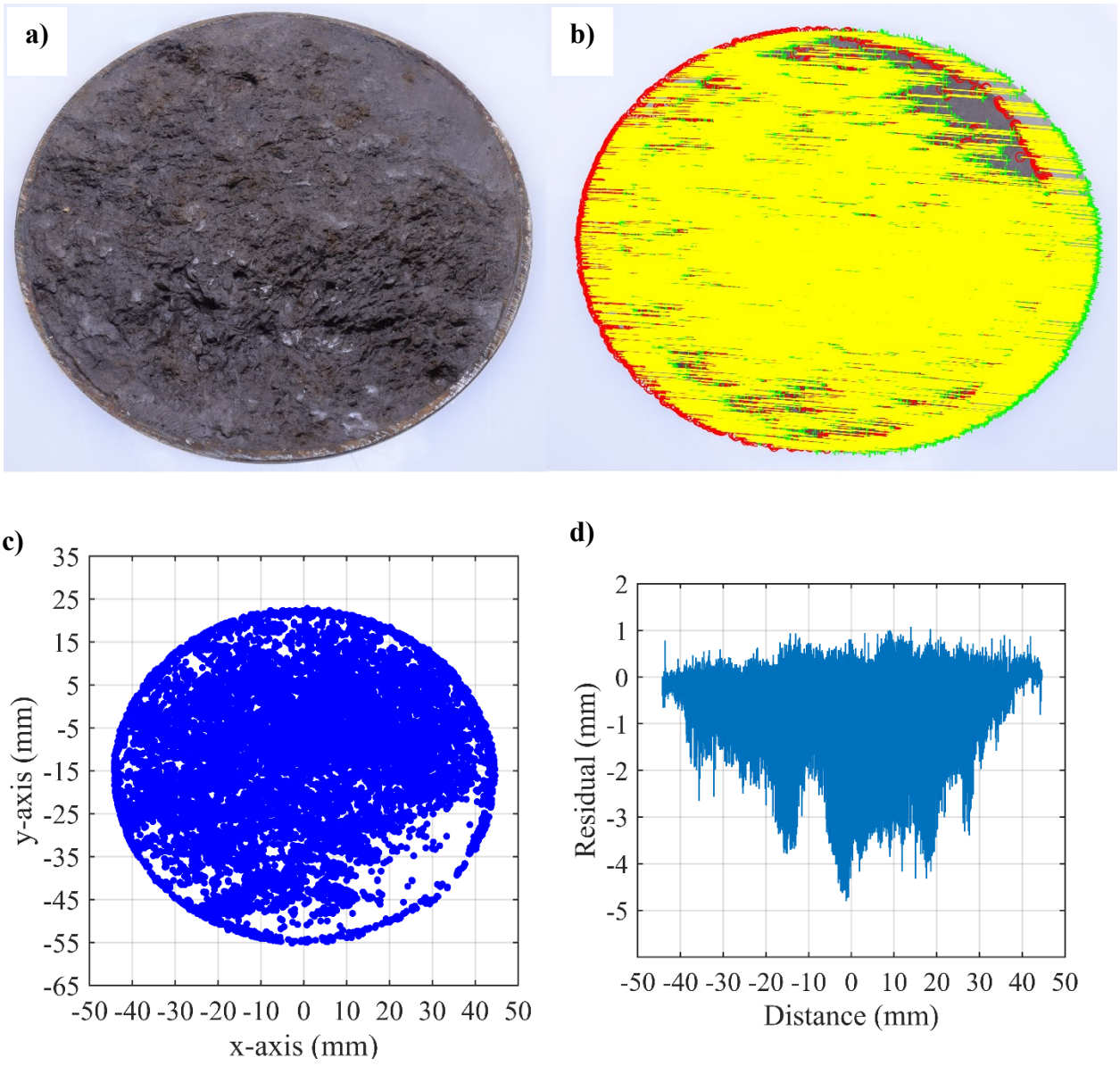

Figure 4.3 Photogrammetry application for the field-retrieved soil sample (Tran et al. 2017)

a) actual photo of the field-retrieved soil sample; b) matched feature points; c) 2D image of the surface sample; d) residuals

Table 4.6 Various measures of roughness and hydraulic shear stress for the field-retrieved soil sample using the photogrammetric and caliper methods

Parameters	Roughness measurement (mm)		Shear stress (Pa)	
	Photogrammetric	Caliper	Photogrammetric	Caliper
Absolute arithmetic average roughness ($R_{\|a\|}$)	0.790	1.594	18.5	23.5
Arithmetic average height ($\bar{z}$)	-0.668	-1.594	17.5	23.5
Average roughness (R_a)	0	0	NA	NA
RMS roughness (R_q)	0.967	1.165	19.5	21.0
Total roughness (R_t)	5.849	2.456	41.0	27.5
Maximum profile peak height (R_p)	1.733	1.244	24.0	21.5
Maximum profile valley depth (R_v)	4.117	2.456	34.5	27.5
Ten Point Height ($R_{z(iso)}$)	-3.689	-2.816	33.0	29.5

This study has been published in the *ASTM Geotechnical Testing Journal:* **Tran, T.** V., Tucker-Kulesza, S. E., and Bernhardt-Barry, M. L., "Determining Surface Roughness in Erosion Testing Using Digital Photogrammetry," *Geotechnical Testing Journal*, Vol. 46, No. 6, 2017, pp. 917–927, https://doi.org/10.1520/GTJ20160277

4.2 Results from the turbidity measurements

Six soil samples from a site in southeastern Kansas were tested using the EFA instrumentation. The first three samples were taken from the same site and the other three were retrieved from another site. All instrumentation was used in these erosion tests. Turbidity measurements were collected, and the erosion parameters were obtained using the stereo-photogrammetry technique. Moreover, additional measurements of the surface roughness were also taken following the traditional method (hand calipers). The erosion rate and hydraulic shear stress were calculated using the distance traveled by the piston over the length of the erosion testing

and using the custom digital photogrammetry program as well as hand calipers, respectively. All soil samples were classified as clay with low plasticity (CL) according to Unified Soil Classification System (USCS), except for Sample 3 which had two different layers. The top of Sample 3 was CL and the bottom layer was high plasticity clay (CH). Therefore sample 3 was broken into two sections, T (top) and B (bottom). A fundamental assumption of the EFA test is that the entire sample in the Shelby tube is uniform during erosion testing.

Figure 4.4 shows turbidity measurements of clean water and turbidity of water in erosion tests conducted from 1m/s to 4 m/s flow velocity for Sample 1 and Sample 3(T) over 3000 seconds (50 minutes) at the downstream of the flow. The black lines are the downstream turbidity measurement of clean water (no erosion test). The blue lines (Figure 4.4 a) and the red lines (Figure 4.4 b) are the turbidity of the water during the erosion tests for Sample 1 and Sample 3(T) at the downstream locations, respectively. In Figure 4.4, the turbidity of clean water was approximately constant but the turbidity measurements of water in erosion tests were higher, indicating that erosion occurred and affected the water clarity. No measurable erosion occurred in Sample 1 until 6 m/s; however, turbidity of water in erosion test for Sample 1 (Figure 4.4 a) are higher than turbidity of clean water. Some erosion took place in Sample 1 from 1 to 4 m/s flow velocity that was not measured in the traditional EFA testing methodology. Results from full erosion tests of all six samples are presented in Table 4.7 and Table 4.8. Based on the turbidity data in each erosion test, the cumulative turbidity difference between the measurements from the water upstream and downstream of the sample were computed. The turbidity of clean water was then deducted from the upstream and downstream data (after removing the noise by Gaussian filtering). This was done because the turbidity of clean water was different at different velocities, likely from turbulence and bubbles (specifically at higher velocities). Then the turbidity difference

between downstream and upstream were calculated for every second. The cumulative sums were computed to determine the final turbidity. The volumes of soil eroded in Table 4.7 and Table 4.8 were calculated based on the volume of the soil extruded in erosion tests and via stereo-photogrammetry technique.

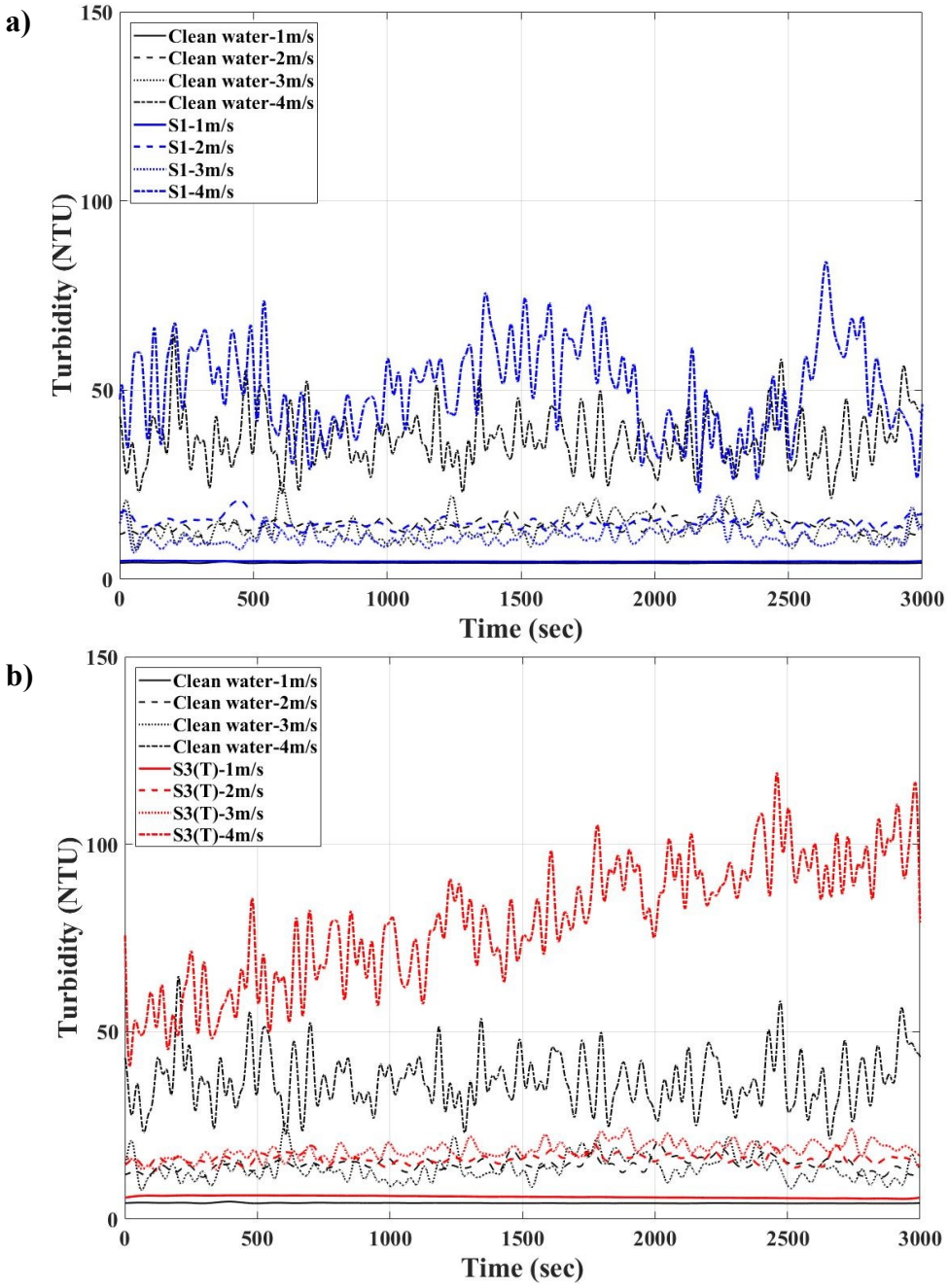

Figure 4.4 Turbidity of clean water and water in erosion tests
a) Sample 1; b) Sample 3(T)

Table 4.7 Summary of EFA testing results for soil samples 1, 2, and 3

Sample	Water velocity (m/s)	Erosion rate (mm/hr)	Shear stress (Pa)			Volume of soil eroded (mm^3/hr)			Cumulative turbidity different (10^3 NTU)
			Photo	Caliper 1	Caliper 2	Photo	Caliper 1	Caliper 2	
1	1	0	4.62	2.50	–	924.9	79.0	–	0.375
	2	0	17.98	12.48	9.99	1,007.6	859.1	382.7	0.554
	3	0	40.45	29.21	–	1,160.2	954.0	–	0.164
	4	0	77.90	55.93	–	1,462.6	1,408.4	–	11.916
	5	0	112.36	96.75	–	1,680.5	1,975.4	–	–
	6	1.8	220.22	134.83	–	12,273.4	12,181.8	–	–
2	1	0	4.49	3.50	3.50	1,657.0	1,162.9	1,161.4	0.401
	2	0	17.98	16.48	16.98	2,969.7	2,338.2	2,677.6	0.765
	3	2.4	52.81	46.07	–	17,531.7	18,822.1	–	2.733
	4	7.8	91.88	89.89	83.89	51,483.2	51,454.9	50,551.8	12.852
	5	67.61	NA	NA	–	NA	NA	–	–
3 (T)	1	0	5.12	3.12	–	1,849.2	645.2	–	0.701
	2	0	18.48	16.48	–	2,641.2	2,420.3	–	0.968
	3	10.8	46.07	42.70	–	66,057.6	66,544.7	–	1.716
	4	30.0	97.88	65.92	–	176,928.8	176,425.5	–	18.242
3 (B)	5	15.0	152.93	103.00	–	81,691.5	84,431.0	–	–
	6	16.8	220.22	457.30	–	101,316.0	100,262.6	–	–
	4	0	73.91	47.94	–	2,306.8	709.8	–	3.42
	3	0	49.44	34.83	–	1,937.0	389.6	–	0.430
	2	0	17.48	13.98	–	1,336.0	226.8	–	0.065
	1	0	4.24	3.37	–	921.6	109.9	–	0.002

Table 4.8 Summary of EFA testing results for soil samples 4, 5, and 6

Sample	Water velocity (m/s)	Erosion rate (mm/hr)	Shear stress (Pa)			Volume of soil eroded (mm^3/hr)			Cumulative turbidity different (10^3 NTU)
			Photo	Caliper 1	Caliper 2	Photo	Caliper 1	Caliper 2	
4	1	0	4.87	3.25	–	1,221.7	849.8	–	0.960
	2	0	19.97	22.47	21.97	5,777.2	6,343.0	5,907.1	4.096
	3	7.2	65.17	65.17	57.30	49,479.2	53,944.5	50,622.6	6.401
	4	7.2	107.86	85.89	–	30,627.7	36,071.1	–	14.318
	5	11.4	184.14	149.81	–	74,382.8	73,782.5	–	–
	6	21.76	301.12	215.73	–	116,179.7	118,667.5	–	–
5	1	0	4.49	3.37	3.00	1,102.1	902.5	546.8	0.436
	2	1.8	22.97	16.98	–	9,035.2	13,141.2	–	1.962
	3	3.6	58.43	37.08	33.71	22,427.0	23,308.4	22,609.1	4.031
	4	7.2	81.90	57.93	–	41,469.4	43,396.0	–	15.022
	5	112	159.17	165.42	–	658,281.8	658,829.2	–	–
	6	288	247.19	305.61	–	1,682,545.5	1,686,844.3	–	–
6	1	0	4.74	3.12	3.12	912.7	653.0	616.6	1.616
	2	3.0	22.47	13.48	10.49	18,526.3	18,492.9	17,699.1	1.554
	3	4.2	46.07	39.33	–	25,098.0	27,238.7	–	5.532
	4	6.0	83.89	65.92	57.93	33,766.2	37,149.0	36,287.2	20.001
	5	13.2	137.33	71.78	–	77,212.0	77,139.8	–	–
	6	18.66	188.76	134.83	–	110,520.7	109,994.5	–	–

Figure 4.5 shows the volume of soil eroded versus cumulative turbidity difference of field-retrieved samples in erosion tests from 1 m/s to 4 m/s flow velocity. Overall, higher volumes of soil eroding from each sample resulted in higher cumulative turbidity difference. This can be seen clearly in Samples 2, 3 (T), 3 (B), 4 (except 3 m/s erosion point), 5, and 6 (except 1 m/s erosion point). For instance, in Sample 2, the amount of erosion and cumulative sum at 2 m/s flow are larger than that at 1 m/s flow velocity. Similarly, this is also true when comparing the volume of soil eroded and cumulative sum between 2 m/s and 3 m/s, 3 m/s and 4 m/s. The relationship between the volume of soil eroded and cumulative turbidity difference is fairly linear. However, more samples need to be tested and a statistical analysis performed in the future to confirm this finding.

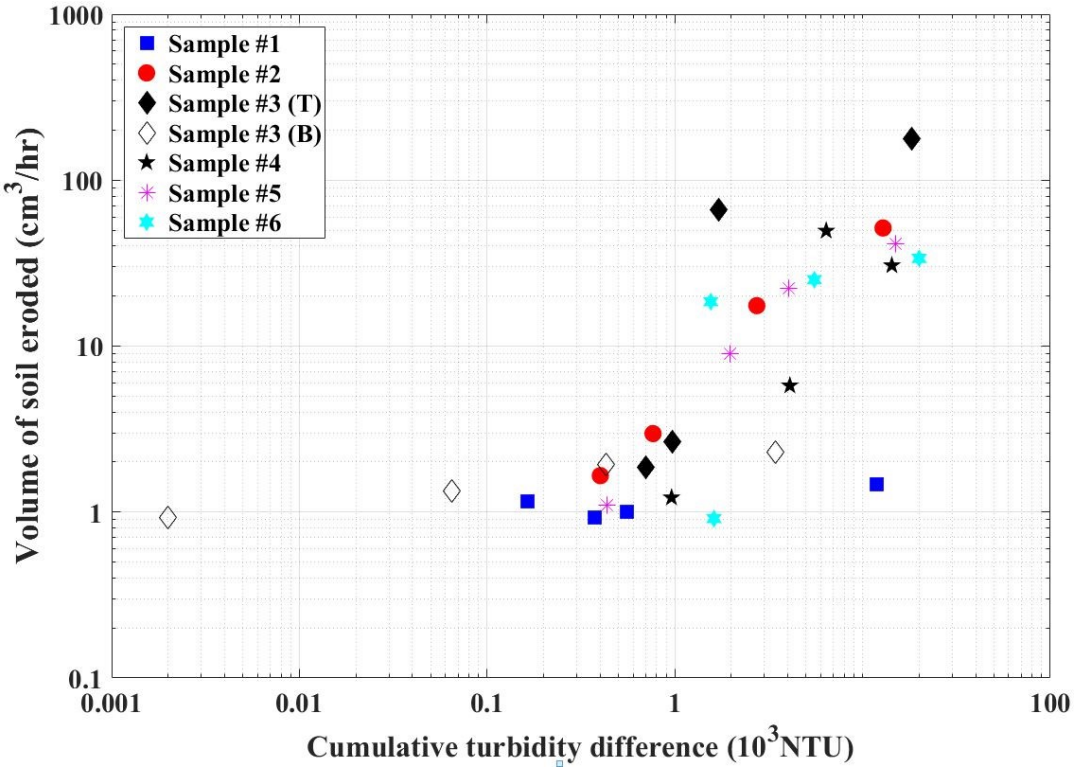

Figure 4.5 Volume of soil eroded vs Cumulative turbidity difference of all samples in erosion tests

The study has been published in *International Foundation Congress and Equipment Expo (IFCEE)* 2018: **Tri V. Tran**; Stacey E. Tucker-Kulesza; and Michelle Bernhardt, "Soil Surface Roughness and Turbidity Measurements in Erosion Testing," *IFCEE 2018: Advances in Geomaterial Modeling and Site Characterization-GSP 295-2018*, pp. 506–515, https://doi.org/10.1061/9780784481585.049

4.3 New erosion characterization chart

The results of erosion tests in the EFA for six field-retrieved soil samples (Table 4.7 and Table 4.8) were plotted according to the HEC–18 as seen in Figure 4.6. This figure includes the calculated applied hydraulic stress (Pa) versus the measured erosion rate (mm/hr). Most of the samples did not have a measurable erosion at flow velocities of 1 and 2 m/s (Samples 1, 2, 3, and 4), while Sample 5 and 6 had no measurable at 1 m/s water velocity. Sample 1 had no measurable erosion until maximum flow velocity of 6 m/s. Sample 3 also had no erosion at 1, 2, 3, 4 m/s in the bottom layer. However, the amount of erosion could be quantified through the stereo-photogrammetry program. Based on the HEC–18 chart, Sample 1 was classified as very low to low erodibility, whereas Samples 2 and 3 were categorized as low to moderate erodibility. Sample 4 was on the edge of low to moderate erodibility and Samples 5 and 6 were considered as moderate erodibility. Erosion points obtained by using hand calipers (C1 and C2) were also plotted in Figure 4.6. They were plotted on the left of the erosion points obtained by using the stereo-photogrammetry method. Hence, using hand caliper method to get the erosion results was more conservative than results from the photogrammetric technique. For example, the erosion points of Sample 4 at 5 and 6 m/s flow velocities were plotted in the low erodibility zone of the HEC–18 chart using the stereo-photogrammetry method; however, they were considered in the moderate erodibility zone using hand calipers. Additionally, different people (noted as C1 and C2) used

hand calipers following the traditional EFA methodology got different erosion points as seen in Figure 4.6. This highlights the operator dependency and why hand calipers are not recommended for future research. The photogrammetric technique gives a unique, repeatable result and accurate measurements.

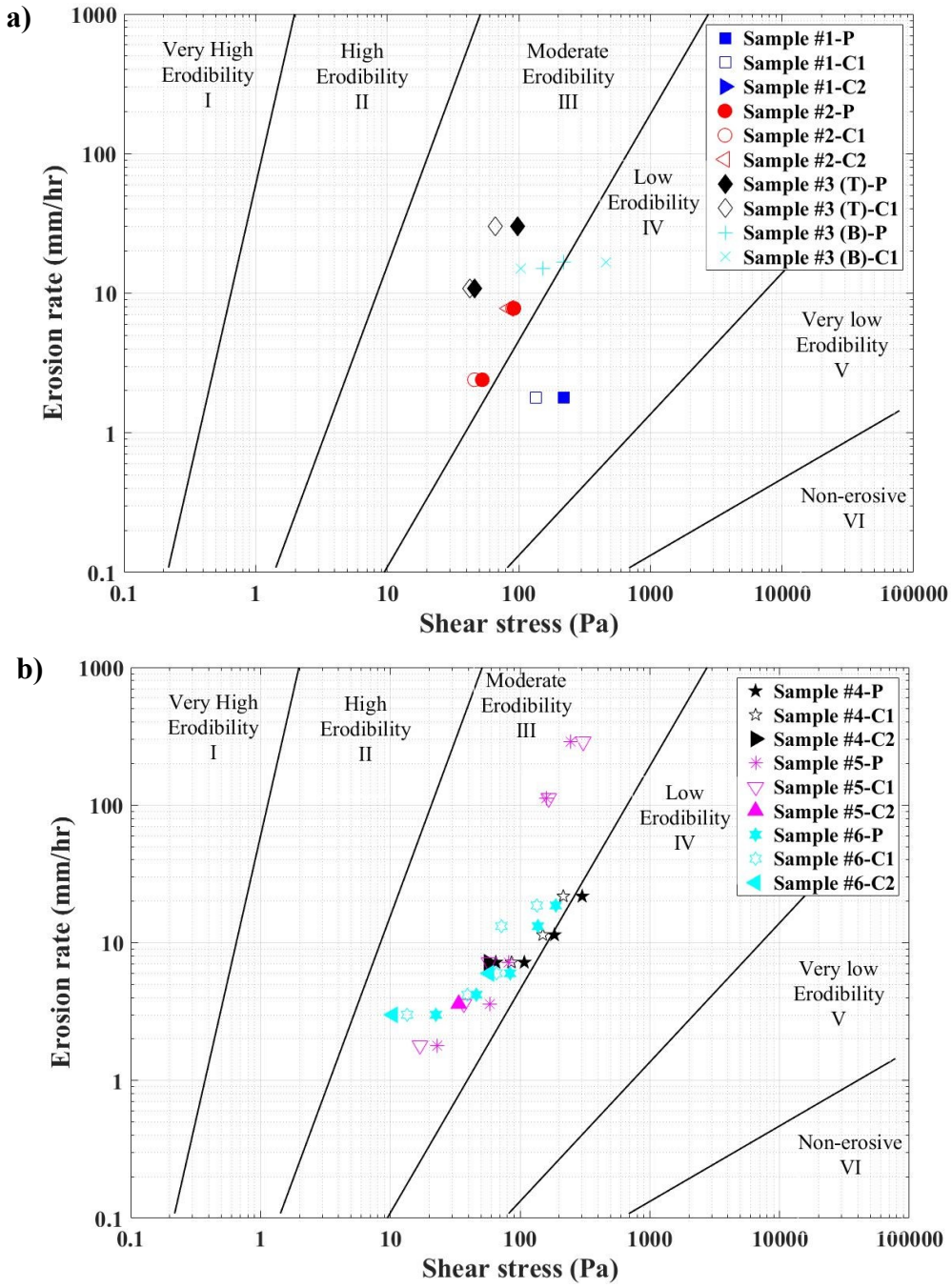

Figure 4.6 Erosion rate versus shear stress according to HEC–18

Note that Figure 4.6 is a log–log plot and therefore all erosion points that have zero erosion cannot be seen in the chart. This is often overcome by plotting zero erosion at 0.1 mm/hr, but this can be misleading as many researchers identify 0.1 mm/hr as the point where critical shear stress is measured. Thus, a new erosion chart was developed. Figure 4.7 shows the volume of soil eroded in erosion tests versus the hydraulic shear stress obtained by the stereo-photogrammetry method. As seen in Figure 4.7, all of zero erosion points in Figure 4.6 according to HEC–18 are now shown in this plot and they can be compared very easily. For instance, Samples 1, 2, and 3 (T) had all zero erosion at 1 and 2 m/s water velocities; but Samples 2 and 3 (T) actually eroded more than Sample 1 as shown in Figure 4.7 a. Similarly, Sample 4 eroded more than Sample 5 and 6 at 1 m/s flow velocity although all of the samples had zero erosion without the photogrammetry calculations. According to Figure 4.7, Sample 1 was classified as low to moderate erodibility, whereas the rest of the samples were categorized as moderate erodibility. Thus, the updated graph is very useful for comparing low erodibility soils while not changing the erosion characterization according to the widely accepted HEC–18 method.

Another proposed chart is based on the turbidity measurement. Figure 4.8 presents the cumulative turbidity difference versus hydraulic shear stress for all samples. Again, all zero erosion points in HEC–18 chart (Figure 4.6) are shown in this plot and are now comparable. In general, higher cumulative turbidity difference resulted in higher hydraulic shear stress, except two erosion points in Figure 4.8 a (3 m/s for Sample 1 and Sample 3 (B)). All samples are still considered as moderate erodibility.

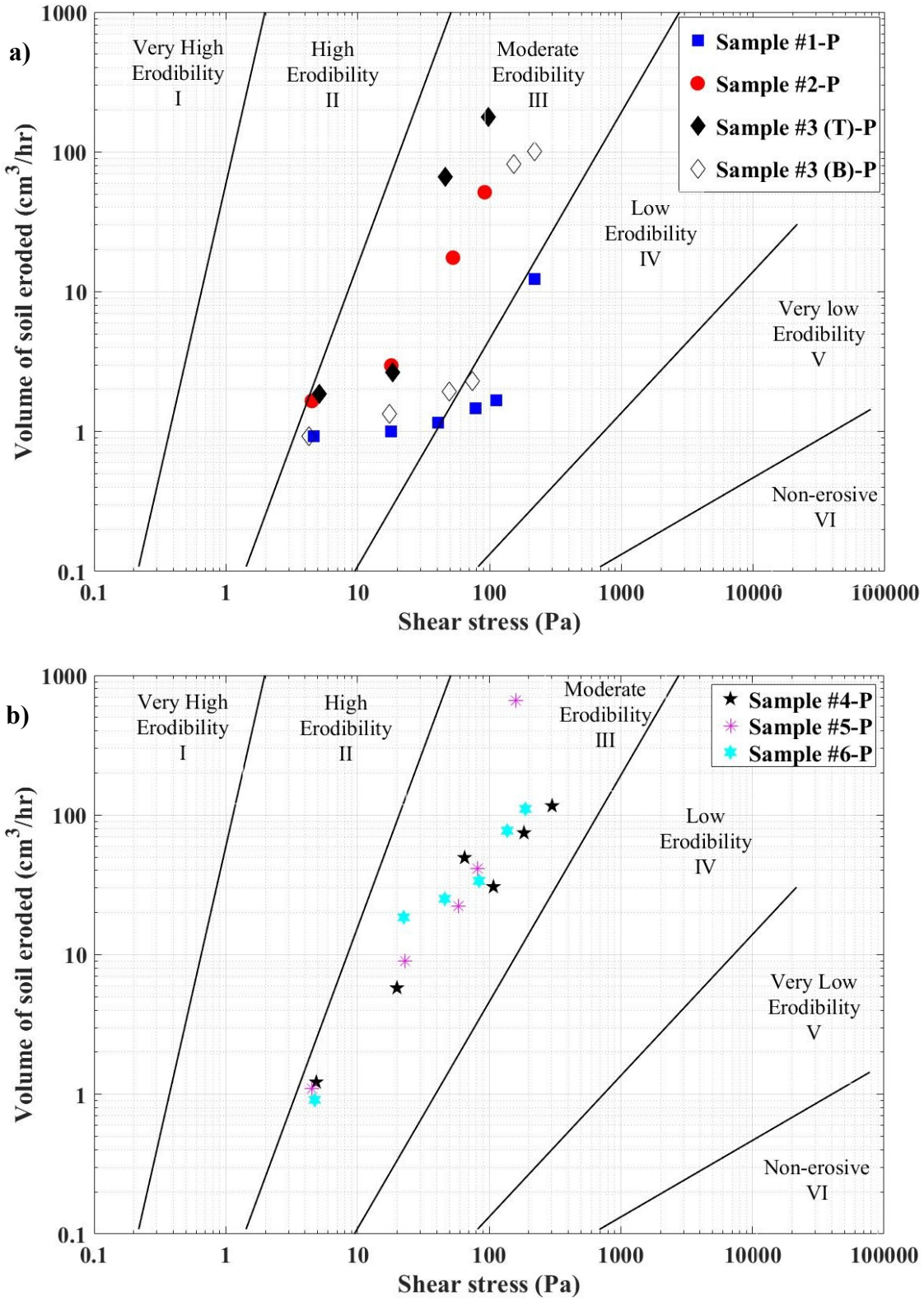

Figure 4.7 Volume of soil eroded versus shear stress

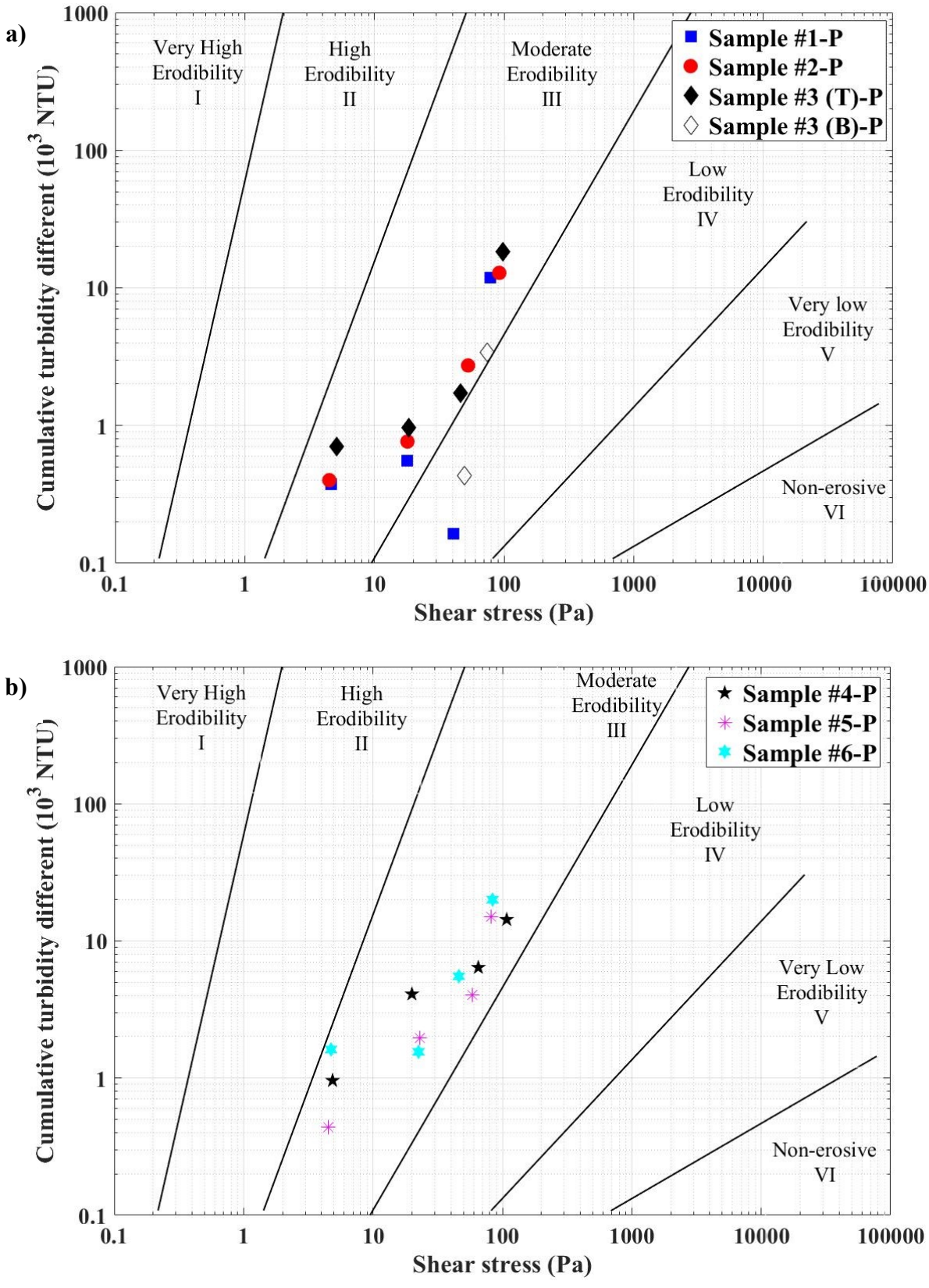

Figure 4.8 Cumulative turbidity difference versus shear stress

4.4 Utilizing the instrumentation of the EFA

4.4.1 Engineered soils

In this study, the EFA tests were conducted to evaluate the enhanced erosion resistance of engineered soils. Ottawa sand samples were treated with a polymer-modified Microbially Induced Carbonate Precipitates (MICP) solution (a mixture of dyed median concentration polymer-modified cementation solution and bacteria solution). This treatment improves the strength of soil in the surficial regions and therefore the treated soil is more erosion resistant. The results of the EFA tests for both treated and untreated samples are shown in Figure 4.9 and summarized in Table 4.9.

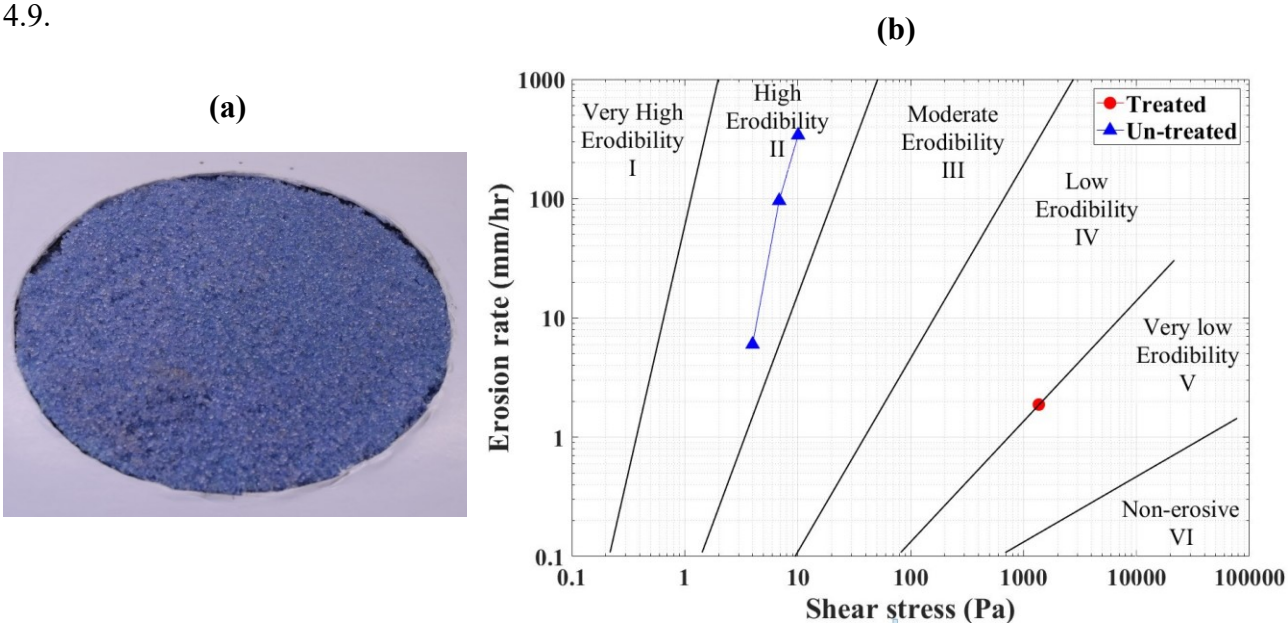

Figure 4.9 a) Photos of the MICP sample; b) Shear stress vs erosion rate (HEC–18)

The replicate samples plot on top of each other for the treated sample and very close to each other for the untreated sample; therefore, Figure 4.9 b shows the results for only one sample (untreated 1 and treated 1). The untreated sample classified as moderate/high erodibility following the HEC–18 soil classification system, whereas the treated sample categorized as low/very low

erodibility on the charts. The results were in good agreement with the results from a flume test conducted by the co-authors (Wang et al. 2018)

Table 4.9 Summary of EFA testing results

Sample	Velocity (m/s)	Water temperature (°C)	Erosion rate (mm/hr)	Shear stress (Pa)	Critical shear stress (Pa)
Un-treated 1	0.1	14.7 – 14.8	0	0.50	2.13
	0.2	14.7 – 14.8	0	1.76	
	0.3	14.7- 14.8	6	3.99	
	0.4	14.7 – 14.8	96	6.86	
	0.5	14.7 – 14.8	340	10.1	
Un-treated 2	0.1	15 - 15.1	0	0.51	2.17
	0.2	15 - 15.1	0	1.81	
	0.3	15 - 15.1	6	3.97	
	0.4	15 - 15.1	102	6.66	
	0.5	15 - 15.1	330	10.7	
Treated 1	1	14.9 – 15.0	0	39.2	1171.5
	2	14.6 – 14.8	0	155.8	
	3	14.8 – 14.9	0	350.6	
	4	14.0 – 15.3	0	607.6	
	5	14.4 – 15.5	0	949.4	
	6	13.8 – 15.4	1.88	1367	
Treated 2	1	14.2 - 14.3	0	39.2	N/A
	2	14.3 – 14.5	0	155.82	
	3	13.9 – 14.4	0	341.76	
	4	13.8 – 15.3	0	607.58	
	5	13.8 – 15.3	0	949.35	

The treated sample had no erosion, except at the very high flow velocity (6 m/s). It would be very difficult to quantify the critical shear stress and the amount of soil erosion if using the traditional EFA test. However, erosion could be obtained if using digital stereo-photogrammetry method. Additional, only one and three erosion points have been shown in Figure 4.9 b for treated and un-treated samples, respectively. The other erosion points could not be seen in the chart

because of the zero erosion. Therefore, utilizing the EFA instrumentation combine with the new erosion characterization chart would help to evaluate the erodibility of this engineered soil.

The treated sample was tested up to 6 m/s to achieve measurable erosion; however, the replicate sample was flushed out of the Shelby tube at the 6 m/s velocity, so the critical shear stress could not be determined. The critical shear stress of the treated sample was over 550 times higher than the air-pluviated sand as shown in Table 4.9. Results of the presented experiments clearly demonstrate that the polymer-modified MICP approach is effective and efficient for preventing water-induced surficial erosion as well as the need for using the instrumentation of the EFA in order to quantify the improvement of an engineered soil.

This study has been published in the *ASCE Journal of Materials in Civil Engineering:* Wang, X., Tao, J., Bao, R., **Tran, T**., and Tucker-Kulesza, S. "Surficial soil stabilization against water-induced erosion using polymer-modified microbially-induced carbonate precipitation," *Journal of Materials in Civil Engineering*, Vol. 30, No. 10, 2018, 04018267, https://doi.org/10.1061/(ASCE)MT.1943-5533.0002490

4.4.2 In-situ soil samples

In this application, undisturbed soil samples from two sites (two agriculture fields) were brought to the laboratory for the controlled erosion testing to obtain the critical shear stress. This research quantified soil erosion to study the erodibility of claypan soils. One sample was collected from a highly productive region of the field and the other from an unproductive area. The results of the EFA tests are presented in Table 4.10. There was no measurable erosion until 3 m/s for the high-yielding area and none until 5 m/s for the unproductive area. However, the amount of soil eroded via photogrammetry was measured and the effective hydraulic stress was calculated. At 6 m/s flow velocity, a block of high-yield soil was eroded instead of particle by particle; hence, the

photos of the soil surface could not be taken and the shear stress was not calculated. Figure 4.10 shows the photos of the two soil samples after EFA testing following 5 m/s flow velocity (left photos) and the resulting measured roughness amplitudes of the samples (right images). The zero elevation is the plane of the Shelby tube. The blue lines above or below zero elevation are the height of the soil above or below the plane of the Shelby tube. They were used to calculate the roughness of the sample and the hydraulic shear stress in Figure 4.11 was then calculated.

Table 4.10 Results of EFA testing for the high yield and low yield soil samples

Sample	Water velocity (m/s)	Erosion rate (mm/h)	Shear stress (Pa)	Volume of soil eroded (mm^3)	Critical shear stress (Pa)
High-yield	1	0	3.0	711.4	35.3
	2	0	11.5	1,337.1	
	3	0.6	25.9	3,733.7	
	4	1.2	40.0	6,012.6	
	5	6.0	115.6	28,290.0	
	6	76.8	NA	NA	
Low-yield	1	0	2.8	942.0	103.5
	2	0	17.5	1,327.0	
	3	0	46.1	5,354.4	
	4	0	88.0	7,398.2	
	5	3.6	143.8	27,996.8	
	6	18.0	220.5	110,491.8	

The critical shear stress for the high yield area (saturated clayey sand soil) was 35.3 Pa whereas the critical shear stress for the low-yield area (low-permeability fat clay) was 103.5 Pa, indicating the low yield region was more erosion resistant. Recall that critical shear stress is a key measurement in soil erodibility and a more accurate calculation of the critical shear stress helped to further characterize the claypan soils in this study. Figure 4.11 shows a comparison of erodibility of the two soil samples. Figure 4.11 a was plotted according to HEC–18 erosion chart while the new erosion characterization chart (volume of soil eroded vs shear stress) is presented in Figure 4.11 b.

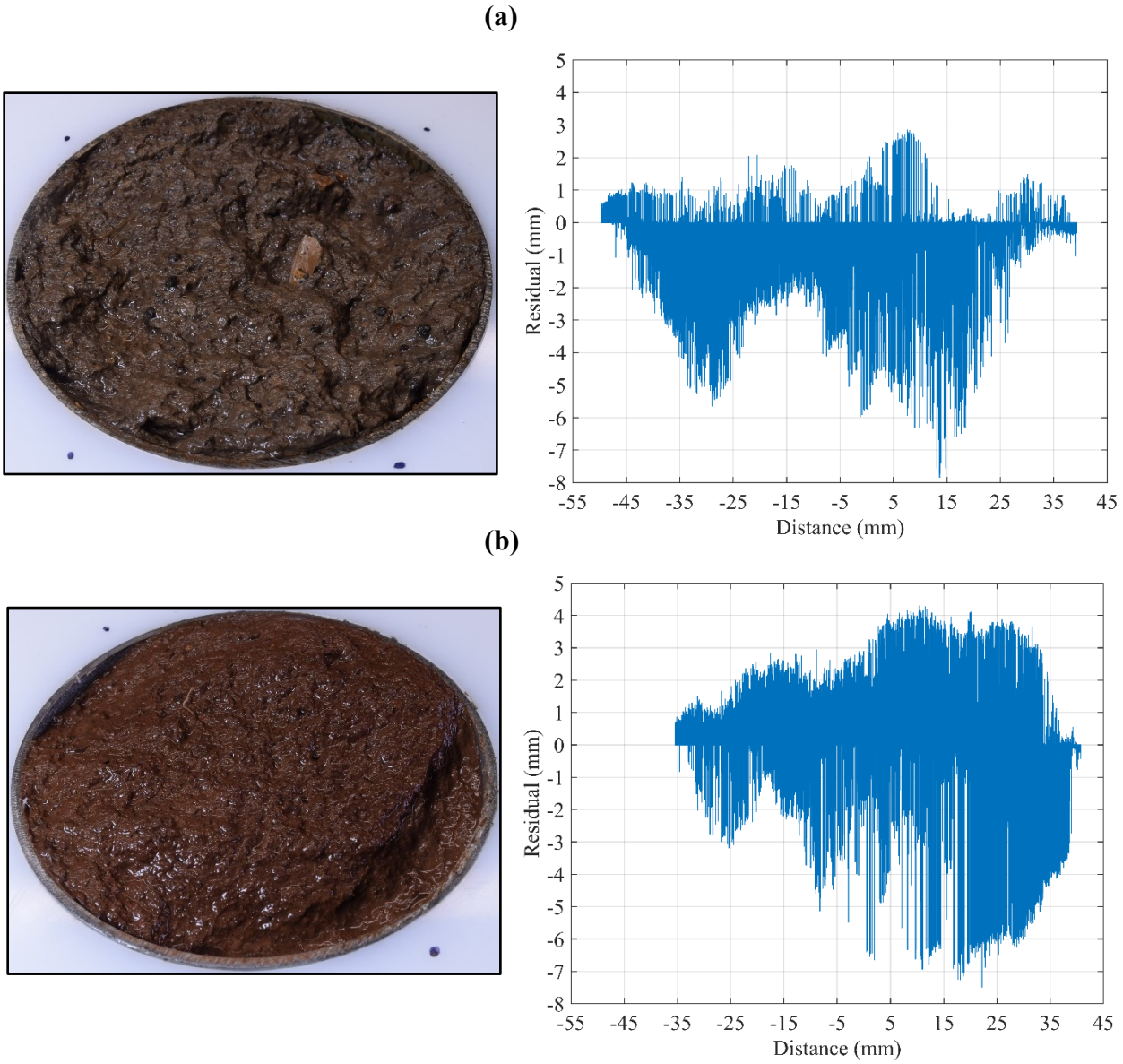

Figure 4.10 Soil samples following 5 m/s flow velocity and roughness measurements calculated with stereo-photogrammetry method (Tucker-Kulesza et al. 2017)

a) Low-yielding area; b) High-yielding area

It is clear that all the zero erosion points are not shown on HEC–18 chart and it may be difficult to compare the erodibility of two soil samples with these limited datasets. However, the new erosion chart allowed comparison of the erodibility between the two samples point by point. For example, both samples had zero erosion at 2 m/s but the hydraulic shear stress of the low-yield sample was greater than that of the high-yield sample. This indicates that the sample from the low

productive area is more resistance to erosion than the high productive area sample. Based on the HEC–18 erosion chart, both samples were classified as low to moderate erodibility. But both samples were likely considered as moderate erodibility according to the new erosion chart.

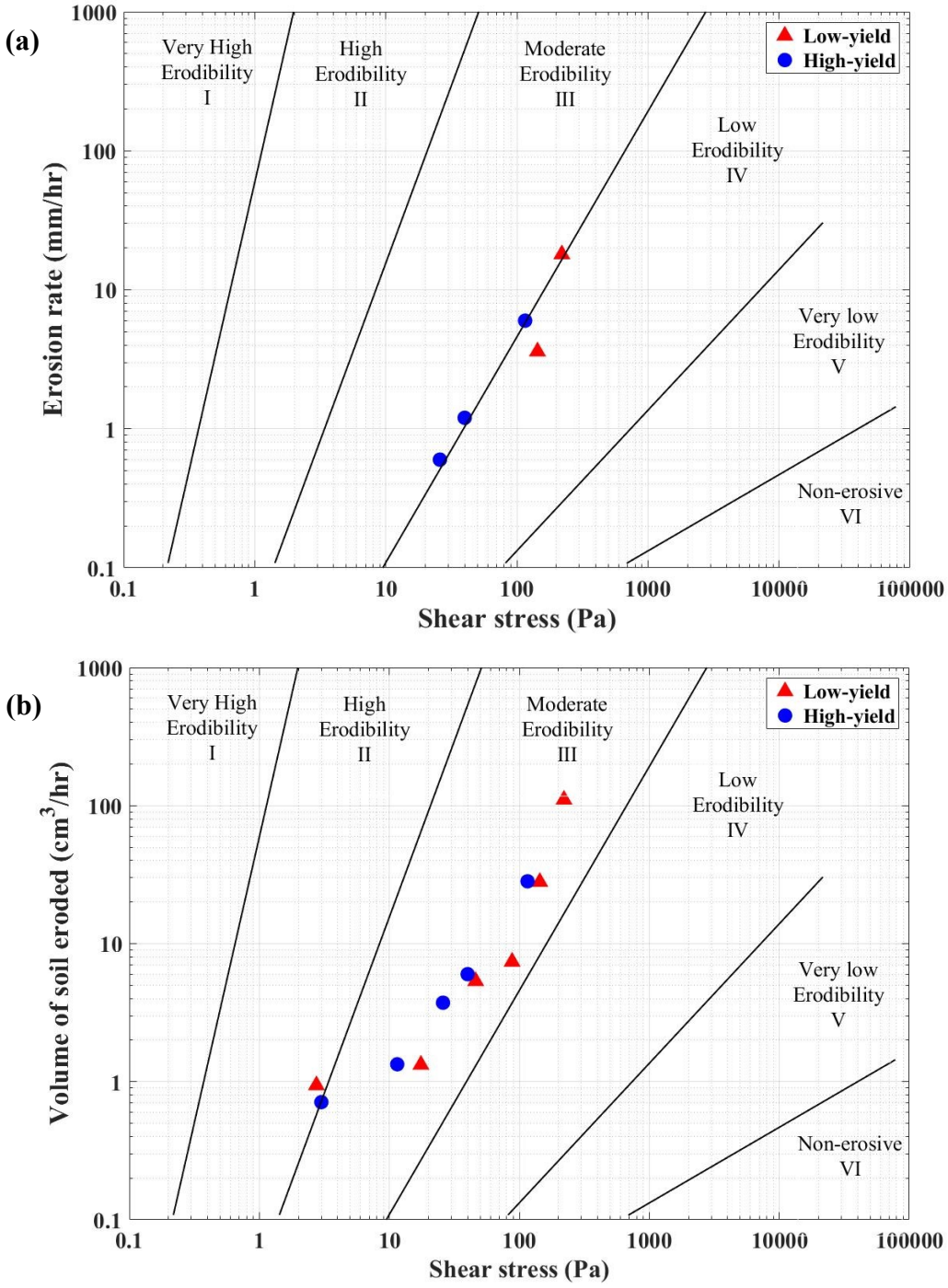

Figure 4.11 Soil erodibility of the low-yield and high-yield samples
a) According to HEC–18 chart; b) According to new erosion characterization chart

This study has been published in *American Society of Agricultural and Biological Engineers*: S. Tucker-Kulesza, G.F. Sassenrath**, Tran, T.**, W. Koehn, L. Erickson, "Site-Specific Erodibility in Claypan Soils: Dependence on Subsoil Characteristics," *Applied Engineering in Agriculture*, Vol. 33, No. 5, 2017, pp. 705–718, https://doi.org/10.13031/aea.12120.

4.5 Effects of temperature on soil erosion

The application of using the instrumentation of the EFA was used to investigate the effects of water and soil temperature on soil erosion as presenting in this section.

4.5.1 Effect of water temperature

In this experiment, six remolded kaolin-sand mixtures samples were tested under different target water temperatures (17, 28, and 36ºC) and each temperature was tested twice. These water temperatures were selected based on average annual temperatures of the Arkansas River near Coolidge, KS. The soil temperature was also monitored with the thermocouples during testing. Each sample was tested at four velocities from 1 to 4 m/s. All erosion data are plotted as erosion rate versus hydraulic shear stress as shown in Figure 4.12. In general, at the same water flow velocity, samples tested under high temperature exhibited greater erosion rate than the other samples tested under lower temperature. No measurable erosion occurred at the minimum water flow velocity, 1 m/s at all temperatures; therefore, these data are not plotted in Figure 4.12. However, as shown in Figure 4.12, all tests at the highest water temperature, 36°C (green square), eroded more than the other samples (17ºC, blue circle, and 28°C, red triangle) for cases with measurable erosion (2, 3, and 4 m/s water flow). The maximum difference in erosion due to the effect of water temperatures occurred at the highest water velocity of 4 m/s. The samples tested at the highest water temperature of 36ºC and highest velocity eroded over three times as much as the sample at the reference water temperature of 17ºC. Only the sample tested at 28°C had

measurable erosion at the lowest velocity of 1 m/s, and this erosion was detected with the photogrammetry method. However, the amount of erosion was less than 0.1 cm^3; so, it was not shown in Figure 4.12 b.

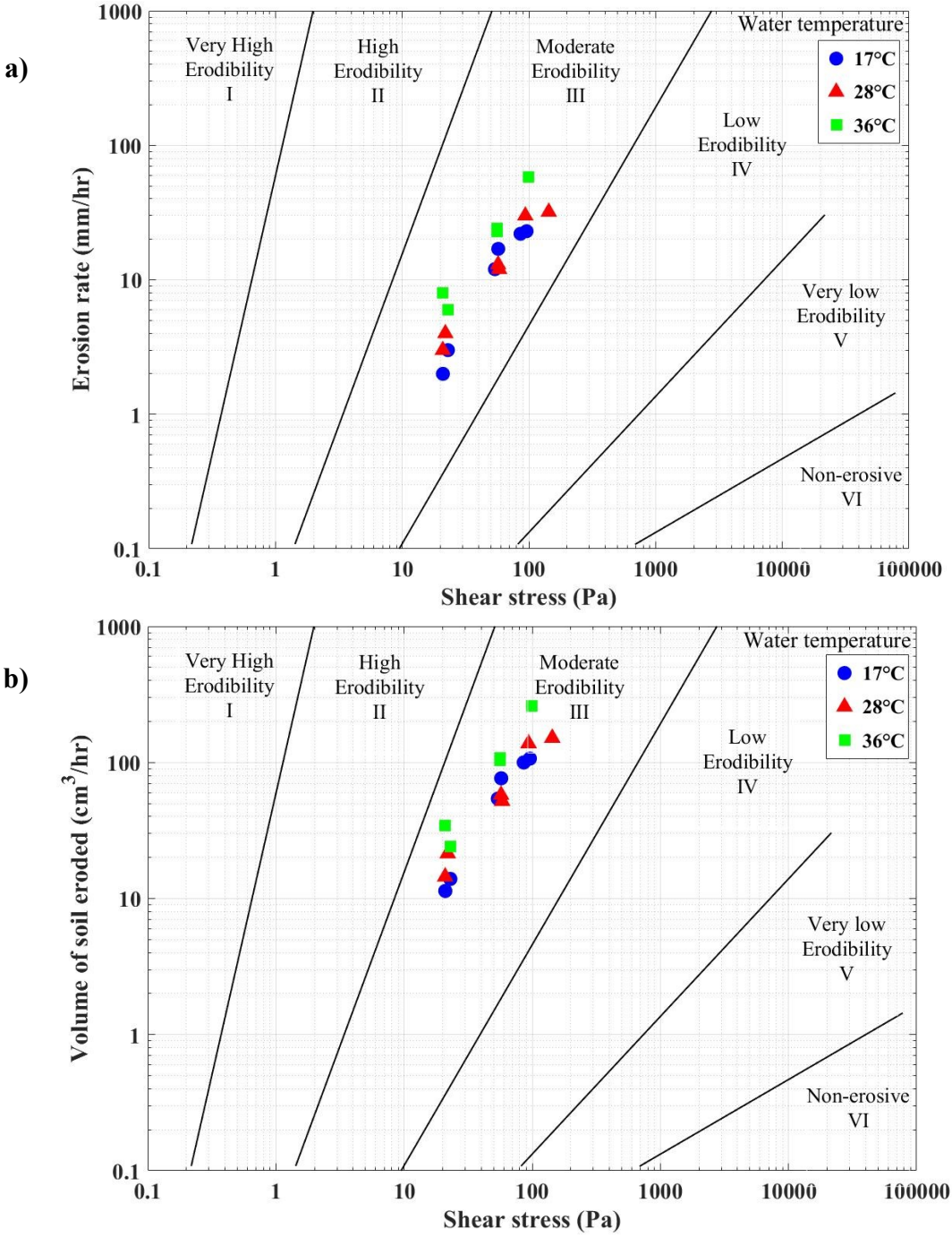

Figure 4.12 Comparison of soil erodibility under different water temperatures a) HEC–18; b) New erosion characterization chart

Table 4.11 Summary of all erosion rates for different water temperature of all samples

Sample	Water temperature (°C)	Soil temperature (°C)	Water velocity (m/s)	Erosion rate (mm/h)	Shear stress (Pa)	Volume of soil eroded (mm^3)	Critical shear stress (Pa)
W1	17	17-18	1 2 3 4	0 3 17 22	2.37 22.97 57.30 85.89	0 13,938.3 76,461.9 99,951.1	9.24
W2	17	17-18	1 2 3 4	0 2 12 23	2.37 20.97 53.93 95.88	0 11,366.3 54,146.3 106,672.1	11.67
W3	28	18-27	1 2 3 4	0 3 13 30	2.49 20.92 57.16 93.65	25.0 14,470.9 57,743.5 137,898.9	8.63
W4	28	18-27	1 2 3 4	0 4 12 32	2.49 21.92 58.28 143.46	92.8 21,445.6 51,936.4 151,290.0	7.35
W5	36	19-35	1 2 3 4	0 6 23 70	2.36 22.86 55.90 NA	0 24,066.1 104,353.1 319,225.7	7.49
W6	36	19-35	1 2 3 4	0 8 24 58	2.36 20.87 55.90 99.37	0 34,466.2 108,197.3 259,718.3	4.67

Table 4.11 shows the erosion rate and corresponding calculated volume of soil eroded of all samples at each water velocity. The volume of soil eroded in Table 4.11 was calculated using the custom stereo-photogrammetry program. Generally, the volume of soil eroded of samples tested at higher water temperatures were greater than the one tested under lower water temperature. The hydraulic shear stresses at 1 m/s water velocity in Table 4.11 were similar for each water temperature because they had the same roughness factor. Note that, the shear stress could not be calculated at the 4 m/s flow velocity for Sample W5 because a clod of soil was plucked from the Shelby tube during testing; therefore, the test was stopped and the soil surface roughness was not

measured. Although 28ºC samples (Sample W3 and W4) had measurable erosion via the photogrammetry method, the erosion was so small; thus, there was no difference in the friction factor. The critical shear stress in Table 4.11 was the shear stress that corresponded to 1 mm erosion (Briaud et al. 2001). The average critical shear stress of the 28ºC and 36ºC samples was lower than 17ºC sample, indicating that these samples were more susceptible to erosion. The samples tested at highest water temperature had the lowest critical shear stresses and exhibited the highest erosion rates. Overall, the erosion rate increased and the critical shear stress decreased with increasing water temperature.

4.5.2 Effect of soil temperature

When water temperature increased in the erosion tests, the soil temperature also increased. As shown in Table 4.11, the temperature of the soil increased from 19ºC to 35ºC during increased water temperature erosion tests. The discontinuities on the graph occurred when the erosion tests had to be stopped to measure the surface roughness and trim the sample before testing the next velocity.

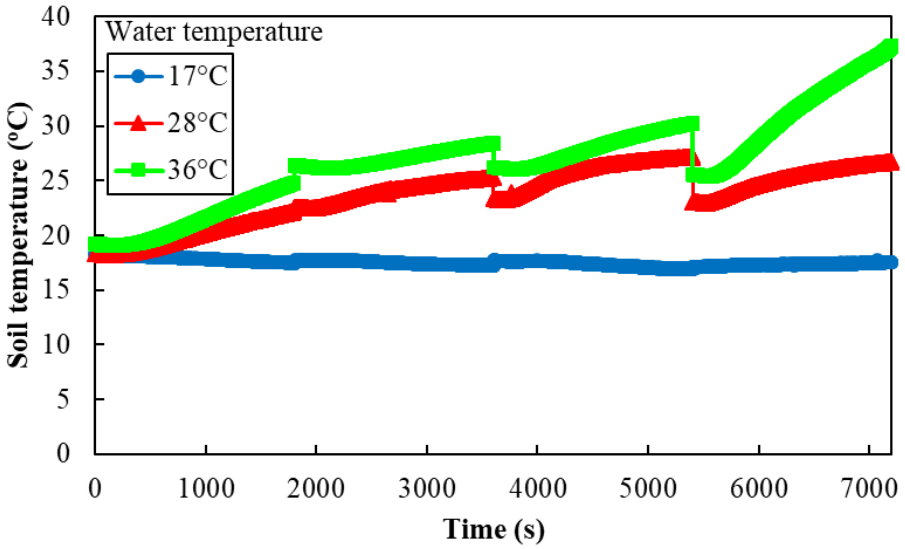

Figure 4.13 Increasing of soil temperature during erosion test at different water temperatures

Based on this phenomenon, in order to determine whether the water temperature alone or compounding effort of water temperature and soil temperature resulted in the change of erosion, eight more samples were tested at different soil temperature while water temperature was maintained at a constant value. This second set of erosion tests was used to disaggregate the effects of water temperature from soil temperature. The erosion tests were conducted at soil temperatures of 19°C, 25°C, 30°C, and 35°C and water temperature of 17°C. The results from the erosion tests are shown in Table 4.12 and Figure 4.14.

Again, no measurable erosion occurred at 1 m/s flow velocity for five of the eight samples. Samples S3, S6, and S8 had measurable erosion via the photogrammetry method. The erosion data points shown in Figure 4.14 were almost at the similar location at the same water flow velocity. All samples tested at 2 m/s flow velocity had the same erosion rate except Sample S2 (soil temperature of 19°C) and the samples at the maximum soil temperature of 35°C (Samples S7 and S8). Samples S7 and S8 eroded 2 times greater than the other samples at water velocity of 2 m/s and an average of 1.5 times more than all other samples 3 m/s. The erosion rate was approximately the same for all samples at the highest water velocity (4 m/s). The results from these experiments proved that when the soil temperature alone increased, the erodibility of soil did not increase as consistently (i.e., higher temperature resulting in higher erosion) as increased water temperature. However, increasing the soil temperature generally resulted in a decrease in critical shear stress as shown in Table 4.12.

Table 4.12 Summary of all erosion rates for different soil temperature of all samples

Sample	Water temperature (°C)	Soil temperature (°C)	Water velocity (m/s)	Erosion rate (mm/h)	Shear stress (Pa)	Volume of soil eroded (mm^3)	Critical shear stress (Pa)
S1	17	19	1 2 3 4	0 2 10 24	2.37 20.47 50.56 87.89	0 10,118.2 46,764.9 109,816.3	11.42
S2	17	19	1 2 3 4	0 0 8 20	2.37 17.48 47.19 95.88	0 2,236.0 38,068.9 93,953.8	21.19
S3	17	25	1 2 3 4	0 2 8 24	3.75 18.98 47.19 87.89	98.8 10,015.9 33,399.1 106,838.3	11.37
S4	17	25	1 2 3 4	0 2 8 26	2.37 18.98 49.44 95.88	0 11,087.7 34,245.0 116,434.5	10.68
S5	17	30	1 2 3 4	0 2 7 20	2.37 21.47 50.56 107.86	0 10,794.9 34,973.9 85,663.7	11.92
S6	17	30	1 2 3 4	0 2 9 20	4.24 20.97 60.67 109.86	782.6 9,027.0 36,647.4 86,777.2	12.61
S7	17	35	1 2 3 4	0 4 12 24	2.37 23.47 60.67 109.86	0 19,037.6 50,813.7 104,382.3	7.65
S8	17	35	1 2 3 4	0 4 12 25	4.12 23.47 65.17 97.88	882.2 19,231.8 57,953.6 110,346.4	8.96

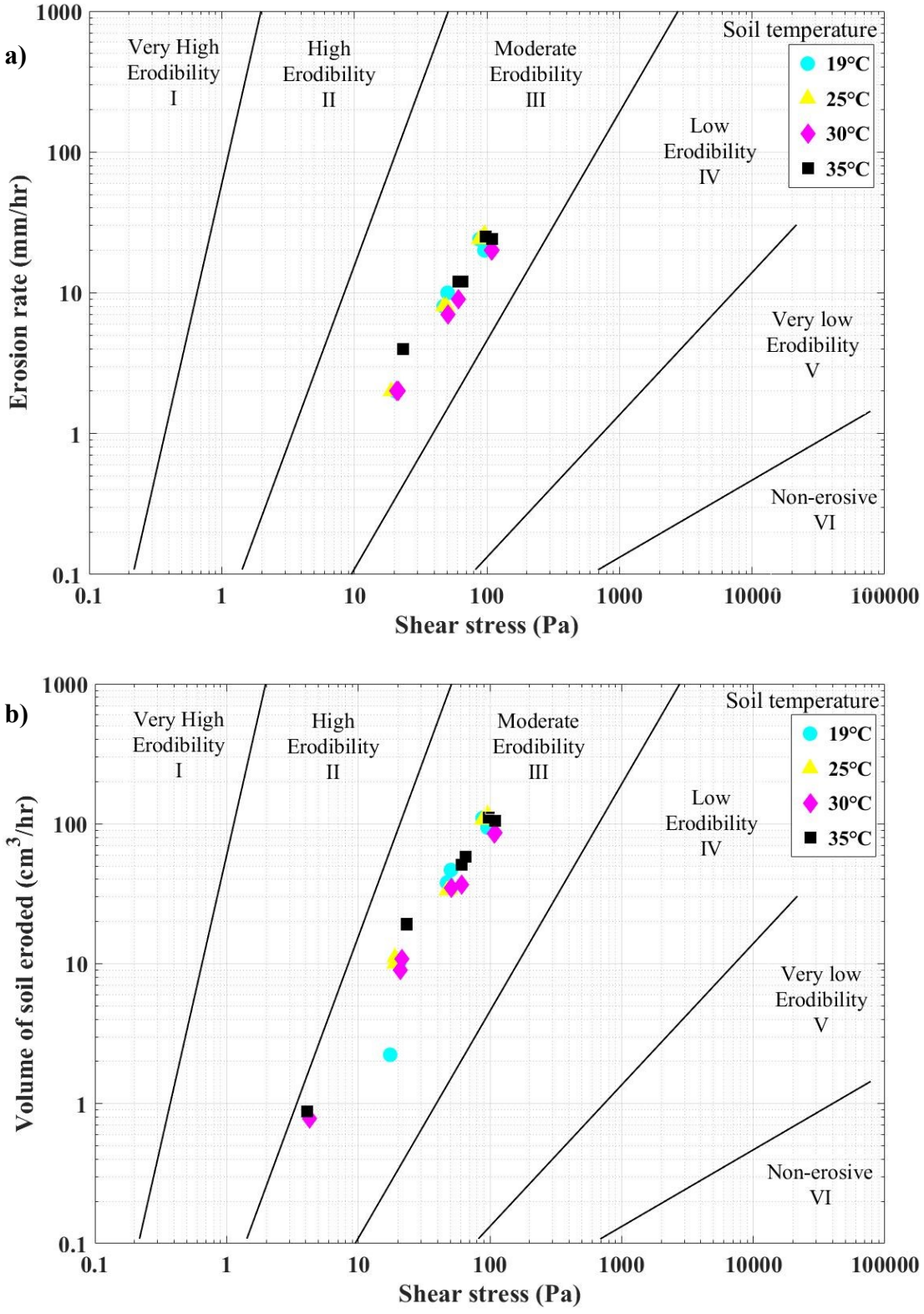

Figure 4.14 Comparison of soil erodibility for all heated samples

a) HEC–18; b) New erosion characterization chart

All soil erosion tests using an EFA are conducted in the laboratory and laboratory conditions vary at each research laboratory (i.e., ambient laboratory temperatures and fluctuation in laboratory temperatures). Moreover, most laboratory conditions do not reflect *in situ* conditions. For instance, ambient laboratory conditions in this study were 19ºC for the soil (from the humidity room) and 17ºC for the water temperatures (from the external water line). These temperatures were lower than the reported *in situ* temperature conditions in many regions of the US and worldwide. A review of USGS data in Kansas showed that the water temperature remains above 17ºC from March to November across the state. The results from this study indicated that when the water temperature was increased above ambient laboratory conditions, the soil erosion increased by as much as 184%. Therefore, soil erosion tests performed in laboratory conditions may be unconservative if the temperature parameters are not controlled in the test. Table 4.11 showed that when the water temperature increased 11ºC (from 17ºC to 28ºC), soil erosion increased approximately 38% at the highest water velocity (4 m/s). When the water temperature was further increased to 36ºC, the soil erosion rate increased 62% at 3 m/s flow velocity.

The effects of both water and soil temperatures in an erosion test on soil erodibility were still controversial. Some hypotheses have been carried out by previous researchers. For example, a study was conducted by Zreik et al. (1998) where erosion tests were run on soft, cohesive soil in a large rotating annular flume. The authors showed that a sample at 29ºC eroded more than a sample at 20ºC and conclude that an increase in soil temperature led to an increase in soil erosion. However, the water temperature in these experiments was not reported and it was also not clear what caused the increase in soil temperature in their study. Zreik et al. (1998) attributed the increase in soil erosion to a decrease in bond strength between the particles at temperature. On the other hand, Mehta and Prachure (2000) attributed the increase in the flowing water temperature to

a reduction in the inter-particle bonds. As mentioned previously, Larionov et al. (2014) hypothesized that increased water temperature increased soil erosion due to the reorientation of electrostatic forces between the monomolecular water layers around the soil particles, but their study was performed on coarse grained soils.

The goal of this study was to provide a better understanding what primarily caused the soil erosion variability, water temperature or soil temperature alone, or whether it was a compounding effect of water temperature and soil temperature. Therefore, two separate sets of erosion tests were conducted. As shown in Table 4.11Table 4.11, Samples W3 and W4 were tested under the water temperature of 28°C and the soil temperature rose during testing up to 27°C. The heated samples S3 and S4 in Table 4.12 were tested at a soil temperature of 25°C, while the water temperature was maintained at 17°C. The erosion rates of Samples W3 and W4 in Table 4.11 were approximately 1.5 times more than Sample S3 and S4 in Table 4.12. Similarly, the erosion rate of Samples W5 and W6 in Table 4.11 (water temperature of 36°C, soil temperature of 35°C) were also higher than Samples S7 and S8 in Table 4.12 (water temperature of 17°C, soil temperature of 35°C). These results showed that an increase in soil temperature would not lead to an increase in soil erosion as measured by Zreik et al. (1998). Thus, water temperature was the main factor that affect soil erodibility. An alternative hypothesis is that the increased water temperature would increase the kinetic energy (the energy that an object possesses due to its motion) of the soil particles in suspension circulating in the EFA flume. This increased motion may have created a "scrubbing effect" at the soil/water interface and therefore, the soil erosion increased. The two turbidity sensors will be used to test this hypothesis by future researchers.

As shown in both tables (Table 4.11 and Table 4.12), another interesting finding in this study was that the critical shear stress decreased in both the controlled water temperature and soil

temperature experiments. In other words, the soil started to erode sooner at higher temperatures in both experiments. The calculated critical shear stress in the soil temperature experiments (Samples S1-S8) were smaller than the water temperature experiments at the highest temperatures. The difference between increased erosion at higher water temperature versus decreased critical shear stress at higher soil temperatures have not been noted in previous studies. As a conclusion, this research confirmed soil erosion increases with an increase in water temperature; however, an increase in soil temperature alone did not result in a significant increase in erodibility of soil. More research is needed to develop a better understanding of how temperature affects the erodibility of cohesive soil.

This study has been submitted to the *ASTM Journal of Testing and Evaluation*: **Tran, T**., Tucker-Kulesza, S., and. Derby, M., "Temperature effects on cohesive soil erodibility," *ASTM Journal of Testing and Evaluation.*

4.6 Summary

This chapter demonstrates the application of the stereo-photogrammetry technique for measuring the surface roughness of the soil sample following an erosion test as well as the use of turbidity sensor and a new erosion characterization to get the precise measurements on soil erodibility. The effects of water and soil temperatures on soil erosion has also been investigated using the instrumentation of the EFA in this study. Moreover, the instrumentation of the EFA was utilized to characterize the erodibility of claypan soil and also can be used to evaluate the enhanced erosion resistance of engineered soils.

Chapter 5 - Scientific Contribution

5.1 Custom stereo-photogrammetry computational program

There are currently no exact methods for determining the surface roughness in soil erosion tests even though it is an important parameter in numerical and physical geotechnical soil models. It is used to obtain the hydraulic shear stress, which is one of the main parameters to determine the erodibility of soil. Different researchers have their own ways to measure this parameter; however, these methods are operator dependent, not applicable to small-scale experiments, or cannot be used for very soft material such as soil. Some of the methods also required highly specialized equipment, making them cost prohibitive. Photogrammetry techniques are used across many fields but have not been used for soil surface roughness measurements. Therefore, developing the stereo-photogrammetry computational program is one of the main contributions of this project (Tran et al. 2017). This method is not user dependent and accurately measures surface roughness while being cost effective. Additionally, the new method can be used for other applications where a measurement of soil surface roughness is required. This study was published in the *ASTM Geotechnical Testing Journal*. The paper can be found in with the reference: **Tran, T.** V., Tucker-Kulesza, S. E., and Bernhardt-Barry, M. L., "Determining Surface Roughness in Erosion Testing Using Digital Photogrammetry," *Geotechnical Testing Journal*, Vol. 46, No. 6, 2017, pp. 917–927, https://doi.org/10.1520/GTJ20160277

5.2 Turbidity measurements in soil erosion tests

Erosion measurements are important for engineering design or remediation purposes. Using turbidity measurements can evaluate the erodibility of materials that are typically difficult to measure, such as fat clays, soft rock, or engineered soils. The turbidity data were used in concert with the photogrammetry method to provide a more accurate measurement of soil erodibility in

the K-State EFA. This finding is a strong contribution not only for the EFA user but also for other erosion testing devices user. The preliminary results of the turbidity method were presented at the *International Foundation Congress and Equipment Expo (IFCEE)* 2018 in Orlando, Florida on March. The final paper has been published and can be found in with the reference: Tri V. Tran; Stacey E. Tucker-Kulesza; and Michelle Bernhardt, "Soil Surface Roughness and Turbidity Measurements in Erosion Testing," *IFCEE 2018: Advances in Geomaterial Modeling and Site Characterization-GSP 295-2018*, pp. 506–515, https:\\doi.org\\10.1061\\9780784481585.049

5.3 New erosion characterization chart

Erosion tests in the EFA are currently plotted according to the HEC–18. This figure includes the calculated applied hydraulic stress versus the measured erosion rate, in length per time. This HEC–18 figure is a log-log plot and precise measurements cannot be directly compared. Moreover, all zero erosion data points cannot be seen in this chart which make it hard to compare low erodibility samples, specifically when investigating small changes in soil properties to gain a better understanding of the root causes of soil erosion. The new erosion characterization chart is based on the HEC–18 erosion classification; however, instead of showing the erosion rate versus the calculated applied hydraulic stress, these charts show the applied hydraulic shear stress versus the volume of soil eroded or the cumulative turbidity difference in erosion tests. By plotting in this way, all of the "zero" erosion data points will be shown which helps to improve visualization of the erodibility of the materials that are difficult to quantify.

5.4 Evaluating the enhanced erosion resistance of engineered soil

Engineered soil may be a way to reduce projected increases in soil erosion. The polymer-modified MICP approach is an effective and efficient method for preventing water-induced surficial erosion. This treatment improves the strength of soil in the surficial regions and therefore

the treated soil is more erosion resistant. Traditional EFA tests could not quantify the amount of erosion for these low erodibility soils. The novel instrumentation in this research should be used to evaluate the impacts of engineered soil on soil erodibility in future research. The study was published in the *ASCE Journal of Materials in Civil Engineering* and can be found in with the reference: Wang, X., Tao, J., Bao, R., **Tran, T**., and Tucker-Kulesza, S. "Surficial soil stabilization against water-induced erosion using polymer-modified microbially-induced carbonate precipitation," *Journal of Materials in Civil Engineering*, Vol. 30, No. 10, 2018, 04018267, https://doi.org/10.1061/(ASCE)MT.1943-5533.0002490

5.5 Investigating the erodibility of claypan soils

Claypan soils are impervious, limiting water infiltration and restricting agricultural productivity. Based on an extensive literature review, no measurements have been conducted to quantify the erodibility of claypans soils to date. Therefore, this study helped to determine the erodibility of claypan soils to better understanding erosion potential of claypan soils. These soils were also used to evaluate the new erosion chart methodology using photogrammetry. The value of the new method, compared to the traditional HEC–18 method was highlighted in Chapter 4. The new method allowed direct comparison of when the soil actually started to erode, versus what was measurable via the traditional HEC–18 chart. In fact, the new methodology was developed after this study was published. The results in the published article are not plotted using the HEC–18 graph because it was not possible to see all of the data and to compare the soil samples with the original methodology. This study can be found in *American Society of Agricultural and Biological Engineers* with the reference: S. Tucker-Kulesza, G.F. Sassenrath**, Tran, T.**, W. Koehn, L. Erickson, "Site-Specific Erodibility in Claypan Soils: Dependence on Subsoil Characteristics,"

Applied Engineering in Agriculture, Vol. 33, No. 5, 2017, pp. 705–718, https://doi.org/10.13031/aea.12120.

5.6 Effect of water and soil temperature on erodibility

The temperature of rivers, lakes, and the oceans are changing. Whether by climate change or from increased and warmer runoff from impervious surfaces, the temperature of eroding fluid is increasing; thus, the erosion rate will change. The current theories explaining how temperature affects the erodibility of soil are still controversial. The finding from this aspect of the study will help to improve the understanding of the effect of temperature on soil erosion. This research confirmed that water temperature was the main factor that affect soil erodibility. Soil erosion increases with an increase in water temperature; however, an increase in soil temperature alone did not result in significantly increasing the erodibility of soil. This study has been submitted to the *ASTM Journal of Testing and Evaluation* with the reference: **Tran, T**., Tucker-Kulesza, S., and. Derby, M., "Temperature effects on cohesive soil erodibility," *ASTM Journal of Testing and Evaluation.*

.

Chapter 6 - Conclusions and Future Work

6.1 Conclusions

6.1.1 Stereo-photogrammetry method

A custom digital stereo photogrammetry method was developed to reconstruct 3D images of soil sample surfaces and a roughness measurement was determined following an erosion test. The model was validated using a manufactured red disk to measure the surface roughness by structured light scanner, photogrammetry, and hand caliper methods. The RMS roughness, R_q, is recommended for all future soil surface roughness measurement because it gave consistent results regardless of the number of measured points. The RMS roughness for the red disk from the photogrammetric program was less than 0.09 mm different than a full scan taken using a structured light scanner; whereas the roughness measured with hand caliper was within 0.26 mm. Therefore, the new photogrammetric method is more accurate. The feasibility of the method has been confirmed in the application examples for the laboratory and field-retrieved soil samples. The number of detected points (13,637 points) in the field-retrieved sample was approximately two times as much as the laboratory soil sample (6,830 points). This was likely because of the surface condition (rougher, multicolored, and darker) of the field-retrieved sample.

The stereo photogrammetry system is automated and the roughness measurements are more precise. This removed the operator dependence without requiring highly specialized equipment. The camera (approximately $500) and MATLAB software are all that is needed for using this method. The surface roughness of soil samples was compared to the traditional method (hand calipers). The results showed that different users with hand calipers get different erosion data points. This finding again confirmed that caliper method is user dependent and is not

recommended using for future research. Furthermore, the point cloud generated from the stereo-photogrammetry method was used to develop a new erosion characterization chart.

6.1.2 Turbidity measurements in erosion testing

Six field-retrieved soil samples from southeastern Kansas were measured using all EFA instrumentation. The turbidity of water in erosion tests was collected and erosion parameters were obtained using stereo-photogrammetry method. This precise roughness measurement was used to support the new addition of turbidity sensors. The results showed that the turbidity sensors are capable of measuring erosion more accurately than the traditional methods used in EFA testing. The turbidity of the water circulating in the flume increased as erosion occurred. Cumulative turbidity difference between the measurements upstream and downstream from the sample were then calculated. In general, higher erosion rate resulted in a higher cumulative turbidity difference. However, the results were not consistent. More samples need to be tested in the future to confirm the finding in this study. The results from turbidity measurements also provided a secondary measurement of erosion. These precise measurements may be used to compare the erodibility of samples that do not easily erode, such as soft rocks or engineered samples.

6.1.3 New erosion characterization chart

In this study, a new erosion chart was developed using the instrumentation of the EFA. The results from erosion tests are commonly plotted using HEC–18 erodibility categorizing plot; however, the drawback of this plot is that all zero erosion points cannot be seen in the graph and the precise measurements cannot be directly compared. The new erosion characterization chart shows the volume of soil eroded in erosion tests versus the calculated hydraulic shear stress and the cumulative turbidity difference versus the calculated hydraulic shear stress. These charts help to improve visualization of the erodibility of the samples that are typically difficult to measure.

The results from six field-retrieved soil samples above were used for analysis and plotted in the new charts. All zero erosion data points were presented in the graph allowing user to compare point by point the erodibility of soils.

6.1.4 Application of the EFA instrumentation to the engineered soils and in-situ soil samples

The EFA tests has been conducted in the study to evaluate the enhanced erosion resistance of engineer soils. Ottawa sand samples were treated with a polymer-modified MICP solution (a mixture of dyed median concentration polymer-modified cementation solution and bacteria solution). This treatment improves the strength of soil in the surficial regions and therefore the treated soil is more erosion resistant. The results of the controlled EFA tests show that the treated sample had no erosion, except at the very high flow velocity (6 m/s). The treated sample classified as low/very low erodibility on the velocity and shear stress charts. The results were agreed well with the results from a flume test conducted by the co-authors. In this study, it would be very difficult to quantify the critical shear stress and amount of soil erosion if using the traditional EFA test. However, measurable erosion could be obtained using instrumentation of the EFA and the new erosion characterization methodology.

The application of the EFA instrumentation has been shown in the study to characterize the erodibility of claypan soils. Soil samples from two sites were brought to the laboratory for the controlled erosion testing. This study quantified soil erodibility in agricultural fields to investigate the erodibility of claypan soils. One sample was collected from a highly productive region of the field and the other from an unproductive area. The hydraulic shear stress was calculated using the digital photogrammetry. There was no measurable erosion of either sample at low water velocity. However, the applied shear stress via photogrammetry was measured and the effective hydraulic

stress was calculated. The critical shear stress for the high yield area (saturated clayey sand soil) was 35.3 Pa whereas the critical shear stress for the low-yield area (claypan soil) was 103.5 Pa, indicating the low yield region was more erosion resistant. Recall that critical shear stress is a key measurement in soil erodibility and a more accurate calculation of the critical shear stress helped to further characterize the claypan soils in this study.

6.1.5 Effect of water and soil temperature on erodibility

This study examined the effect of water and soil temperatures in remolded kaolin-sand mixtures on surface soil erodibility using the instrumentation of the EFA. Two different set of erosion tests were conducted. At first, six soil samples were tested under water temperatures of 17ºC, 28ºC, and 36ºC. The results showed that the soil tested under high water temperatures (i.e., 28ºC and 36ºC) exhibited higher erosion rates than the samples tested under 17ºC water temperature. During testing, the soil temperature was also monitored by two thermal couples (at the middle and the edge of soil sample). The results indicated that increasing the water temperature lead to an increase in soil temperature. Thus, eight more soil samples were tested at various soil temperatures at the laboratory water temperature (17ºC) to determine whether water temperature or soil temperature independently or combined of both parameters effect soil erosion. The obtained results indicated increasing the soil temperature alone did not consistently impact the soil erosion rates; therefore, the variability in soil erosion was primarily due to the change in water temperature. The other finding in this study was that soil tended to erode sooner at the high soil temperature. This finding has not been reported in the previous erosion studies. The effect of water and soil temperature on cohesive soil may be used to hypothesize the influence of temperature on cohesive soil erosion, which is needed to improve soil erosion models that are typically over conservative. This study also highlights the need for controlling the water temperature during

erosion testing, which has not been done in the past in order to more accurately measure the soil erosion to be representative of field conditions.

In conclusion, the interactions among the physical, geochemical, and biological properties of soil need to be further investigated to find the correlations between multiple properties and soil erodibility. The objective of this research was to instrument an erosion device to establish a methodology for future researchers to study these interactions. The finding from this study (i.e., stereo-photogrammetry method, turbidity measurement, new erosion characterization methodology) will allow future researchers to take a deeper look into soil erosion, especially fine-grained soil. The instrumentation of this study was used to specifically identify the influence of temperature change on soil erosion. This is the first study to establish that the fluid (water) temperature influences the soil temperature and the fluid temperature is primarily the controlling factor related to soil erodibility.

6.2 Future work

Turbidity measurement in an erosion test was shown to be very useful. It is not only able to evaluate the erodibility of materials that are difficult to erode but it may also be used in the future to reduce the amount of time spent on the erosion test. Thus, finding relationship between the turbidity measurements and volume of soil eroded in erosion test will be a strong contribution in the future in term of economics. Instead of spending an hour for each velocity in an EFA test, one may only test for approximately 10 minutes and predict the future data based on turbidity measurements. Additional research is needed on filtering and data processing of the turbidity sensors so they can consistently be used to report EFA results. This will allow the evaluation of shortening the EFA test so more experiments can be conducted by practitioners as opposed to assuming soil properties conservatively due to cost constraints.

In this study, the water used in erosion tests was from a connected water line that was treated for commercial uses. Therefore, this does not simulate field water conditions which may have different properties. The properties of water in the river or stream, such as the organic matter (dissolved organic carbon), inorganic nutrients, turbidity, and dissolved solids are likely very different from potable tap water. Thus, there is a need for a study that investigates the effect of clean water versus river (for example) water in erosion tests. There is also limited information regarding the effects of recirculating water versus using clean water throughout an EFA test. This can be evaluated by having a second reservoir in the EFA where the water flow from downstream will go to the second tank. The first reservoir will be used to get the clean water from the water line so that the pump can drive the water through the test section in the EFA. The clean versus recirculated water experiments were planned in this research, however the second reservoir was not available during the project.

Finally, as stated in Chapter 1, erosion in cohesive soils is a complex function of physical, geochemical, and biological soil properties. The interactions among the physical, geochemical, and biological properties of soil need to be further investigated to find the relationship between multiple properties and erodibility of the soils (Grabowski et al. 2011). The physical soil properties consist of mean particle size, particle size distribution, bulk density, water content, and temperature. These properties have been extensively investigated by many researchers in the past. However, there is very little research in the literature to the best of the author's knowledge that investigate the effect of geochemical properties of soil on erosion. One of these properties is the organic matter content. Soil organic matter is important to soil fertility, sustainable agriculture systems, and crop productivity. Crop yields are often larger in soils with more organic matter compared to those with less (Johnston et al. 2009). Organic matter content influences soil erosion

(Guerra 1994); however, it has not been evaluated. The influence of organic matter on soil erodibility of soil can now be measured with the novel instrumentation of the EFA. Additionally, the new erosion characterization chart is capable showing small changes as needed in soil erosion tests.

References

Alarcon, V. J., and Sassenrath, G. F., "Modeling cotton (*Gossypium* spp.) leaves and canopy using computer aided geometric design (CAGD)," *Ecological Modelling*, Vol. 222, No. 12, 2011, pp. 1951-1963, https://doi.org/10.1016/j.ecolmodel.2011.03.037

Alexandru, A., "Introduction in Architectural Photogrammetry", *Journal of Young Scientist*, Vol. 4, 2016, pp. 119–124

Amos, C.L., Bergamasco, A., Umgiesser, G., Cappucci, S., Cloutier, D., DeNat, L., Flindt, M., Bonardi, M., Cristante, S., "The stability of tidal flats in Venice Lagoon — the results of in-situ measurements using two benthic, annular flumes," *Journal of Marine Systems*, Vol. 51, No. 1, 2004, pp. 211–241

Arneson, L. A., Zevenbergen, L. W., Lagasse, P. F., and Clopper, P. E., "Evaluating scour at bridges," Report No. FHWA-HIF-12-003, 2012

ASTM D2216-10, 2010, Standard Test Methods for Laboratory Determination of Water (Moisture) Content of Soil and Rock by Mass, ASTM International, West Conshohocken, PA, www.astm.org

Avnimelech, Y., Ritvo, G., Meijer, L. E., and Kochba, M., "Water content, organic carbon and dry bulk density in flooded sediments," *Aquacultural engineering*, Vol. 25, No. 1, 2001, pp. 25-33

Bale, A. J., Stephens, J. A., and Harris, C. B., "Critical erosion profiles in macro-tidal estuary sediments: Implications for the stability of intertidal mud and the slope of mud banks," *Continental Shelf Research*, Vol. 27, No. 18, 2007, pp. 2303–2312, https://doi.org/10.1016/j.csr.2007.05.015

Ballio, F. and Radice, A., "A Non-Touch Sensor for Local Scour Measurements," *Journal of Hydraulic Research*, Vol. 41, No. 1, 2003, pp. 105–108, https://doi.org/10.1080/00221680309499934

Benahmed, N. , and Bonelli, S., "Investigating Concentrated Leak Erosion Behavior of Cohesive Soils by Performing Hole Erosion Tests," *European Journal of Environmental and Civil*

Engineering, Vol. 16, No. 1, 2012, pp. 43-58, https://doi.org/10.1080/19648189.2012.667667

Bemis, S. P., Micklethwaite, S., Turner, D., James, M. R., Akciz, S., Thiele, S. T., and Bangash, H. A., "Ground-based and UAV-based photogrammetry: A multi-scale, high-resolution mapping tool for structural geology and paleoseismology," *Journal of Structural Geology*, Vol. 69, 2014, pp. 163-178

Bernhardt, M. L., Briaud, J. L., Kim, D., Leclair, M., Storesund, R., Lim, S. G., Bea, G. R., and Rogers, J. D., "Mississippi River Levee Failures: June 2008 Flood," *International Journal of Geoengineering Case History*, Vol. 2, No. 3, 2011, pp. 127–162

Bloomquist, D., Sheppard, D. M., Schofield, S., Crowley, R. W., "The rotating erosion testing apparatus (RETA): A laboratory device for measuring erosion rates versus shear stresses of rock and cohesive materials," *Geotechnical Testing Journal*, Vol. 35, No. 4, 2012, pp. 641-648, https://doi.org/10.1520/GTJ104221

Brady, N.C. and Weil, R.R., "The Nature and Properties of Soils," Prentice Hall, Upper Saddle River, 2002, pp. 960, New Jersey

Briaud, J., Bernhardt, M., and Leclair, M., "The Pocket Erodometer Test: Development and Preliminary Results," *Geotechnical Testing Journal*, Vol. 35, No. 2, 2012, pp. 342-352, https://doi.org/10.1520/GTJ102889. ISSN 0149-6115

Briaud, J.L., Ting, F., Chen, H.C., Gudavalli, R., Perugu, and S., Wei, G., "SRICOS: Prediction of Scour Rate in Cohesive Soils at Bridge Piers," *Journal of Geotechnical and Geoenvironmental Engineering*, Vol. 125, No. 4, 1999, pp. 237-246, https://doi.org/10.1061/(ASCE)1090-0241(1999)125:4(237)

Briaud, J. L., Ting, F., Chen, H. C., Cao, Y., Han, S. W., and Kwak, K. W., "Erosion Function Apparatus for Scour Rate Predictions," *Journal of Geotechnical and Geoenvironmental Engineering,* Vol. 127, No. 2, 2001, pp. 105–113, https://doi.org/10.1061/(ASCE)1090-0241(2001)127:2(105)

Brubaker, K. L., Ghelardi, V., Goodings, D., Guy, L., and Pathak, P., "Estimation of Long Term Scour at Maryland Bridges Using EFA/SCRICOS," Report MD-04-SP107B4E, 2004,

Department of Civil & Environmental Engineering, University of Maryland, College Park, MD 20742

Calappi, T., Miller, C. J., & Carpenter, D. (2010). Revisiting the HEC–18 Scour Equation. In *Scour and Erosion* (pp. 1102-1109). ASCE

Coleman, S. E., Lauchlan, C. S., and Melville, B. W., "Clear-Water Scour Development at Bridge Abutments," *Journal of Hydraulic Research*, Vol. 41, No. 5, 2003, pp. 521-531

Cooner, S. A. and Balke, K. N., "Use Of Photogrammetry For Investigation Of Traffic Incident Scenes," Report 4907-2, Texas Transportation Institute, The Texas A&M University, System College Station, Texas

Crowley, R. W., Bloomquist, D., Shah, F. D., Holst, C. M., "The sediment erosion rate flume (SERF): A new testing device for measuring soil erosion rate and shear stress," *Geotechnical Testing Journal*, Vol. 35, No. 4, 2012, pp. 649-659, https://doi.org/10.1520/GTJ103814

Dade, W.B., Nowell, A.R.M., Jumars, P.A., "Predicting erosion resistance of muds," *Marine Geology*, Vol. 105, No. 1–4, 1992, pp. 285–297, https://doi.org/10.1016/0025-3227(92)90194-M

Debnath, K., Nikora, V., Elliott, A., "Stream Bank Erosion: In Situ Flume Tests," *Journal of irrigation and drainage engineering*, Vol. 133, No. 3, 2007, pp. 256-264, https://doi.org/10.1061/(ASCE)0733-9437(2007)133:3(256)

Derenyi, E. E., 1982, Photogrammetry for Civil and Forest Engineers: Lecture Notes, Department of Surveying Engineering University of New Brunswick

Droppo, I. G., Lau, Y. L., and Mitchell, C., "The effect of depositional history on contaminated bed sediment stability," *Science of the Total Environment*, Vol. 266, No. 1, 2001, pp. 7-13

Fischer, L., Kääb, A., Huggel, C., and Noetzli, J., "Geology, Glacier Retreat and Permafrost Degradation as Controlling Factors of Slope Instabilities in a High-Mountain Rock Wall: The Monte Rosa East Face," *Natural Hazards and Earth System Science*, Vol. 6, No. 5, 2006, pp. 761-772

Gadelmawla, E. S., Koura, M. M., Maksoud, T. M. A., Elewa, I. M., & Soliman, H. H., "Roughness parameters," *Journal of Materials Processing Technology*, Vol. 123, No. 1, 2002, pp. 133-145

Grabowski, R., Droppo, I., and Wharton, G., "Erodibility of Cohesive Sediment: The Importance of Sediment Properties," *Earth-Science Reviews,* Vol. 105, No. 3-4, 2011, pp. 101–120, https://doi.org/10.1016/j.earscirev.2011.01.008

Guerra, A., "The effect of organic matter content on soil erosion in simulated rainfall experiments in W. Sussex, UK," *Soil Use and Management*, Vol. 10, No. 2, 1994, pp. 60-64, https://doi.org/10.1111/j.1475-2743.1994.tb00460.x

Haghighi, I., Chevalier, C., Duc, M., Guédon, S., and Reiffsteck, P., "Improvement of hole erosion test and results on reference soils," *Journal of Geotechnical and Geoenvironmental Engineering*, Vol. 139, No. 2, 2012, pp. 330-339

Hamdan, N., Zhao, Z., Mujica, M., Kavazanjian Jr, E., and He, X., "Hydrogel-assisted enzyme-induced carbonate mineral precipitation," *Journal of Materials in Civil Engineering*, Vol. 28, No.10, 2016, https://doi.org/10.1061/(ASCE)MT.1943-5533.0001604

Hansen, L. T., Breneman, V. E., Davison, C. W., and Dicken, C. W, "The cost of soil erosion to downstream navigation," *Journal of Soil and Water Conservation*, Vol. 57, No. 4, 2002, pp. 205-212

Hanson, G. J. and Cook, K. R., "Apparatus, test procedures, and analytical methods to measure soil erodibility in situ," *Applied Engineering in Agriculture*, Vol. 20, No. 4, 2004, pp. 455-462

Hartley, R., and Zisserman, A., 2004, Multiple View Geometry in Computer Vision, 2nd ed., Cambridge University Press, New York

Houwing, E. J., "Determination of the critical erosion threshold of cohesive sediments on intertidal mudflats along the Dutch Wadden Sea coast," *Estuarine, Coastal and Shelf Science*, Vol. 49, No. 4, 1999, pp. 545-555

Isakson, M. J. and Chotiros, N. P., "Finite Element Modeling of Acoustic Scattering from Fluid and Elastic Rough Interfaces," *IEEE Journal of Oceanic Engineering*, Vol. 40, No. 2, 2015, pp. 475-484

Jepsen, R., Roberts, J., and Lick, W., "Effects of bulk density on sediment erosion rates," *Water, Air, and Soil Pollution*, Vol. 99, No. 1-4, 1997, pp. 21-31, Springer Netherlands

Johnston, A. E., Poulton, P .R., and Coleman, K., "Chapter 1 Soil Organic Matter: Its Importance in Sustainable Agriculture and Carbon Dioxide Fluxes," *Advances in Agronomy*, Vol. 101, 2009, pp. 1-57, https://doi.org/10.1016/S0065-2113(08)00801-8

Kandiah, A., "Fundamental aspects of surface erosion of cohesive soils," PhD Thesis, University of California, Davis, 1974

Kimiaghalam, N., Clark, S. P., and Ahmari, H., "An Experimental study on the effects of physical, mechanical, and electrochemical properties of natural cohesive soils on critical shear tress and erosion rate," *International Journal of Sediment Research*, Vol. 31, 2016, pp. 1-15, https://doi.org/10.1016/j.ijsrc.2015.01.001

Karim, Z.Md. and Tucker-Kulesza, S., "Predicting Soil Erodibility Using Electrical Resistivity Tomography," *Journal of Geotechnical and Geoenvironmental Engineering*, Vol. 144, No. 4, 2018, https://doi.org/10.1061/(ASCE)GT.1943-5606.0001857

Lambrou, T. P., Anastasiou, C. C., and Panayiotou, C. G. (2009). "A Nephelometric Turbidity System for Monitoring Residential Drinking Water Quality," In SENSAPPEAL 43-55.

Lança, R.M., Fael, C. S., Maia, R. J., Pêgo, J. P., and Cardoso, A.H., "Clear-Water Scour at Comparatively Large Cylindrical Piers," Journal of Hydraulic Engineering, Vol. 139, No. 11, 2013, pp. 1117–1125, https://doi.org/10.1061/(ASCE)HY.1943-7900.0000788

Larionov, G. A., Bushueva, O. G., Dobrovol'skaya, N. G., Kiryukhina, Z. P., Krasnov, S. F., and Litvin, L. F., "Effect of the water temperature and soil moisture on the erodibility of chernozem samples: A model experiment," *Eurasian Soil Science,* Vol. 47, No. 7, 2014, pp. 734–736, https://doi.org/10.1134/S1064229314070096

Larsen, R. J., Ting, F. C., and Jones, A. L., "Flow Velocity and Pier Scour Prediction in a Compound Channel: Big Sioux River Bridge at Flandreau, South Dakota," *Journal of Hydraulic Engineering*, Vol. 137, No. 5, 2010, pp. 595–605

Lau, Y. L. and Droppo, I. G., "Influence of antecedent conditions on critical shear stress of bed sediments," *Water Research*, Vol. 34, No. 2, 2000, pp. 663-667

Lick, W. and McNeil, J., "Effects of sediment bulk properties on erosion rates," *Science of the Total Environment*, Vol. 266, No. 1, 2001, pp. 41-48

Liu, T., Burner, A. W., Jones, T. W., and Barrows, D. A., "Photogrammetric techniques for aerospace applications," *Progress in Aerospace Sciences*, Vol. 54, 2012, pp. 1-58

Liu, Y. and Kang, J., "Application of Photogrammetry: 3D Modeling of a Historical Building," presented at the Construction Research Congress 2014: Construction in a Global Network, Atlanta, GA, American Society of Civil Engineers, Reston, VA, https://doi.org/10.1061/9780784413517.023

Luhmann, T., Robson, S., Kyle, S., and Harley, I., 2007, Close Range Photogrammetry: Principles, Techniques and Applications, John Wiley and Sons, Inc., Hoboken, New Jersey

Maas, H.-G. and Hampel, U., "Photogrammetric Techniques in Civil Engineering Material Testing and Structure Monitoring," *Photogrammetric Engineering and Remote Sensing*, Vol. 72, No. 1, 2006, pp. 39–45, https://doi.org/10.14358/PERS.72.1.39

MATLAB R2015a, The MathWorks Inc., Natick, MA, 2000

Mehta, A.J. and Parchure, T.M., "Surface erosion of fine-grained sediment revisited," In: Flemming, B.W., Delafontaine, M.T., Liebezeit, G. (Eds.), Muddy Coast Dynamics and Resource Management, 200, pp. 55-84, Elsevier, London

Moody, L. F., "Friction Factors for Pipe Flow," *Transactions of the American Society of Mechanical Engineers*, Vol. 66, No. 8, 1944, pp. 671-684

Moore, W.L. and Masch, F.D., "Experiments on the scour resistance of cohesive sediments." *Journal of Geophysical Research*, Vol. 67, No. 4, 1962, pp. 1437-1449

Morgan, R.P.C., "Soil Erosion and Conservation," Blackwell, 2005, pp. 304, Oxford

Munson, B. R., Young, D. F., and Okiishi, T. H., 1990, Fundamentals of Fluid Mechanics, Wiley, New York

Panagiotopoulos, I., Voulgaris, G., and Collins, M. B., "The influence of clay on the threshold of movement of fine sandy beds," *Coastal Engineering*, Vol. 32, No. 1, 1997, pp. 19-43

Partheniades E. 2007. Engineering Properties and Hydraulic Behavior of Cohesive Sediments. CRC Press, Taylor & Francis Group. London ISBN: 9780849375552

Poon, C. Y. and Bhushan, B., "Comparison of Surface Roughness Measurements by Stylus Profiler, AFM and Non-Contact Optical Profiler," *Wear*, Vol. 190, No. 1, 1995, pp. 76-88

Porter, K., Simons, R., and Harris, J., "Comparison of Three Techniques for Scour Depth Measurement: Photogrammetry, Echosounder Profiling and a Calibrated Pile," *Coastal Engineering Proceedings*, Vol. 1, No. 34, 2014, pp. 64

Raposo, M., Ferreira, Q., and Ribeiro, P. A., "A Guide for Atomic Force Microscopy Analysis of Soft-Condensed Matter," Modern research and educational topics in microscopy, 1, 2007, pp. 758-769

Ravens, T. M., "Comparison of two techniques to measure sediment erodibility in the Fox River, Wisconsin," *Journal of Hydraulic Engineering*, Vol. 133, No. 1, 2007, pp. 111-115, https://doi.org/10.1061/(ASCE)0733-9429(2007)133:1(111)

Richardson, E. V., Pagan-Ortiz, J. E., Schall, J. D., & Price, G. R. (2003). *Monitoring and Plans for Action for Bridge Scour: Instruments and State Departments of Transportation Experiences* (No. E-C049)

Rowell, D.L., "Soil Science: Methods and Applications," Longman, Harlow, 1994, pp. 350

Samuel, H. C., Frazier, P., Joel, G. M., John, E. C., and Oktay, G., "Erosion Characteristics of Alabama Soils Obtained with the Erosion Function Apparatus and Correlations with Classification Properties," Report 930-490, 2003, Alabama Department of Transportation, Montgomery, AL, September

Sang, J., Allen, P., Dunbar, J., and Hanson, G., "Development of semi-physically based model to predict erosion rate of kaolinite clay under different moisture content," *Canadian Geotechnical Journal*, Vol. 52, No. 5, 2015, pp. 577-586, https://doi.org/10.1139/cgj-2012-0274

Schaaff, E., Grenz, C., Pinazo, C., Lansard, B., "Field and Laboratory Measurements of Sediment Erodibility: A Comparison," *Journal of Sea Research*, Vol. 55, No. 1, 2006, pp. 30-42

Shan, H., Shen, J., Kilgore, R., and Kerenyi, K., "Scour in Cohesive Soils," Report No. FHWA-HRT-15-033, 2015

Shan, H., Kerenyi, K., Guo, J., Shen, J. Wagner, A., and Xie, Z., "An ex-situ scour testing device for characterizing erosion of cohesive soils," 6th International Conference on Scour and Erosion (ICSE-6), 2012, Paris

Shanahan, C. and Montoya, B. (2016). "Erosion reduction of coastal sands using microbial inducedcalciteprecipitation," Geo-Chicago 2016: Sustainability and Resiliency in Geotechnical Engineering, number GSP 269, https://ascelibrary.org/doi/abs/10.1061/9780784480120.006

Sheppard, D. M. and Miller Jr. W., "Live-Bed Local Pier Scour Experiments," *Journal of Hydraulic Engineering*, Vol. 132, No. 7, 2006, pp. 635-642

Simons, R. R., Weller, J., and Whitehouse, R. J. S., 2007, "Scour development around truncated cylindrical structures," presented at the 5th Coastal Structures International Conference, CSt07, Venice, Italy, University College London, London, United Kingdom, pp. 2–4

Stahlmann, A. and Schlurmann. T., "Physical Modeling of Scour around Tripod Foundation Structures for Offshore Wind Energy Converters," *Proceedings of 32nd Conference on Coastal Engineering (ICCE)*, American Society of Civil Engineers (ASCE), Shanghai, China, July 2010

Straub, T. D. and Over, T. M., "Pier and Contraction Scour Prediction in Cohesive Soils at Selected Bridges in Illinois," Report FHWA-ICT-10-074, 2010, U.S. Geological Survey, Urbana, IL

Tran, T. V., Tucker-Kulesza, S. E., and Bernhardt-Barry, M. L., "Determining Surface Roughness in Erosion Testing Using Digital Photogrammetry," *Geotechnical Testing Journal,* Vol. 46, No. 6, 2017, pp. 917–927, https://doi.org/10.1520/GTJ20160277

Tucker-Kulesza, S., Sassenrath, G.F., Tran, T., Koehn, W., Erickson, L. "Site-Specific Erodibility in Claypan Soils: Dependence on Subsoil Characteristics," *Applied Engineering in Agriculture*, Vol. 33, No. 5, 2017, pp. 705–718, https://doi.org/10.13031/aea.12120

Thomsen, L. and Gust, G., "Sediment erosion thresholds and characteristics of suspended aggregates on the western European continental margin," *Deep Sea Research Part I: Oceanographic Research Papers*, Vol. 47, No. 10, pp. 1881-1897

Thomsen, L. M., Baartman, J. E. M., Barneveld, R. J., Starkloff, T., and Stolte, J., "Soil Surface Roughness: Comparing Old and New Measuring Methods and Application in a Soil Erosion Model," Soil, Vol. 1, No. 1, 2015, p. 399, https://doi.org/10.5194/soil-1-399-2015

Van Ledden, M., Van Kesteren, W. G. M., and Winterwerp, J. C., "A conceptual framework for the erosion behaviour of sand–mud mixtures," *Continental Shelf Research*, Vol. 24, No. 1, 2004, pp. 1-11

Verstraeten, G., Poesen, J., Govers, G., Gillijns, K., van Rompaey, A., van Oost, K., "Integrating science, policy and farmers to reduce soil loss and sediment delivery in Flanders (Belgium)," *Environmental Science and Policy*, Vol. 6, No. 1, 2003, pp. 95–103, https://doi.org/10.1016/S1462-9011(02)00116-8

Wan, C. F. and Fell, R., "Laboratory tests on the rate of piping erosion of soils in embankment dams," *Geotechnical Testing Journal*, Vol. 27, No. 3, 2004, pp. 295-303, https://doi.org/10.1520/GTJ11903

Wang, X., Tao, J., Bao, R., Tran, T., and Tucker-Kulesza, S., "Surficial soil stabilization against water-induced erosion using polymer-modified microbially-induced carbonate precipitation", *ASCE Journal of Materials in Civil Engineering*, Vol. 30, No. 10, 2018, https://doi.org/10.1061/(ASCE)MT.1943-5533.0002490

Whiteman, T., Lichti, D. D., and Chandler, I., 2002, July, "Measurement of Deflections in Concrete Beams by Close-Range Digital Photogrammetry," Proceedings of the Symposium on Geospatial Theory, Processing and Applications, pp. 9–12, Ottawa, Canada

Winterwerp, J. C. and Van Kesteren, W. G., "Introduction to the physics of cohesive sediment dynamics in the marine environment" Vol. 56, 2004, Elsevier

Yatsui, T., Hirata, K., Nomura, W., Tabata, Y., and Ohtsu, M., "Realization of an Ultra-Flat Silica Surface with Angstrom-Scale Average Roughness Using Nonadiabatic Optical Near-Field Etching," *Applied Physics B*, Vol. 93, No. 1, 2008, pp. 55-57

Zreik, D., Germain, J., and Ladd, C., "Erosional and Mechanical Strengths of Deposited Cohesive Sediments," *Journal of Hydraulic Engineering,* Vol. 124, No. 11, 1998, pp. 1076–1085, https://doi.org/10.1061/(ASCE)0733-9429(1998)124:11(1076)